CHALMERS
UNIVERSITY OF TECHNOLOGY

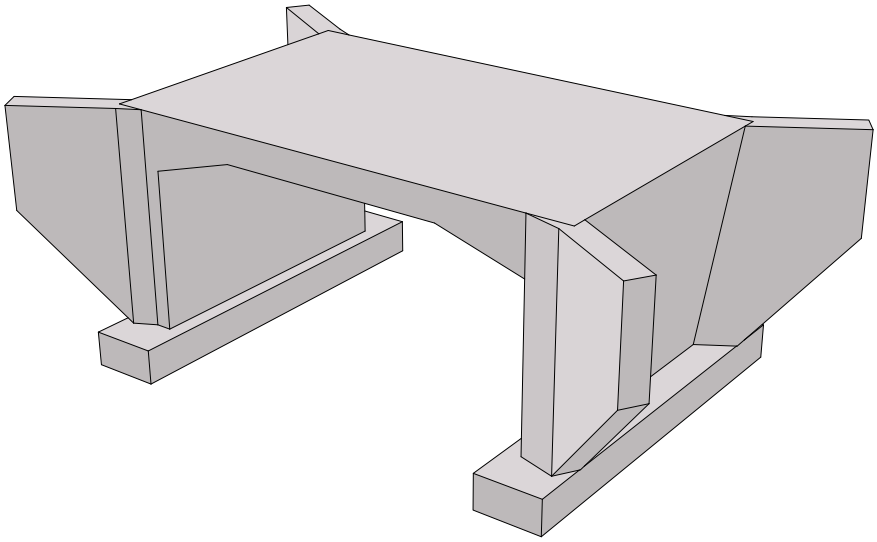

Parameter Study and Optimization of Slab Frame Bridges

Optimized Design Considering Environmental, Economical and Constructability Impact in a Preliminary Stage

Master's thesis in Master Programme Structural Engineering & Building Technology

ANDREAS ALHEDE
KAROLINA BESKOW

Department of Architecture and Civil Engineering
CHALMERS UNIVERSITY OF TECHNOLOGY
Gothenburg, Sweden 2020

Master's thesis ACEX30

Parameter Study and Optimization of Slab Frame Bridges

Optimized Design Considering Environmental, Economical and Constructability Impact in a Preliminary Stage

Master's Thesis in the Master's Programme Structural Engineering and Building Technology

ANDREAS ALHEDE
KAROLINA BESKOW

CHALMERS
UNIVERSITY OF TECHNOLOGY

Department of Architecture and Civil Engineering
Division of Structural Engineering
Concrete Structures
Chalmers University of Technology
Gothenburg, Sweden 2020

Parameter Study and Optimization of Slab Frame Bridges
Optimized Design Considering Environmental, Economical and Constructability Impact in a Preliminary Stage

Master's Thesis in the Master's Programme Structural Engineering and Building Technology

ANDREAS ALHEDE
KAROLINA BESKOW

Examensarbete ACEX30
Institutionen för Arkitektur och Samhällsbyggnadsteknik
Chalmers tekniska högskola, 2020

Department of Architecture and Civil Engineering
Division of Structural Engineering
Concrete Structures
Chalmers University of Technology
SE-412 96 Gothenburg
Sweden
Telephone +46 (0)31 772 1000

Cover: Type of slab frame bridges investigated. Typeset in LaTeX

Printed by Chalmers Reproservice
Gothenburg, Sweden 2020

Parameter Study and Optimization of Slab Frame Bridges
Optimized Design Considering Environmental,Economical and Constructability Impact in a Preliminary Stage
Master's Thesis in the Master's Programme Structural Engineering and Building Technology
ANDREAS ALHEDE
KAROLINA BESKOW
Department of Architecture and Civil Engineering
Division of Structural Engineering
Concrete Structures
Chalmers University of Technology

Abstract

Slab frame bridges are one of the most common bridge types in Sweden with a potential in optimizing the design on the emissions from carbon dioxide and the costs. Older graphs with recommendations for dimensions of cross-sections published by the Swedish Road Administration, Vägverket (1996), are considered as conservative and outdated.

This thesis presents updated dimensions that fulfils codes and standards that are used today. The optimization parameters have been identified through theory of slab frame bridges and a parameter study where different cross-sections have been analysed with respect to environmental, economical and constructability impact. The parameters have thereafter been optimized in a two-dimensional analytical study by implementing the moment distribution method and in a three-dimensional numerical study. Differences in the results between the different studies are discussed as well as the differences to the Swedish Road Administration's graphs over preliminary dimensions.

The theory of slab frame bridges and the parameter study show a correlation between the environmental and economical impacts where slender, heavy reinforced, cross-sections are to prefer when optimizing. Results from the preliminary design study shows a noticeable difference against the ones given by the Swedish Road Administration. Today's standards and optimization techniques enables an optimized design of slab frame bridges, where a slender cross-section decreases the environmental impact to a lower investment cost.

Keywords: slab frame bridge, preliminary design, moment distribution method, analytical optimization, numerical optimization.

Parameterstudie och optimering av plattrambroar
Optimerad utformning med avseende på miljömässiga, ekonomiska och byggbarhetstekniska aspekter i ett preliminärt skede
Examensarbete inom masterprogrammet Structural Engineering and Building Technology
ANDREAS ALHEDE
KAROLINA BESKOW
Institutionen för arkitektur och samhällsbyggnad
Avdelningen för kontruktionsteknik
Betongbyggnad
Chalmers tekniska högskola

Sammanfattning

Plattrambroar är en av de vanligaste brotyperna i Sverige och det finns potential att optimera broarnas tvärsnitt för att på så sätt minimera koldioxidutsläpp och kostnader. Existerande grafiska hjälpmedel med preliminära dimensioner för tvärsnitt utgivna av Vägverket (1996) anses konservativa och föråldrade.

Detta arbete presenterar uppdaterade dimensioner på parametrar som uppfyller dagens normer och föreskrifter. Optimeringsparametrar har identifierats med hjälp av teori om plattrambroar och en parameterstudie som studerat olika tvärsnitt med avseende på dess miljömässiga, ekonomiska och byggbarhetstekniska aspekter. Parametrar har sedan optimerats i en tvådimensionell analytisk studie, där momentförskjutningsmetoden tillämpats, samt i en tredimensionell numerisk studie. Skillnader i resultat mellan de olika studierna, samt skillnaderna mot Vägverkets grafer över preliminära dimensioner diskuteras.

Teorin och parameterstudien visar på att sambandet mellan de miljömässiga och ekonomiska aspekterna korrelerar och där slankare, tungt armerade, tvärsnitt är att föredra vid optimering. Resultatet från den preliminära designstudien visar på anmärkningsvärda skillnader mot de som ges av Vägverket och där dagens föreskrifter och optimeringstekniker möjliggör en design av framtida plattrambroar med slankare tvärsnitt till en lägre kostnad och med mindre påverkan på miljön.

Nyckelord: plattrambro, preliminär design, momentförskjutningsmetoden, analytisk optimering, numerisk optimering.

Contents

List of Figures

List of Tables

Preface

This Master's thesis has been written within the Master's program Structural Engineering and Building Technology at Chalmers University of Technology and is the end of a total of five years at Chalmers. The work was carried out at WSP bridge department in Gothenburg during spring 2020.

We both attended two courses in concrete, Concrete Structures and Structural Concrete, and two courses in the finite element method, FEM Basics and FEM Structures, available at Chalmers. The courses raised a great interest in concrete structures and numerical modelling, which motivated us writing about this topic.

We would like to thank our supervisor's at WSP, Daniel Josefsson and Hallvard Pagander Milveden. Thank you for your support and enthusiasm during the project. The examiner of the thesis, Mario Plos, docent in concrete structures at Chalmers. Thank you for your guidance through the project. Moreover, a great thank you to all teachers involved in the courses during our education. Thank you for your engagement.

I, Andreas Alhede, would also like to give a special thank you to my friend, Gabriel Edefors, and my family. Thank you for motivating me, without you this would have meant nothing to me.

I, Karolina Beskow, would like to thank my family for all your support and motivation during my education.

Andreas Alhede and Karolina Beskow, Gothenburg, June 2020

Acronyms

BC Boundary condition. vii, x–xii, xiv, 42, 44–52, 54–57, 73–81, 83, 84

DOF Degree of freedom. 16

EC Eurocode. 10–12, 32, 35, 40, 53, 69
EMC Embodied carbons. 20, 23, 71

LM1 Load model 1. x, xi, 11, 35, 37, 38, 47, 65

SLS Serviceability limit state. 13, 35, 40, 53
SRA Swedish Road Administration. 71, 87–89, 92
STA Swedish Transport Administration. 10, 25

ULS Ultimate limit state. 12, 35, 40, 53

Nomenclature

α_{cem}	Cement content [kg/m^3]
α_{Qi}	Adaptation factor for concentrated loads
α_{qi}	Adaptation factor for distributed loads
$\beta_{clinker}$	Clinker content in cement [%]
Δp	Assumed passive earth pressure [kPa]
$\delta_{\Delta p}$	Horizontal displacement caused by the assumed passive earth pressure Δp
δ_{pas}	Fictitious horizontal displacement of the frame caused by q_{pas}
δ_{res}	Actual horizontal displacement of the frame
δ_{sur}	Fictitious horizontal displacement of the frame caused by q_{sur}
$\gamma_{G,j,inf}$	Safety partial factor for favourable permanent loads
$\gamma_{G,j,sup}$	Safety partial factor for unfavourable permanent loads
$\gamma_{Q,1}$	Safety partial factor for unfavourable variable loads
$\gamma_{Q,i}$	Safety partial factor for favourable variable loads
μ	Utilization ratio
$\Psi_{0,i}$	Combination factor
$\Psi_{1,i}$	Combination factor
$\Psi_{2,i}$	Combination factor
ξ	Reduction factor
A_1	Cross-sectional area of the frame leg [m^2]
A_2	Cross-sectional area of the bridge deck slab [m^2]
B	Width of the bridge [m]
d	Effective height of a concrete section
E	Young's modulus of elasticity [Pa]
$G_{k,j,inf}$	Characteristic, favourable permanent loads
$G_{k,j,sup}$	Characteristic, unfavourable permanent loads
H	Height of frame legs [m]
I_1	Moment of inertia of the frame leg [m^4]
I_2	Moment of inertia of the bridge deck slab [m^4]

L	Theoretical span length of the bridge deck slab [m]
n_i	Number of load fields
Q_{ik}	Characteristic axle-loads from vehicles
q_{ik}	Characteristic distributed loads from vehicles
q_{res}	Counteracting lateral earth pressure
t_{f1}	Thickness of the frame leg at the level of the foundation slab [m]
t_{f2}	Thickness of the frame leg at the level of the haunch [m]
t_{hs}	Thickness of the haunch at the inside of the frame leg [m]
t_s	Thickness of the bridge deck slab / thickness at the end of the haunch [m]
v_{con}	Concrete volume $[m^3]$
w	Width of one lane [m]
z	Part of frame leg subjected to lateral earth pressure [m]

1
Introduction

1.1 Background

Concrete slab frame bridges are frequently used around the world and it is the most common bridge type in Sweden, especially for short spans (Trafikverket, 2008, p. 28). Slab frame bridges are limited, due to economical reasons, to a span width of approximately 25 meters (Almén, 2016, p. 5). A slab frame bridge consists of a bridge deck, frame legs and wing walls. It can be constructed with either open or closed foundation slab, with traffic on one or two levels and as single or multi-span bridge. The connections between the bridge deck and the frame legs are designed to transfer section forces. A typical slab frame bridge can be seen in Figure 1.1.

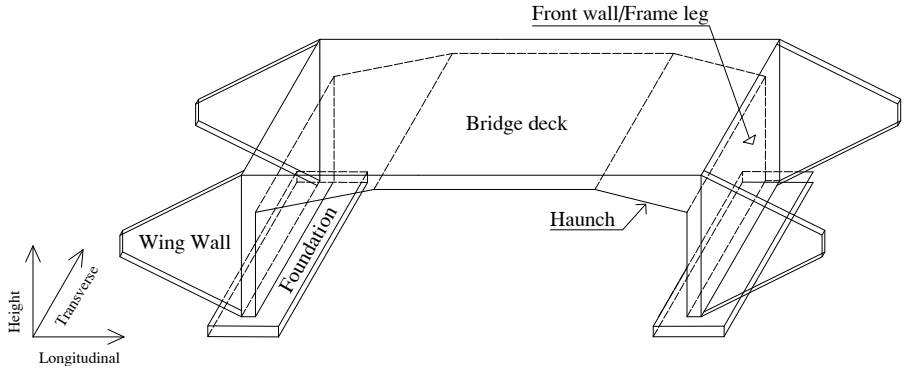

Figure 1.1 A common type of slab frame bridge with open foundation.

The construction sector plays an important role in the consumption of energy and raw material and on the emissions of carbon-dioxides. In 2017 the construction and real estate sector was responsible for 19 % of Sweden's total emission of green-house gases (Boverket, no date). The Swedish government decided in 2017 that Sweden should be climate neutral with respect to emission green-house gases by the year 2045. The construction and infrastructure sector has set internal goals where the sector's emissions of carbon dioxide should be reduced with 50 % by the year 2030 compared to 2015 (Fossilfritt Sverige, 2018, p. 7). To reach this goal the construction industry needs to implement new techniques and new ways of working.

In order to give a tender for design of a structure in an effective way, the designers needs to guess dimensions without performing detailed calculations in early stages.

Today, graphs and previous experience are used as guidelines for the choice of dimensions of slab frame bridges at an early stage. These graphs are old and based on information of dimensions of existing slab frame bridges, see Figure 1.2. Practicing engineers are concerned that these diagrams result in bridges that are not optimized with regard to material use, but also that the design process for optimization of slab frame bridges is very time-consuming.

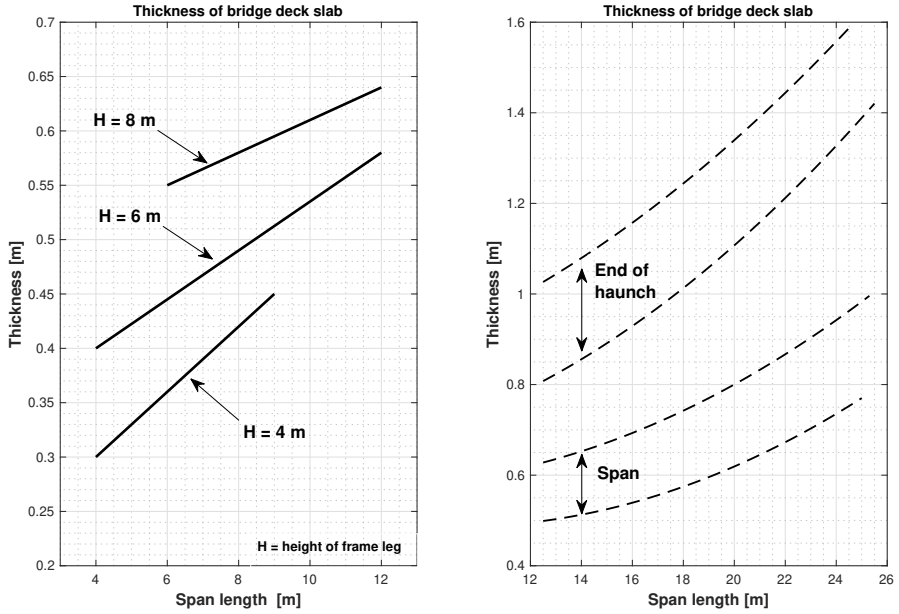

Figure 1.2 Suggestion on dimensions of deck thickness in the bridge deck of slab frame bridges (Vägverket, 1996, p. 42-43).

By implementing new knowledge and corresponding updated design codes it might be possible to design slab frame bridges which are more optimized than previously. It should be noted that this applies if the dimensions assumed in early stage are chosen accordingly. A more optimized structure would mean that the environmental impact and economic cost can be reduced as a result of the reduced amount of material. The effect may be particularly large for such a common type of structure as concrete slab frame bridges.

1.2 Aim and objectives

The aim of the project is to get a deeper understanding on how the design of slab frame bridges can be optimized by identifying and take into account the main parameters that affect the design. The intention is to develop graphs for preliminary design that facilitate optimized sizing. The goal is to enable a reduction of the environmental and economic impact of future concrete slab frame bridges by implementing the diagrams at early stages of the bridge design process.

1.3 Limitations

In order to make this study doable the study will be limited with respect to the following aspects:

- Slab frame bridges designed for road traffic only
- Straight slab frame bridges; vertical frame legs perpendicular to road direction
- Symmetric cross-section along the longitudinal section of the bridge
- Single span bridges
- Open foundation slab
- Reinforced concrete, with a predefined reinforcement amount limited to two layers $\phi 25$ in the tensile zone
- Wing walls are taken into account by adding equivalent forces from the wing walls on the frame legs
- Design of reinforcement is limited to the longitudinal direction of the bridge.

1.4 Specific issues under investigation

In order to fulfil the aim of the thesis, following aspects are investigated:

- Which are the main parameters that affect the design of slab frame bridges?
- Is there any significant differences in the results between an analytical two-dimensional optimization and a numerical three-dimensional optimization?
- How much can the cross-sectional area be reduced for a slab frame bridge that has been preliminary designed from the updated graphs compared to an already designed slab frame bridge?

1.5 Methodology

This master's thesis consists of three different phases. The first phase of the project will present theory of slab frame bridges to identify and evaluate critical parameters that affect the design. The parameters are related to the geometry of the bridge and its different structural parts. Interviews with experienced designers will be performed as a complement to and verification of the theory. An investigation regarding the environmental impact and economic cost of a concrete slab frame bridge will be performed to identify the basis for optimization. Interviews with contractors will be performed and evaluated as input for limitations of the optimization with respect to constructability. When the most critical parameters have been identified from the literature study a second phase of the project will start.

In the second phase the identified and selected parameters will be evaluated in a parameter study for a two-dimensional model. Expressions for design moments in critical sections of the frame will be used by implementing elementary cases for frames. Relations between the dimensions of the structural parts will be predicted and used for the optimization process in phase three. The two-dimensional analysis

will be used to simplify and limit the extent of the third phase by stating relevant load cases and giving start values for the iteration.

In the third phase of the study the programming language Python will be used to build a plug-in code to the finite element software BRIGADE/Plus, where structural analyses will be executed. The results from BRIGADE/Plus will then be evaluated until the design fulfils requirements stated in design codes. The process will continue until an optimized design of the slab frame bridge has been achieved.

Results from the study will be presented in graphs where parameters can be achieved as a function of the span length which can be used in a preliminary design of slab frame bridges. Dimensions of parameters of existing slab frame bridges will be compared and discussed with the results obtained from the numerical analyses. Moreover, a comparison study of the carbon dioxide impact will be performed for slab frame bridges with dimensions obtained from the optimization and older designs, respectively.

2

Design of slab frame bridges

The following chapter includes the theory of slab frame bridges, how they can be designed and their structural parts. The chapter continues with describing different loads that act on a slab frame bridge and how they are combined in the design process. The traditional design process is described as well as the complexity of the optimization procedures. Environmental impact and economical aspects of a slab frame bridge follows and how these aspect affects the design. Conclusion are drawn regarding optimal cross-section with respect to environmental impact and cost, which are used further on as basis for the optimization. The chapter ends with constructability.

2.1 Slab frame bridges

The slab frame bridge has traditionally been very popular in Sweden and constitutes 46 % of all bridges in Sweden (Solat Yavari, 2017, p. 983). It is commonly seen along bicycles roads, railways and smaller roads. The structural parts consist of a bridge deck slab, frame legs (or frame walls) and wing walls. The frame legs are connected to one continuous (closed) or two separate foundation slabs, creating either an open or closed frame. Figure 1.1 shows an open slab frame bridge. Slab frame bridges are rigid in their connections between the frame legs and the bridge deck with continuous reinforcement through the connections (Trafikverket, 2008, p. 28). A typical reinforcement layout for a slab frame bridge with pinned and fixed boundary conditions, respectively, is shown in Figure 2.1. In addition to the reinforcement shown in Figure 2.1, minimum reinforcement is added at all surfaces as well as reinforcement in the transverse direction of the bridge.

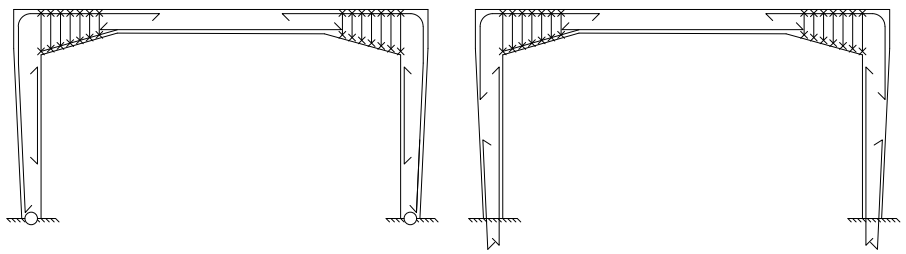

Figure 2.1 Typical layout of main reinforcement for a slab frame bridge with pinned connections to the foundation (left) and fixed connections to the foundation (right).

The slab frame bridge is similar to the girder frame bridge where the bridge deck slab is supported by girders under the slab connected to the frame legs. The general definition for these types of bridges is given by Trafikverket (2008, p. 15, 20) and can be read as:

- **Girder frame bridge:** The main structural parts should consist of one or more girders with a width (B) which is less or equal to five times the height (H), $B \leq 5H$.
- **Slab frame bridge:** The main structural part can be considered as a plate if the width (B) is larger than five times the height (H), $B > 5H$

Slab frame bridges can be both straight or skewed depending on the geometry of the road. A straight slab frame bridge has frame legs perpendicular to the road direction. Figure 2.6 (right) shows a plan-view of an straight and a skewed slab frame bridge, where φ is the angle of inclination.

2.1.1 Bridge deck

The bridge deck slab transfers loads to the frame legs. The loads can be carried in one or two directions depending on the support condition of the slab (Engström, 2014, p. 1-2). Since the deck slab in a slab frame bridge is supported by frame legs on the opposite sides of the slab it acts mainly as a "one-way slab" (beam action). However, the behavior of the slab is highly dependent on the load that is applied. Uniformly distributed loads results in pure beam action while concentrated loads (axle loads from vehicles, for instance) results in a slab that distributes the load in two directions (plate action) (Engström, 2014, p. 2) and biaxial bending, see Figure 2.2 and 2.3.

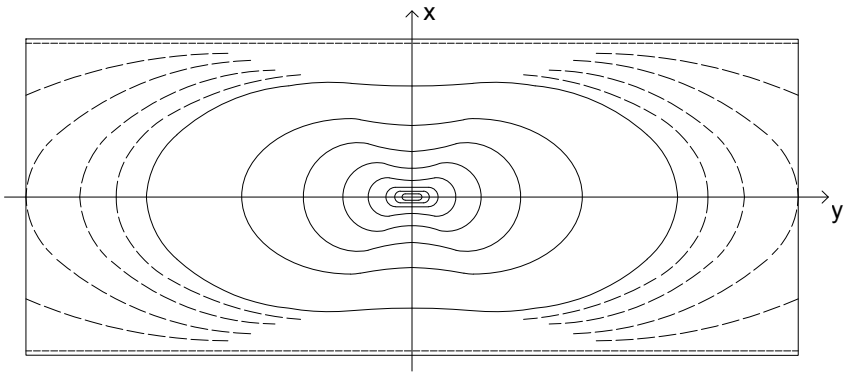

Figure 2.2 Example of a two-way behaviour for a simply supported slab on two opposite edges: Influence area for the mid-section and how the bending moment m_x is affected by a concentrated load (Pucher, 1958).

Figure 2.3 shows a slab element which is divided into strips in its plane, longitudinal and transverse. The slab is simply supported on all edges, is subjected to a uniformly distributed load and acts in plate action ("two-way"). A relation between the out of

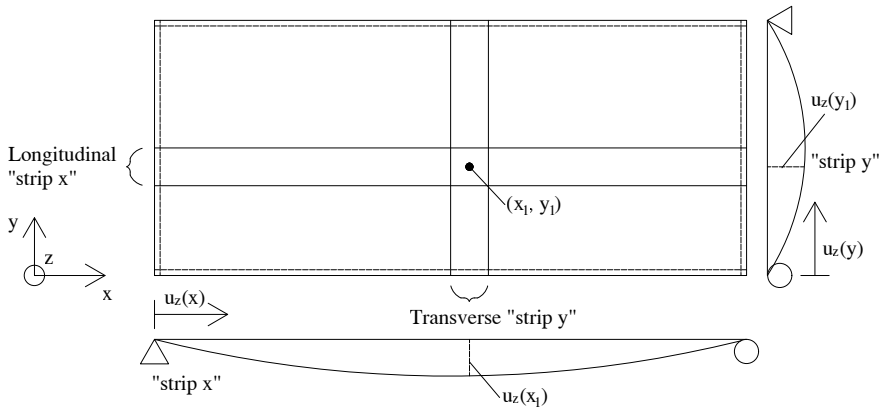

Figure 2.3 A simply supported slab on all edges, divided into strips in the longitudinal and transverse direction.

plane deformation in the two strips can be determined. The deformation in a certain point must be equal in both strips - in order to fulfil the compatibility condition, i.e: $u_z(x_1) = u_z(y_1)$

2.1.2 Frame legs

The frame legs carry the load from the bridge deck slab but are also subjected to lateral earth pressure, and surcharge loads. The lateral earth pressure counteracts lateral movements of the frame caused by horizontal loads. The rigid connections between the frame legs and the bridge deck stabilize the structure and makes it possible to carry horizontal forces. It is recommended that the frame legs are of equal height because of the earth pressure. If the frame legs are of different height the resulting lateral earth pressure will not be in equilibrium and additional stresses will be induced in the shorter frame leg (Vägverket, 1996, p. 41). The height of the frame leg for a reinforced slab frame bridge should be at least 1/4 of the span length. In cases with span lengths up to 12 meter ans when the foundation consist of soft soil (clay, for instance) it is advised to make use of a closed frame (Vägverket, 1996, p. 41).

The stiffness in the connection between the frame legs and the foundation is important for the overall behavior of a frame structure, as can be seen in Figure 2.4. The frame legs can be either cast together with the foundation or not. When the frame legs are cast together with the foundation the boundary condition depends on the geotechnical condition. In a simplified analysis based on hand-calculations it is common to assume either a fixed boundary condition (for instance when the foundation is cast on a bedrock) or pinned. However, for any type of soil, it is more realistic to assume a partially fixed connection by including the stiffness of the soil.

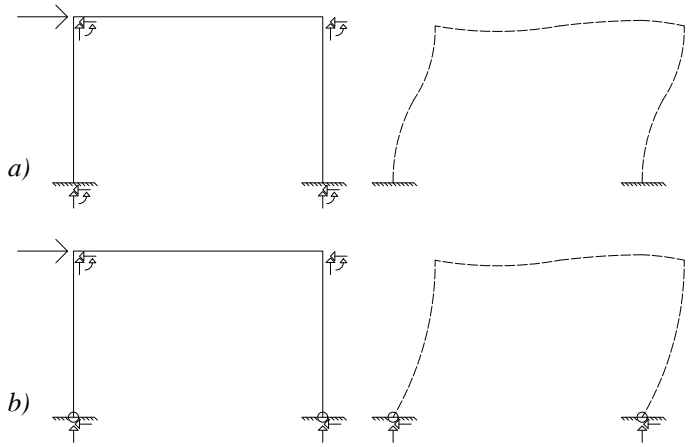

Figure 2.4 Principal sketch on how the boundary condition between the frame legs and the foundation influence the behavior due to horizontal forces. a) In case of fixed connections. b) In case of pinned connections.

2.1.3 Haunches

Haunches are used to increase the shear capacity in critical sections, frame corners, and to transfer moment and shear force to the frame legs. By using haunches, the amount of shear reinforcement can be reduced. According to the former Road Administration of Sweden, Vägverket (1996), different types of haunches are recommended depending on the span length, see Figure 2.5. For span lengths up to 12 m the haunch are normally predefined as a right-angled triangle with dimensions of the cathetus of 500 mm. For longer spans the thickness of the haunch is designed and the length is often around a quarter of the span length.

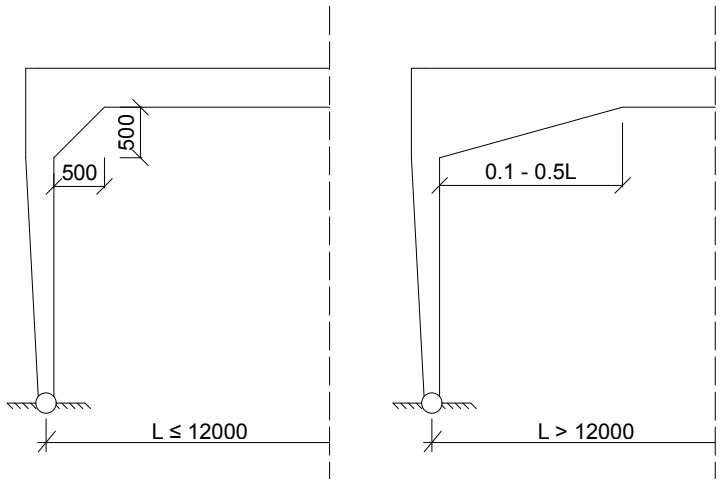

Figure 2.5 Recommendations according to Vägverket (1996) for execution of haunches. Dimensions in millimeter.

2.1.4 Wing walls

Wing walls are used to keep adjacent soil in place and give an extra contribution to the stiffness of the frame legs as a result (Difs & Karlsson, 2015, p. 14). The arrangement of the wing walls depends on how the embankment is formed as well as the geometry of the bridge. The wing walls are normally arranged such that they follow the bisection. Figure 2.6 shows a straight and a skewed slab frame bridge and how the wing walls are arranged for the two cases following the bisection.

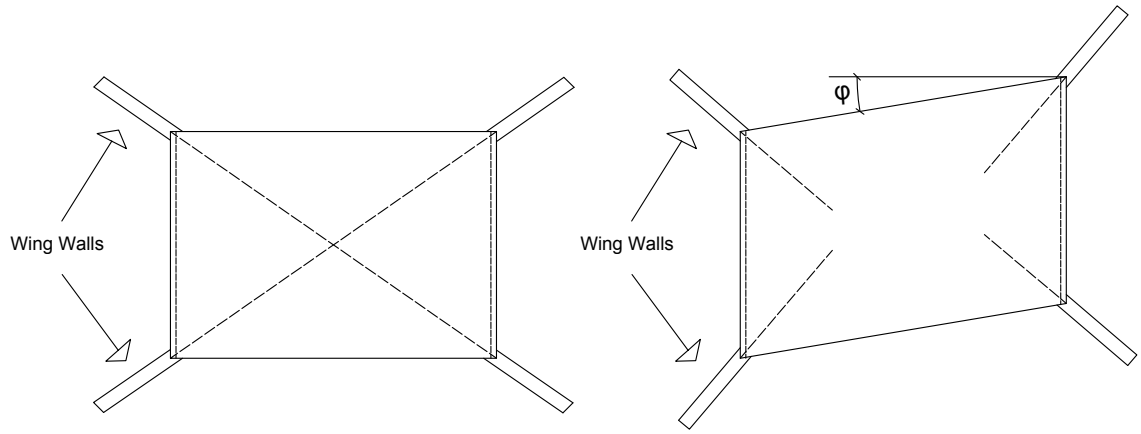

Figure 2.6 Top-view over wing-walls parallel to the bisection of the slab for a straight slab frame bridge (left) and for a skewed slab frame bridge (right).

2.2 Loads

A structure is subjected to different kinds of loads that it needs to be designed for. It is the designer's responsibility to design a robust structure to ensure the safety. The common approach to fulfil the requirements is to design all cross-sections to withstand all possible load combinations and load positions. Besides the load-carrying capacity the structure must fulfil requirements regarding serviceability and fatigue.

2.2.1 Type of loads

There are many different types of loads that needs to be designed for. The loads can for instance be static or dynamic and can act in the vertical or horizontal direction. Loads that typically are of interest in the design of a slab frame bridge are listed below.

Permanent loads

- **Self-weight:** Constant in time and acts in the vertical plane.
- **Paving:** Constant in time and acts in the vertical plane.
- **Shrinkage:** Increases with time and creates restraint forces.

- **Creep:** An effect of loading the concrete. Depends on time and the magnitude of the loads.
- **Earth Pressure:** Acts both in the vertical and horizontal plane. The lateral earth pressure is of particular interest in the design of slab frame bridges.
- **Pore water pressure:** Acts both in the vertical and horizontal plane.
- **Differential displacement:** Uneven settlement of the foundations may result in horizontal and vertical displacement at the support.

Variable loads

- **Vertical traffic load:** Not constant in time and with a variation of magnitude and position.
- **Acceleration/braking:** Caused by traffic loads and acts in the horizontal plane.
- **Transverse horizontal load:** Caused by a quick in-plane motion from vehicles.
- **Centrifugal force:** An horizontal force from vehicle loads is developed when the bridge deck is performed with a horizontal radius.
- **Surcharge load:** Vertical loads from vehicles on the embankment creates a uniformly distributed lateral earth pressure on the frame legs.
- **Accidental load:** These are loads that are included to ensure the load-bearing capacity in case of an accident.
- **Wind load:** Acts horizontally on the bridge and vehicles driving over the bridge.
- **Temperature effects:** Hydration of young concrete creates internal stresses that can induce cracking of concrete. In the normal service state temperature changes of the surrounding air creates stress-independent strains. If the concrete is prevented from movements, restraint forces occurs which can induce cracking.

2.2.2 Vehicle models used in the design of road bridges

In Sweden it is the Swedish Transport Administration (Trafikverket) and the Swedish Transport Agency (Transportsstyrelsen), that sets the regulations for all bridges that are to be designed. The Swedish Transport Agency (STA) demands the designer to design according to the requirements and recommendations stated in the European standard, Eurocode (EC).

According to EC, CEN (2003b, p. 33), the traffic loads should be implemented in design by using several load models. Number of lanes subjected to traffic loads within the width of the bridge is given as a function of the width itself and is explained in Table 2.1 and Figure 2.7.

There are several load models defined in EC for vertical traffic load (CEN, 2003b). These models are equivalent traffic load models that give approximately the same load effect as the real traffic situation on the bridge. Load model 1 (LM1) and

Table 2.1 Calculation of number of lanes and corresponding widths (CEN, 2003b, p.33)

Lane-width	**Number of load fields**	**Width of one load field**	**Width of remaining area**
w $< 5.4\ m$	$n_1 = 1$	$3\ m$	w - $3\ m$
$5.4\ m \leq$ w $< 6\ m$	$n_1 = 2$	$\frac{w}{2}$	0
$6\ m \leq$ w	$n_1 = integer(\frac{w}{3})$	$3\ m$	$w - 3$ x n_1

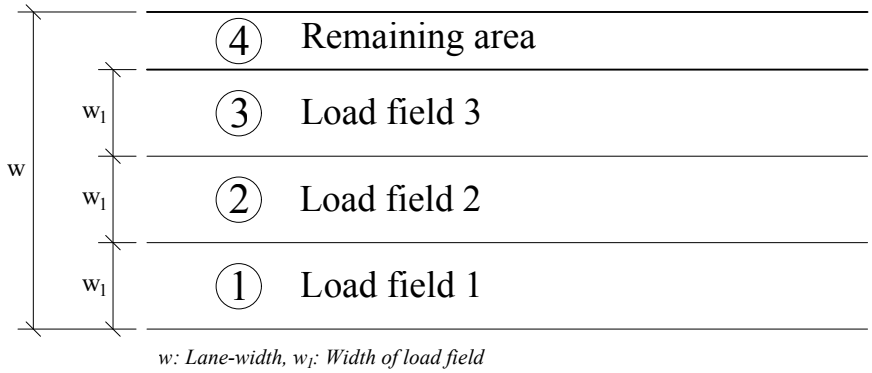

Figure 2.7 Example of load fields (CEN, 2003b, p. 31).

Fatigue load model 3 are used in this thesis.

2.2.2.1 Load model 1

Load model 1 (LM1) consist of a uniformly distributed load per unit area and one group of concentrated axle loads. The uniformly distributed traffic load act vertically over the bridge deck. The concentrated axle loads act vertically and with a position given in EC. Figure 2.8 shows how LM1 is applied.

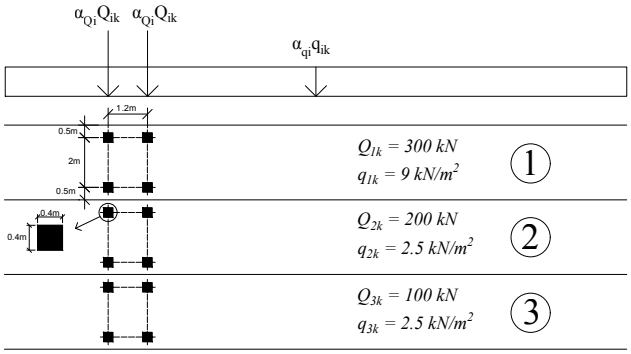

Figure 2.8 Illustration of how LM1 is applied on different traffic lanes (CEN, 2003b, p. 34).

The reduction factors α_{Qi} and α_{qi} account for road conditions. In the Swedish national annex, α_{Qi} is set to 0.9 for traffic lane 1 and 2 and 0.0 for traffic lane 3. α_{qi} is 0.8 for traffic lane 1 and 1.0 for traffic lane 2 (Transportstyrelsen, 2018, p. 36).

2.2.2.2 National Vehicle model

The Swedish Transport Agency requires the designer to also take national load models into account, here referred to as vehicle models (Transportstyrelsen, 2018, p. 35). These models are used to represent the actual vehicles and axle combinations that pass over the bridge. There are fourteen vehicle models ,A - N, according to Transportstyrelsen (2018, p. 35) which are presented in appendix B.

2.2.2.3 Fatigue load model 3

Fatigue load model 3 consists of 4 concentrated axle loads, each with two identical wheels. Each axle load is of magnitude 120 kN. The local placement of the load model is presented in Figure 2.9.

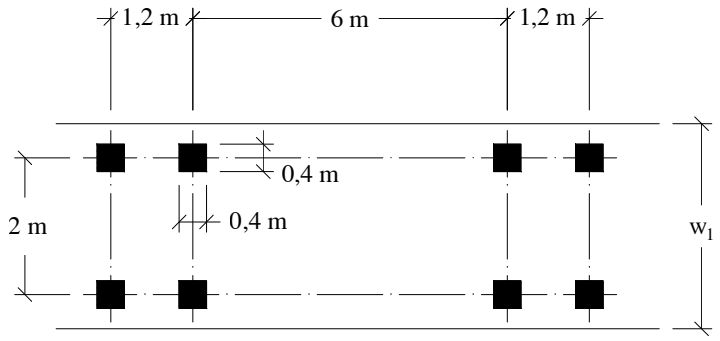

Figure 2.9 Fatigue model 3 (CEN, 2003b, p. 45).

2.2.3 Load combinations

The ultimate limit state (ULS) is in EC, CEN (2002, p.40) divided into different categories that are used depending on what is going to be designed. The different groups are defined as follows:

- **EQU:** Loss of static equilibrium for a structure, or a part of it, when it is regarded as a rigid body.
- **STR:** Internal failure or large deformations of the load-bearing structure or the structural parts where the strength of the material is decisive.
- **GEO:** Failure or large deformation of the foundation where the strength of the soil or bedrock is decisive.
- **FAT:** Failure of the load-bearing structure or its structural parts caused by fatigue.

The different categories of failure stated above has their own expression of combining loads. Permanent and variable loads are combined. In case of several permanent and/or variable loads it has to be investigated which combination of loads that gives the worst case scenario with respect to each category, when the loads are considered as either favorable or unfavorable.

The expression for loss of static equilibrium (EQU) is defined according to CEN (2002, p. 48) and yields:

$$\sum_{j\geq 1} \gamma_{G,j,sup} G_{k,j,sup} + \gamma_{G,j,inf} G_{k,j,inf}" + "\gamma_{Q,1} Q_{k,1}" + "\sum_{i\geq 1} \gamma_{Q,i} \Psi_{0,i} Q_{k,i} \tag{2.1}$$

The same expressions are used for STR and GEO and is stated in Equations 2.2 and 2.3. Equation 2.2 is desicive when permanent loads gives the most unfavourable effect and Equation 2.3 when variable loads gives the most unfavourable effect (CEN, 2002, p. 48).

$$\sum_{j\geq 1} \gamma_{G,j,sup} G_{k,j,sup} + \gamma_{G,j,inf} G_{k,j,inf}" + "\gamma_{Q,1} \Psi_{0,1} Q_{k,1}" + "\sum_{i\geq 1} \gamma_{Q,i} \Psi_{0,i} Q_{k,i} \tag{2.2}$$

$$\sum_{j\geq 1} \xi\gamma_{G,j,sup} G_{k,j,sup} + \gamma_{G,j,inf} G_{k,j,inf}" + "\gamma_{Q,1} Q_{k,1}" + "\sum_{i\geq 1} \gamma_{Q,i} \Psi_{0,i} Q_{k,i} \tag{2.3}$$

"+" in (2.1), (2.2) and (2.3) means that the loads are combined with each other, G, and Q corresponds to permanent loads and variable loads, respectively. According to EC, there are three different methods that uses different sets of equations for load combination in ULS, set A-C. According to Trafikverket (2019b, p. 76), method two should be used for STR and method three for GEO. Method two should be combined with set B, and method three as a combination with set B and C. Values of the partial safety factor γ, the reduction factor ξ and the combination factor Ψ are given in set B and C (CEN, 2002, p. 58, 63–64) and in Trafikverket (2019b). According to Transportstyrelsen (2018, p. 10) the variable loads and unfavourable permanent loads should be multiplied with a partial factor γ_d considering safety class. The partial factor γ_d is 0.83 for safety class 1, 0.91 for safety class 2, 1.0 for safety class 3 and 1.1 for safety class 4. For bridges for road traffic with a theoretical span length shorter than 15 meters safety class 2 should be applied. Safety class 3 applies for bridges with longer spans (Transportstyrelsen, 2018, p. 9).

In Serviceability limit state (SLS), three different load combinations are used; Characteristic combination, Frequent combination and Quasi-Permanent combination (CEN, 2002, p.40).

The Characteristic combination is used for irreversible limit states, see Equation 2.4.

$$\sum_{j\geq 1} G_{k,j,sup} + G_{k,j,inf}" + "Q_{k,1}" + "\sum_{i\geq 1} \Psi_{0,i} Q_{k,i} \tag{2.4}$$

Frequent combination is used for reversible limit states and yields:

$$\sum_{j\geq 1} G_{k,j,sup} + G_{k,j,inf}" + "\Psi_{1,1} Q_{k,1}" + "\sum_{i\geq 1} \Psi_{2,i} Q_{k,i} \tag{2.5}$$

The Quasi-permanent combination is applied for long term effects and is expressed as:

$$\sum_{j\geq 1} G_{k,j,sup} + G_{k,j,inf}" + "\sum_{i\geq 1} \Psi_{2,i} Q_{k,i} \tag{2.6}$$

Load combination for check of deflection is frequent values of the vertical traffic load (Trafikverket, 2019b, p.77).

2.3 Finite element analyses for concrete structures

3D finite element analyses are used widely in design of concrete structures and provide a possibility of accurate structural analyse. However, there are several issues regarding the nature of the model and the evaluation of results that needs to be considered (Johansson, Plos, & Pacoste, 2012, p.7).

2.3.1 Restraint forces in linear elastic FE-analyses

One issue that has been discussed is the effect of restraint forces forces from temperature loads and shrinkage in a linear elastic finite element analyses, especially for design of slab frame bridges. A linear elastic analyses will predict large tensile forces in the transverse direction of the bridge, due to the connection between the bridge deck and frame leg (Zangeneh Kamali, Johansson, & Svedholm, 2013, p. 9). In reality, cracking of concrete will lead to a stiffness reduction and hence a reduction of the restraint forces (Zangeneh Kamali et al., 2013, p. 9). According to Zangeneh Kamali et al. (2013, p. 37), it is recommended to ignore the effects of temperature differences in the linear elastic FE-analyses and design the bridge with respect to temperature and shrinkage in the transverse direction manually.

2.3.2 Post processing

A three-dimensional structure will give rise to a bending moment in two directions, in the longitudinal and transverse direction of the bridge, respectively, and a torsional moment. According to Johansson et al. (2012, p. 24) the reinforcement

moment resistance must be able to balance the complete linear moment field, and it is therefore of importance to include the effect of the torsional moment in design.

Design reinforcement moment is determined as following (Johansson et al., 2012, p. 24):

$$m_{rx} = m_x \pm \mu \left| m_{xy} \right| \quad , \quad m_{ry} = m_y \pm \mu \left| m_{xy} \right| \tag{2.7}$$

m_x and m_y are the linear bending moments in x- and y-direction (longitudinal and transverse direction, respectively) and m_{xy} is the torsional moment. μ is a factor that can be chosen with that, according to Johansson et al. (2012, p.24), normally is chosen close to 1. Associated membrane forces are evaluated as:

$$n_{rx} = n_x \pm \mu \left| n_{xy} \right| \quad , \quad n_{ry} = n_y \pm \mu \left| n_{xy} \right| \tag{2.8}$$

Finite element analyses also generates shear force in two directions. The structure should be designed for the resultant shear force, which can be expressed as (Johansson et al., 2012, p. 25):

$$v_0 = \sqrt{v_x^2 + v_y^2} \tag{2.9}$$

2.4 Traditional design process

The traditional design process for structural design of concrete members is based on trial and error or past experience (Behrooz & Hinton, 1999, p. 2). Initially the designer assumes dimensions and performs analyses of the structure and compare results against requirement from design codes. If the initial configurations meet the requirements of the code, the section is approved. Otherwise the configurations are updated until the sections fulfil the requirements (Behrooz & Hinton, 1999, p. 2). One consequence of this design process is that it is time consuming if the assumed initial parameters are chosen wrong. Another consequence is that there is no way to know weather the approved configurations result in the best and most optimized design considering environmental impact and cost.

Since almost all bridges are unique it is not economically defensible to spend time on an optimized design for each individual bridge. A design scheme showing the traditional design process can be seen in Figure 2.10.

2.4.1 Complexity of finding the most optimized design

In order to explain the complexity of finding the most optimized bridge design one may study the *optimization objectives*. The most optimized design is the design

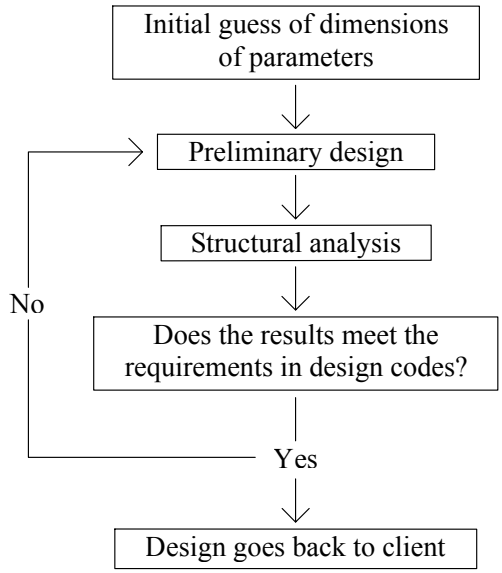

Figure 2.10 Traditional design process applied in the design of slab frame bridges.

beyond which there is no other design that has a lower environmental impact, lower cost and higher utilization ratios. The complexity of finding the optimal design requires an iterative process that quickly becomes huge because of the large amount of parameters that has to be analysed. The iteration process is very time consuming and the number of iterations increases exponentially to the parameters that are included in the optimization process (Venkataraman & Haftka, 2004, p. 380).

The level of complexity of a structural optimization can be broken-down and divided into sub-levels, the *model complexity level*, the *analysis complexity level* and the *optimization complexity level* (Venkataraman and Haftka, 2004, p. 378-380).

Model complexity level
The model complexity level is associated with the computational time due to the size of the topology of the finite element model (Venkataraman & Haftka, 2004, p. 378). The degree of complexity is related to the degree of freedom (DOF) within the system and constitutes the number of equations in the system. The degrees of freedom increase substantially when a 3D-problem is analysed. Hence, use of symmetry is a useful trick to reduce the size of matrices and vectors in the system. Furthermore, element types and boundary conditions also affect the model complexity.

Analysis complexity level
The complexity regarding the analysis is dependent on which type of analysis that will be executed. A linear elastic analysis, which has a constant rate of change, is the simplest and should be used, if possible, to reduce the computational time. When material and/or geometrical nonlinearities are included in a non-linear analysis the rate of change is no longer constant and thus the computational time increases. The degree of analysis complexity is highly dependent on the problem that is of interest (Mathisen, 2012, p. 6-10).

Optimization complexity level
Venkataraman and Haftka (2004) describe the optimization complexity level as a function of the optimization algorithm applied. The simplest optimization method is the graphical optimization where one or two variables are of interest and the probabilistic optimization as the most complex and time consuming.

Complexity triangle
The complexity levels can be summarized and visualized in a complexity triangle, see Figure 2.11. The general definition of the most optimized design stated earlier can now, with the understanding of complexity of optimization and the understanding of Figure 2.11, reformulate the definition into a more case specific formulation. The need of finding the theoretically most optimized design with the highest level of model, analysis and optimization complexity requires a substantial amount of work and may not be time or economic defensible in a designer's point of view. Instead, the designer should aim for an optimization level that lies somewhere within the triangle, where the complexity levels are delicately balanced.

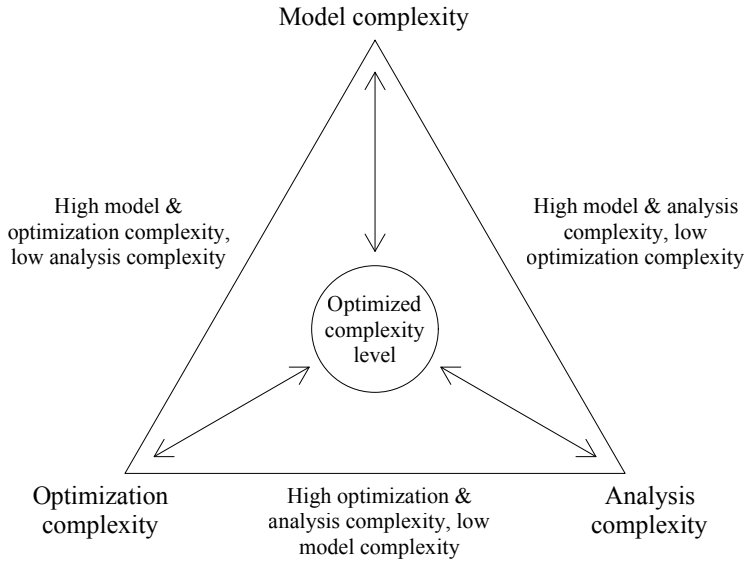

Figure 2.11 Level of complexity can be described by a complexity triangle. The border of the triangle represent the highest level of complexity. The optimized design is found inside the circle.

2.5 Structural optimization

Optimization problems arise everyday but with different complexities and in different areas. Evolution has formed animals and vegetation for millennia to best match their conditions and will continue to optimize them to match the future conditions. Engineers have always, in one way or another, aimed for an optimization process but with different methods in different engineering areas. For all types of optimization

problems there are three central parts that are included in an optimization process, the *objectives*, the *optimization parameter* and *constraints* (Bhatti, 2000, p. 2).

The objective of an optimization problem can be found by answering the question why there is need for optimization. The overall goal does not need to be one but several.

The optimization parameter is a quantitative variable that will be optimized in order to fulfil the objective. Similar to the objective, the optimization parameter can consist of several variables. The variables must affect the objective of the optimization process (primary) and can not be of secondary importance (Bhatti, 2000, p. 2).

The structural design of a bridge must always follow regulations regarding safety of the structure but it is also common that the contractor specifies other conditions. These regulations and conditions constitute constraints for an optimization. The constraint can be either implicit or explicit and affects the output of the optimization (Sioshansi & Conejo, 2017, p. 3).

An optimization problem can be visualized with its different components, as illustrated in Figure 2.12, or in mathematical form.

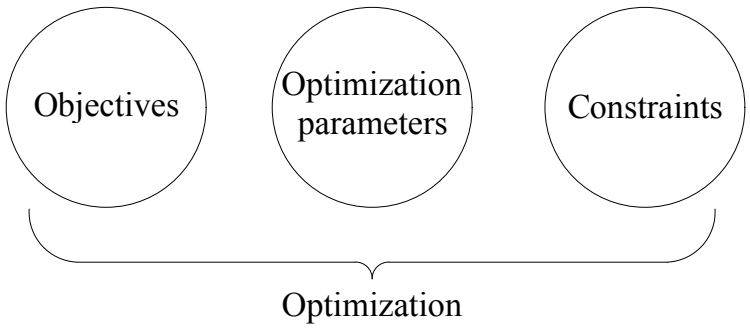

Figure 2.12 Parameters that influence the optimization process.

2.5.1 Optimization classes and optimization algorithms

Optimization problems can be either continuous or discrete. A continuous optimization problem is a problem that can take any value within a certain range as long as it fulfils the constraints (Gould and Leyffer, 2003, p. 1). A continuous optimization parameter in the design of a slab frame bridge can be the thickness and span length of the bridge deck. The complexity of solving a continuous optimization problem depends on where the objective function has a linear or nonlinear relation. A discrete optimization problem is a problem where one or several variables only can take discrete (integer) values (Lee, 2004, p. 1).

There are several different optimization methods to implement in an optimization process. The methods which are explained are the stochastic and the deterministic method which are either constrained or unconstrained, or a combination of both.

The stochastic optimization is based on that the optimization parameters are chosen randomly and is not to prefer in the optimization process of slab frame bridges, since the optimization parameters are predefined. Francisco, Revollar, Vega, and Lamanna (2005, p. 336), implies that a stochastic optimization with constraints is often time consuming and that the risk of producing an infeasible solution is substantial. The implementation of a deterministic optimization with constraints gives a better model in the optimization of a slab frame bridge since the optimization parameters will be predefined.

Depending on the complexity of the optimization problem different optimization algorithms for solving the problem can be applied. Bhatti (2000) explains how the graphical optimization algorithm can be used when one or two variables are to be optimized. The solution is obtained by specifying a certain range for each variable. By execution of the data in this range the solution is found. The graphical optimization requires, however, that the solution is given within the range of data. Otherwise the optimized solution can not be found and the operation tends to be time-consuming.

A more complex and time-consuming way of finding an optimized solution is the probabilistic optimization algorithm. The algorithm is not only dependent on one objective function but several and is based on reliability (Venkataraman & Haftka, 2004, p. 380). No parameters are predefined but stochastic.

An optimization algorithm that is easy to implement is the iterative optimization algorithm. By defining a set of variables with a certain range, the optimization process can be iterated for each step (Wynn, Eckert, & Clarkson, 2007, p. 2). The designer can then decide which execution that gives the best design. In an iterative optimization process it is important to minimize the number of iterations to reduce the computational time (Wynn et al., 2007, p. 2).

2.6 Stopping criterion

In optimization it is of importance to define the point where the calculation can be stopped since the optimization problems often include computationally heavy objectives and constraint functions (Zielinski & Laur, 2008). The point when the calculations can be stopped is when a global optimum is reached and the absolute lowest value of the objective function is found. Detection of a suitable stopping criterion is a difficult task and varies depending on optimization algorithm. However, in engineering applications, the aim is normally to find a solution that is adequate within a practical time range (Solat Yavari, 2017, p. 17). This means that a more suitable stopping criterion for practical engineering applications is a limit on the calculation time as for example maximum numbers of iterations.

2.7 Environmental impact of concrete structures

The environmental impact of a construction material can be defined as its Embodied carbons (EMC). The EMC is the sum of the fuel and process related emissions of carbon dioxides (Geoff & Craig, 2008). The carbon impact of a reinforced concrete structure is the sum of the carbon impact from reinforcement steel and concrete, respectively.

2.7.1 Concrete

Concrete is a flexible and durable construction material but it also has a large environmental impact due to emissions of carbon dioxides. The main part of concrete's carbon impact arises from the production of cement with 90 % of the total emissions of carbon-dioxides. The main ingredient in cement is typically clinker. Clinker is manufactured by heating limestone up to 1400-1500 degrees Celsius. This process requires large amount of energy and emits carbon-dioxides when the limestone is transformed into clinker (Betonginitiativet, 2018). The carbon impact of concrete can be approximated as:

$$(EMC)_{concrete} = v_{con} \cdot \alpha_{cem} \cdot \beta_{clinker} \cdot (EMC)_{clinker} \tag{2.10}$$

where

v_{con} = concrete volume $[m^3]$

α_{cem} = cement content $[kg/m^3]$

$\beta_{clinker}$ = clinker content in cement [%]

$(EMC)_{clinker}$ = embodied carbons in clinker [kg CO_2-eq/kg]

From the expression above it can be seen that the carbon impact of concrete is influenced by the cement content and the clinker content in the cement. A high cement content results in a larger carbon impact. The cement content of concrete is defined as the water-to-cement-ratio, w/c-ratio. There are several concrete classes which are defined by their w/c-ratio which corresponds to the strength of the concrete. The cement content of different concrete classes is presented in Table 2.2. The w/c-ratio is often given by required exposure class of the concrete.

The other factor affecting the carbon impact of concrete is the clinker content in the cement. There's different types of cement with varying clinker contents. In Sweden, the most common cement type for infrastructure is CEM I which has a clinker content of 90-100 %. Environmentally improved cement types are created by substituting some of the clinker to another binder as for example fly-ash or ground granulated blast-furnace slag (ggbs). Clinker content and corresponding EMC-values for different types of cement are presented in Table 2.3.

Table 2.2 Cement content in concrete classes, from AB Svenska Byggtjänst and Cementa AB (1994)

Concrete class	w/c-ratio	Cement content	Unit
C28/35	0.55	348	kg cement/m^3 concrete
C30/37	0.5	355	kg cement/m^3 concrete
C32/30	0.45	390	kg cement/m^3 concrete
C35/45	0.4	413	kg cement/m^3 concrete
C45/55	0.36	450	kg cement/m^3 concrete
C50/60	0.34	460	kg cement/m^3 concrete

Table 2.3 Clinker content and EMC for different cement types.

Cement type	Clinker content	CO_2-eq	Reference
CEM I, Norcem	91 %	758 kg/ton	(Norcem AS, 2013)
CEM I, Cementa	95-100 %	873 kg/ton	(Cementa AB, 2014a)
CEM II/A-V, Cementa	80-94 %	678 kg/ton	(Cementa AB, 2014b)
CEM II/A-V, Norcem	76 %	637 kg/ton	(Norcem AS, 2014)
CEM II/B-M, Norcem	73 %	604 kg/ton	(Norcem AS, 2014)

2.7.2 Reinforcement steel

The carbon impact of steel is mainly a cause of the manufacturing-process of steel and internal transports. The production process of steel can have larger or smaller carbon impact depending on energy source and use of raw material. There is one company, Celsa, that produces reinforcement with energy from 100% hydroelectricity and the material is from recycled waste. Celsa's reinforcement has a carbon impact of of 370 kg CO_2-eq/ton reinforcement (Celsa Steel Service AS, 2015). This type of reinforcement has traditionally not been used in large scale since it is more expensive compared to traditional reinforcement. The mean value for carbon impact of reinforcement in infrastructure in Europe is 1030 kg CO_2-eq/ton reinforcement (Trafikverket, 2019a). The global mean value for reinforcement consists of 30 % recycled steel and has a embodied carbon value of 2043 CO_2-eq/ton reinforcement (Ecoinvent, 2019). A summary of the embodied carbons of a selection of types of reinforcement steel is presented in Table 2.4.

Table 2.4 EMC for reinforcing steel.

Type	CO_2-eq	Unit	Reference
Reinforcement steel, Global	2043	kg/ton	(Ecoinvent, 2019)
Reinforcement steel, Celsa	370	kg/ton	(Celsa Steel Service AS, 2015)
Reinforcement steel, Europe	1030	kg/ton	(Trafikverket, 2019a)

2.8 Production cost of concrete structures

The production cost of a structure is calculated as the sum of material cost and cost for execution. For a reinforced concrete structure the cost is therefore a function of the material cost of concrete and reinforcement, and the cost of labour work for execution of concrete and mounting of reinforcement. Costs for mounting the concrete form itself has been neglected to simplify the calculations.

2.8.1 Concrete

The total cost for concrete consist of material cost and cost of concrete work, as for example vibrating during casting. Unit prices for material and execution of concrete is presented in Table 2.5 which, according to Yavari, Pacoste, and Karoumi (2016), is acquired from construction companies in Sweden.

Table 2.5 Unit prices for Concrete, from Yavari et al., (2016).

Description	Price	Unit
Material C35/45	1800	SEK/m^3
Concrete work frame leg	750	SEK/m^3
Concrete work bridge deck	800	SEK/m^3

2.8.2 Reinforcement

The total cost for reinforcement consist of material cost of reinforcement bars and cost for mounting of reinforcement. The labour cost of mounting reinforcement is influenced by the difficulty of mounting since that strongly effects the time required per kg reinforcement. A thin section results in both higher amount of reinforcement and higher ratio between reinforcement and concrete compared to a thicker section. Unit prices for reinforcement steel is presented in Table 2.6.

Table 2.6 Unit prices for Reinforcement.

Description	Price	Unit	Reference
Reinforcing steel	9000	SEK/ton	(Yavari et al., 2016)
Reinforcing steel	6100[1]	SEK/ton	(Göransson and Nilsson, 2017)
Reinforcement work frame leg	17500	SEK/ton	(Yavari et al., 2016)
Reinforcement work bridge deck	17500	SEK/ton	(Yavari et al., 2016)

[1]Göransson and Nilsson (2017) presents the total amount of reinforcing steel and the corresponding total material costs. Hence, the unit price has been calculated by Alhede and Beskow.

2.9 Optimal cross-section with respect to environmental impact and production cost

From the carbon impact and cost of concrete and reinforcement presented in section 2.7 and 2.8 it is possible to determine optimum ratio between concrete and reinforcement with respect to the two criteria. A simply supported bridge deck with length 10 meter and varying slenderness is compared with respect to the total carbon impact and total cost. Four different decks with different slenderness; L/18, L/21, L/24 and L/30 and corresponding decks heights 560 mm, 480 mm, 420 and 330 mm are investigated. A two-dimensional analyses is performed with a meter strip of the deck. The required reinforcement amount for each bridge deck is calculated based on design codes in ULS with respect to bending moment and shear force. The total mass of concrete and reinforcement for each beam is multiplied by the corresponding EMC-value and unit price according to previous section.

The bridge deck is subjected to a uniformly distributed load of 20 kN/m. The maximum flexural reinforcement requirement in span is assumed to be 50 % higher than the mean requirement. The materials and corresponding EMC-values (using equation (2.10)) and unit prices assumed in the comparison is shown in Table 2.7. One should note that both the material costs and the production costs (for the bridge deck) are included in the price. Factors for compensating the complexity in constructability are neglected since the interview in section 2.10 shows that it is no remarkable difficulties to account for, considering the deck slab.

Table 2.7 Assumptions for comparison.

Material	**Type/Class**	CO_2**-eq**	**Price**
Reinforcement	Mean Europe	8034 kg/m^3	184080 - 206700 SEK/m^3
Concrete	C35/45 CEM I	360 kg/m^3	2400 SEK/m^3

2.9.1 Results

The results from the comparison is presented in Table 2.8 in terms of concrete and reinforcement amount and total carbon impact and cost. Observe that the results only are valid for the bridge deck studied. The costs are presented within an interval where the lower values are calculated based on a cost for the reinforcement of 6100 SEK/ton (see Table 2.6) and the upper value based on a cost for reinforcement of 9000 SEK/ton.

2.9.2 Conclusion

It can be seen that the thickest bridge deck has the highest total carbon impact. The results show the same trend for all combinations of material presented in section 2.7 when it comes to the carbon impact. Hence, from an environmental point of view it is more efficient to optimize the bridges in terms of the slenderness.

Table 2.8 Results from comparison.

Slenderness	**Reinforcement**	**Concrete**	**Total CO_2-eq**	**Price**
L/18	0.0220 m^3	5.58 m^3	2185 kg	17440 - 17940 SEK
L/21	0.0251 m^3	4.77 m^3	1921 kg	16070 - 16640 SEK
L/24	0.0283 m^3	4.17 m^3	1729 kg	15215 - 15860 SEK
L/30	0.0408 m^3	3.26 m^3	1501 kg	15330 - 16260 SEK

It can clearly be seen that the costs decrease with an increased slenderness until a slenderness of L/24. Below this limit the costs increase and can be explained by that the section is heavily reinforced. However, the costs do not increase substantially and one may argue that a further investigation is needed in order to calculate the price in more detail. The costs are also highly dependent on the price of the reinforcing steel.

From the comparison it can be concluded that the bridges shall be optimized based on slenderness in order to reduce the carbon impact and the costs. The increase in costs for very slender structures is small and will be neglected. However, the comparison study gives an indication on how the environmental impact and costs varies for different cross-section types but a further study is needed to confirm the trend.

It should be noted that the comparison is general and not based on detailed design of an entire bridge but on a separate slab with simplified preliminary design. There might exist cases where the optimal combination of concrete and reinforcement differs from the results presented, see Figure 2.13.

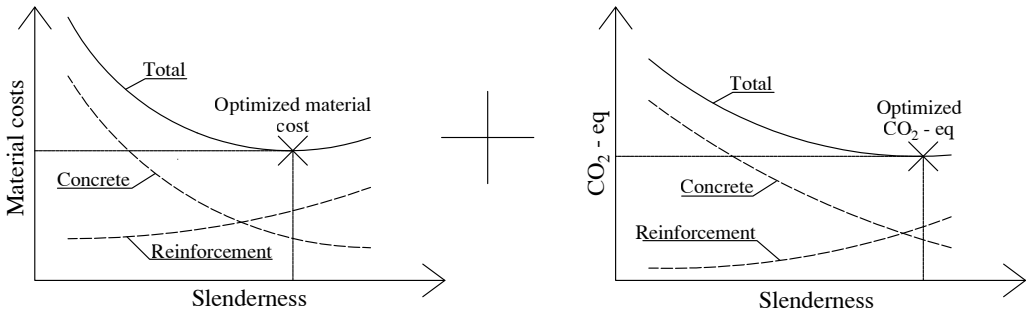

Figure 2.13 How an optimized solution of an engineering optimization problem may be illustrated with respect to material costs and environmental impact.

2.10 Constructability

An optimization process does not only require the engineer to meet the design criteria regarding the structural response, it is also important to include practical constraints in order to avoid a "fictitious" optimization that is not practicable. The border between where an engineering solution turns out to be practical unfeasible is diffuse, and in many cases the engineering solution is feasible but with increased investment costs and additional construction time as a result.

If an engineering optimization process affects the constructability, factors taking the complexity into account can be defined. According to Chalouhi (2019, p. 17-19) the complexity is related to the investment cost, since an increased complexity is related to the time needed to construct an element.

Through an interview with two experienced contractors of slab frame bridges and one experienced advisor at Swedish Transport Administration, the need for any constructability factors to adjust the investment cost can be predicted. The interviewees answered several questions regarding constructability of slab frame bridges. The contractors answered similarly and as following[2]:

- The work cost is not considerably affected by the slenderness of the cross-section.
- The complexity in mounting the top reinforcement increases for slender cross-sections.
- The complexity in mounting the reinforcement does not increase with an increased number of reinforcement layers, as long as the designer follows regulations and recommendations.
- The work cost does not necessarily increase for mounting of the third reinforcement layer, compared to the second reinforcement layer. The contractors was, however, a bit unsure.
- Shear reinforcement is always complicated when using it in frame legs; closed stirrups are tricky to get in place and to enclose the longitudinal reinforcement while open stirrups are tricky to mount in place.

The advisor at STA (Swedish Transport Administration) had a slightly different approach[3]:

- The minimum thickness of a cross-section should be 400 mm when using two layers of reinforcement, to ensure that the reinforcement is active with a sufficient internal lever arm.
- In design, one should as far as possible aim for using one layer of reinforcement. In critical sections such as corner and mid-span, two layers may occur.

[2] According to Hannrup, G. (personal communication, 4 May 2020) and Johansson, N. (personal communication, 27 April 2020)

[3] According to Karlsson, M. (personal communication, 6 May 2020)

- The complexity in mounting the reinforcement increases with an increased number of reinforcement layers. The mounting cost of a third layer of reinforcement is approximated to double the cost of the second layer.
- Shear reinforcement should as for as possible be avoided in both frame legs and bridge deck. However, it can not always be avoided in the bridge deck. Especially in corner sections. In frame legs, the large compressive normal force can be utilized and increases therefore the concrete shear capacity. The concrete shear capacity would therefore be enough, given a sufficient construction height.
- Shear reinforcement is complicated due to the complexity of getting the stirrups in the right place with overlapping splice. It is even more tricky in frame legs compared to bridge deck.

The interviews in their entirety can be found in Appendix A.

3

Optimization study for slab frame bridges

The following chapter is a description of the basis for the optimization presented in chapter 4 and 5. The geometry of the bridges investigated in the optimization is presented as well as optimization parameters, constraints and objectives for the optimization. The chapter also include which loads and load combinations that were used in the optimization study.

3.1 Slab frame bridges investigated

The geometry of the slab frame bridges that were investigated is the following; straight bridges with a constant width of 6 meters and with constant dimensions in transverse direction. Edge beams and wing walls were not included in the models. Equivalent forces from the wing walls were added to the edges of the frame legs. The wing walls were assumed to be inclined 45 degrees from the frame legs when calculating the equivalent forces.

The haunches can be designed in different ways and this study focused on four different layouts of the longitudinal section, see models a-d in Figure 3.1. Frames with spans up to 12 m were modelled with haunches of predefined dimensions (Figure 3.1, a-b). Frames with spans 12 $m \leq$ L $\leq$ 25 m were modelled with haunches for which the length is a function of the span length (Figure 3.1, c-d), and the thickness of the haunches were to be designed. If the difference in thickness between the haunch and the bridge deck slab was less than 0.1 m, the thickness of the haunch was defined as the thickness in span plus the additional difference of 0.1 m (i.e., $t_{haunch} = t_{span} +$ 0.1 m). This was due to economical reasons of the formwork, it is not economically defensible to construct a form with a low inclination of the haunches. The thickness of the frame legs were kept constant for span lengths up to 12 m. For longer spans, the frame legs were designed with a linear variation in thickness, if the thickness was larger than 0.4 m. The frames were given fixed or pinned boundary conditions, respectively.

The frames were optimized in two different studies. An analytical two-dimensional study and a numerical three-dimensional study.

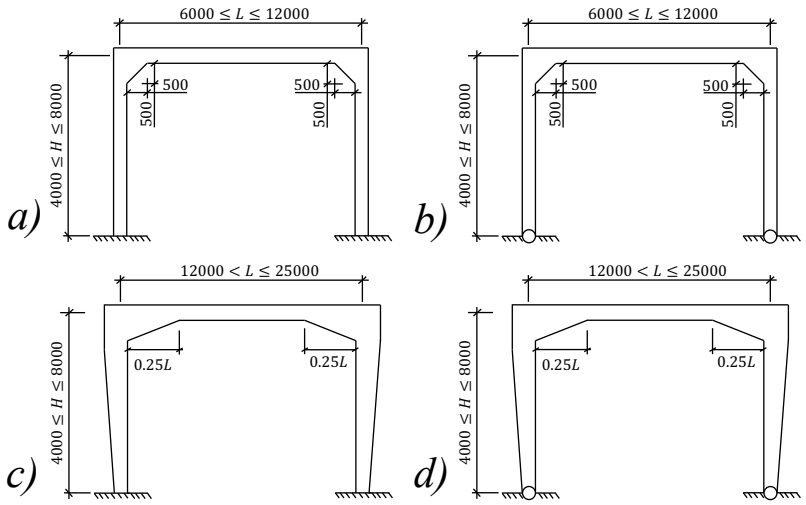

Figure 3.1 Two-dimensional representation of the models studied. a) & c) fixed, b & d) pinned.

3.2 Parameters studied

The variables studied were distinguished as "input variables" and "optimization parameters". Input variables were variables that were defined beforehand in order to optimize the "optimization parameters" of the bridges. Input variables were in this study the theoretical span length, the theoretical height of the frame legs and the geometry of the haunches. The input variables constituted geometrical constraints in the structural optimization, as presented in section 2.5.

Optimization parameters were variables that were optimized, given the input variables. The optimization parameters were the thickness of the bridge deck, thickness of the haunches, thickness of the frame legs at the support and thickness of the frame legs below the frame corner. The notations used in the study is illustrated in Figure 3.2. The thickness parameters of the different structural parts were essential for the amount of material used and so also for the economic cost and were therefore valid parameters in the optimization study. The thickness of each member contributes to the stiffness and played a major role to the internal force distribution of the frame. A representation of the optimization parameters is shown in Figure 3.2. The optimization parameters were:

- Thickness of frame leg at support, t_{f1}
- Thickness of frame leg below haunch, t_{f2}
- Thickness of bridge deck, t_s
- Thickness of haunch, t_{sh}

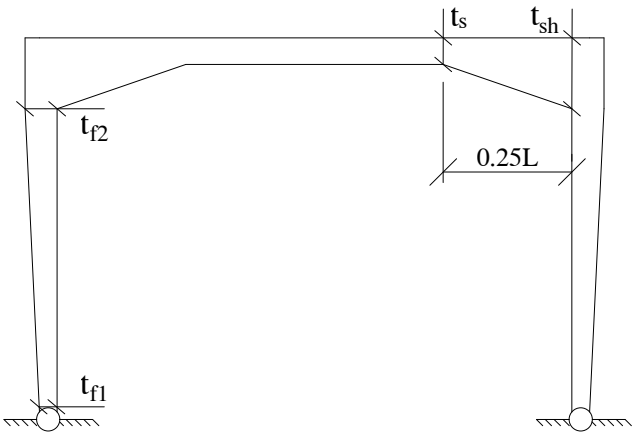

Figure 3.2 Notations used for the optimization parameters.

3.3 Material properties

The material qualities used in the study are presented in Table 3.1. Strength parameters for concrete were defined according to CEN (2004, p. 29) and can be found in Appendix F.

Table 3.1 Material properties

Slenderness	**Reinforcement**
Concrete class	C35/45
Reinforcement	K500C-T

3.4 Loads included

There are several loads that need to be taken into account in the design of a slab frame bridge. The loads that were included in the analyses are presented in Figures 3.3 to 3.8.

The bridge is subjected to both permanent and variable loads. Permanent loads that were taken into account was the self-weight of the structure, paving, earth pressure on the frame legs, shrinkage and differential settlement of the frame legs. Differential settlements of the frame legs cause displacement induced forces. When any displacement of the frame occur, either by vertical settlement of the soil or horizontal displacement, internal forces arise in the frame. Figure 3.4 shows two common types of displacement induced forces. All other loads presented in this section were taken into account as variable loads.

Figure 3.5 shows a symbolic traffic load model including a distributed load and point loads from axles of vehicles. Design traffic load model for varying span lengths was investigated in Section 3.5.1

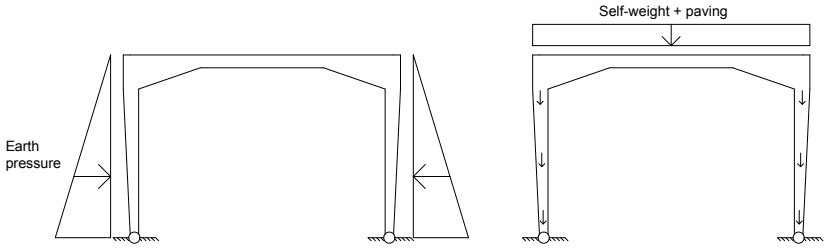

Figure 3.3 Earth pressure (left) and self-weight (right).

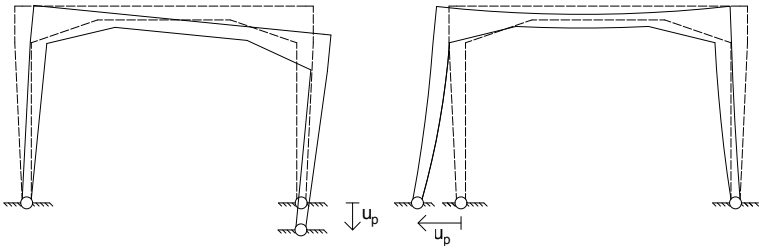

Figure 3.4 Any displacement of the frame leads to internal forces. Vertical settlement (left) and horizontal displacement (right).

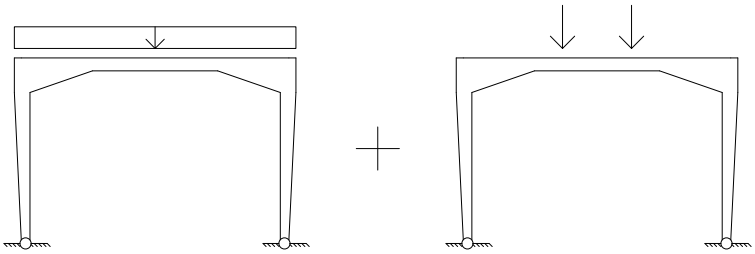

Figure 3.5 Vertical traffic load.

The frame is subjected to surcharge loads when a vehicle is on the embankment behind the bridge, creating a lateral earth pressure. There are two cases of surcharge loads that need to be considered; surcharge load from one side and from both sides. When the surcharge load is applied on the embankment from one side it results in a passive earth pressure from the counteracting soil on the other side of the bridge. The surcharge load is acting with a constant magnitude over the depth whereas the passive earth pressure is, according to Trafikverket (2016, p. 33), assumed to counteract with a triangular shape (see Figure 3.6). The magnitude of the passive earth pressure depends on the horizontal deflection of the frame, caused by the surcharge load and can be compared with the effect of a spring. The same applies for the braking force. See section 3.4.2 for a further explanation of this phenomena.

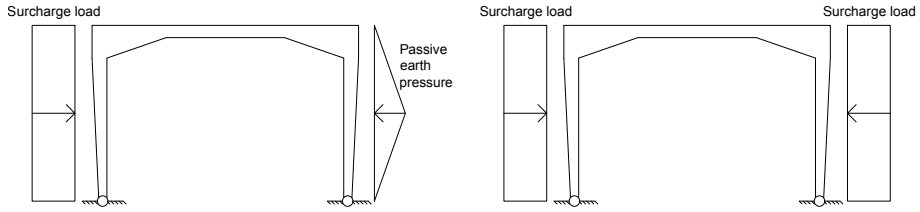

Figure 3.6 Two cases of surcharge loading.

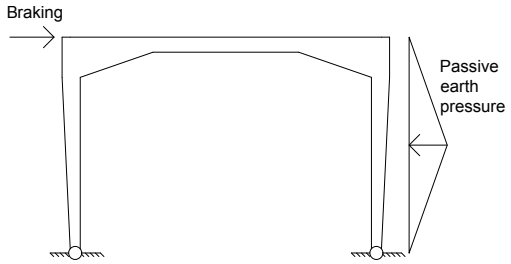

Figure 3.7 Braking force. The passive earth pressure arise as a result of the horizontal displacement of the frame due to the braking force.

Since the wing walls were excluded in the model, equivalent forces from the wing walls were added on the edges of the frame legs to include the effect of the wing walls. Forces from the wing walls arise from earth pressure on the wing walls, surcharge load acting on the wing walls and self-weight from the wing walls. The equivalent forces were added to the edges of the frame legs.

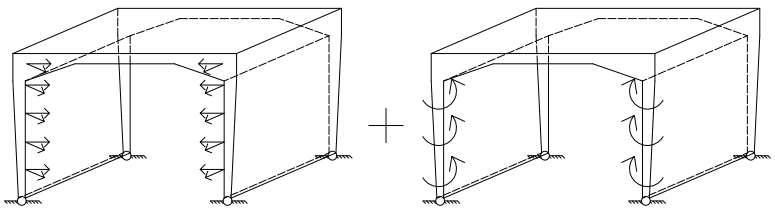

Figure 3.8 Loads from wing wall on the frame. Equivalent lateral forces and bending moment.

3.4.1 Restraint forces

The effect of temperature, shrinkage and creep was important to include in the design since it give rise to early cracking of the concrete. When movement of the concrete is prevented, restraint forces appears. Shrinkage give rise to contraction and temperature variations gives rise to expansion and/or contraction which results in tensile and/or compressive stresses. Creep was included in the design by calculating the effective modulus of elasticity.

In EC, CEN (2003a), the effect of several cases of temperature variations should be included in the design of structures. Following cases was defined:

1. Uniform high temperature
2. Uniform low temperature
3. Temperature gradient 1, with higher upper surface temperature
4. Temperature gradient 2, with lower upper surface temperature
5. Temperature difference between structural parts

In this thesis, the fifth loading case with temperature difference between structural parts was excluded since the structural response was assumed to not differ from the other temperature load cases to a greater extent. Loading case 1 was accompanied with a counteracting (passive) earth pressure. The earth pressure was simplified as a triangular shape just like the passive earth pressure due to surcharge and braking force.

The effect of shrinkage was simulated by applying an equivalent temperature decrease. The strain from shrinkage was represented by the strain due to the equivalent temperature.

3.4.2 Determination of passive earth pressure due to braking and surcharge load

The frame is subjected to lateral earth pressure on both sides of the bridge which are in horizontal force balance. When surcharge loading takes place behind one of the frame legs an additional lateral earth pressure is induced on the frame. The additional earth pressure is acting with a constant magnitude on one side of the frame creating a horizontal displacement of the frame. When the frame is pushed against the soil a passive earth pressure is activated, which counteracts the horizontal movement of the frame. The shape of the passive earth pressure was assumed to be triangular with its highest magnitude at the middle of the height of the frame. The magnitude of the passive earth pressure is dependent on the horizontal displacement of the frame caused by the surcharge load (q_{sur}). The horizontal displacement caused by q_{sur} is in turn dependent on the magnitude of the passive earth pressure, since the passive earth pressure will prevent the free movement of the frame. As a visualization one may think about a case where one frame leg is subjected to a surcharge load and the other frame leg is supported on a spring bed.

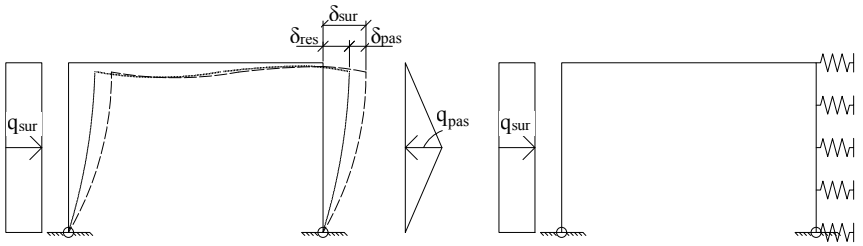

Figure 3.9 The actual displacement of the frame (δ_{res}), the fictitious displacement from the surcharge load (δ_{sur}) and the fictitious displacement from the passive earth pressure (δ_{pas}).

The procedure of finding the resisting earth pressure can be explained as:

1. Calculate the horizontal displacement δ_{sur} of the frame caused by the surcharge load q_{sur}.
2. Calculate the magnitude of the passive earth pressure (Δp) by assuming an initial displacement of the frame of 10 mm.
3. Calculate the horizontal displacement $\delta_{\Delta p}$ of the frame caused by the assumed passive earth pressure Δp.
4. Determine the actual displacement of the frame, δ_{res}, as a relation to δ_{sur} and δ_{pas}.
$$\delta_{res} = \delta_{sur} - \delta_{pas} \tag{3.1}$$
5. Divide Δp by 10 mm to obtain a scale factor that explains the magnitude of the passive earth pressure per unit of displacement. If the scale factor is multiplied by the actual displacement of the frame the actual resisting earth pressure can be obtained:
$$q_{res} = \delta_{res} \frac{\Delta p}{10\ mm} \tag{3.2}$$
6. The displacement of the frame from the passive earth pressure can be calculated by dividing the the horizontal displacement $\delta_{\Delta p}$ by the assumed passive earth pressure Δp. This explains the actual displacement of the frame per unit load. Multiply the fraction with the resisting earth pressure q_{res} to obtain the displacement of the frame caused by the passive earth pressure:
$$\delta_{pas} = q_{res} \frac{\delta_{\Delta p}}{\Delta p} \tag{3.3}$$

The expressions in (3.1) - (3.3) does all contain one unknown. By implementing (3.1) in (3.2) and then (3.2) in (3.3) the following expression is obtained after some mathematical operations:

$$q_{res} = \frac{\delta_{sur} \dfrac{\Delta p}{10\ mm}}{1 + \dfrac{\delta_{\Delta p}}{10\ mm}} \tag{3.4}$$

In order to ease the analyses in the 2D study, and to calculate q_{res} without getting use of numerical computational programs, theory of structural mechanics was applied. For each load case and support conditions, expressions of the horizontal displacement were determined and (3.4) was used subsequently.

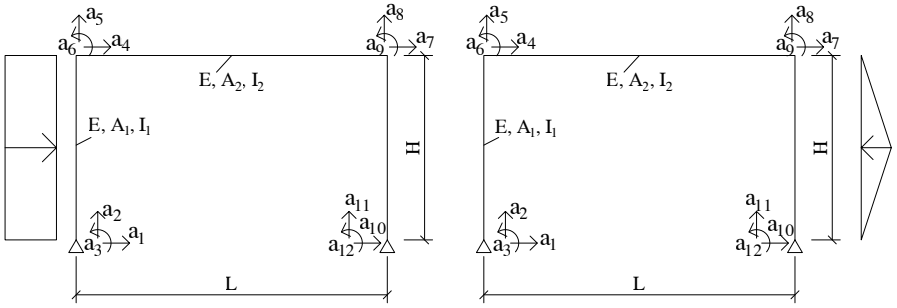

Figure 3.10 The lateral earth pressure from the surcharge load is causing a horizontal displacement (a_7) of the frame (left) which leads to a counteractive passive earth pressure (right) that gives an additional displacement (a_7), but with opposite signs.

The displacement a_7 in Figure 3.10 caused by the surcharge load for a pinned frame yields:

$$\delta_{sur} = q_{sur}H^3\frac{96A_2H^4I_1I_2^2 + 10A_1A_2H^4I_2^2L^2 + 144A_2H^3I_1^2I_2L + 19A_1A_2H^3I_1I_2L^3}{48EI_1I_2A_1L^2(2A_2I_2H^3 + 3A_2I_1LH^2 + 3I_1I_2L)}$$

$$+ q_{sur}H^3\frac{6A_1A_2H^2I_1^2L^4 + 144HI_1^2I_2^2L - 12A_1I_1^2I_2L^4}{48EI_1I_2A_1L^2(2A_2I_2H^3 + 3A_2I_1LH^2 + 3I_1I_2L)} \tag{3.5}$$

The displacement caused by the counteracting triangular earth pressure is given in (3.7). It is important to note that the magnitude of the additional counteracting earth pressure is so far assumed, based on a support displacement of 10 mm. The expression for the additional earth pressure is given in (3.6) and follows the recommendation given by the Swedish Transport Administration (Trafikverket, 2016, p. 32-33).

$$\Delta p = C\gamma_s\frac{10\ mm}{H}z \qquad [kN/m^2] \tag{3.6}$$

Where

$$\begin{aligned} \text{C} &= 300 \quad \text{(Unfavourable)} \\ \text{C} &= 600 \quad \text{(Favourable)} \end{aligned}$$

$$\delta_{\Delta p} = -\Delta p H^3 \frac{384A_2H^4I_1I_2^2 + 42A_1A_2H^4I_2^2L^2 + 576A_2H^3I_1^2I_2L + 79A_1A_2H^3I_1I_2L^3}{384EI_1I_2A_1L^2(2A_2I_2H^3 + 3A_2I_1LH^2 + 3I_1I_2L)}$$

$$- \Delta p H^3 \frac{24A_1A_2H^2I_1^2L^4 + 576HI_1^2I_2^2L - 48A_1I_1^2I_2L^4}{384EI_1I_2A_1L^2(2A_2I_2H^3 + 3A_2I_1LH^2 + 3I_1I_2L)} \tag{3.7}$$

The procedure described above can also be used for other load cases that give rise to the same phenomena. In Appendix D expressions for the displacement of the frame corner can be found in case of a braking force (pinned and fixed boundary conditions), surcharge load with fixed boundary condition and counteracting soil pressure with fixed boundary condition.

For the numerical three-dimensional analyses, the displacements of the frame were extracted from the finite element analyses. The magnitude of the counteracting load was calculated according to equation 3.4 and after that the loads were updated for the main analyses.

3.5 Design load combination

The bridges were designed to meet the requirement stated in EC for ULS, SLS and Fatigue Limit State. The design load combination in ULS was assumed to be given by equation 2.3. Based on this assumption, the way of combining loads according to equation 2.2 was neglected to ease the design process in the analytical study, and to reduce the computational time in the numerical study. Design bending moment and shear force in critical sections was determined from one of those combinations. In SLS, several load combinations were used. The design load combination for deflection is for frequent load values where the vertical traffic load was the only load taken into account. Design load combination for crack width is quasi permanent equation presented in 2.6.

Design section forces and deflections in ULS, SLS and fatigue constituted structural constraints in the optimization.

3.5.1 Design variable load

LM1 and vehicle-model A-N, presented in section 2.2.2.1 and 2.2.2.2, was evaluated for a simply supported beam in the program STRIPSTEP2. The maximum moment and shear force for the worst placement of each load model was evaluated. The design loads for span 6 to 25 meters is presented in Figure 3.11 and 3.12.

For bending moment it can be seen that LM1 was decisive until a span length of around 22 meters which after vehicle-model I gives a slightly larger bending moment. Since the difference was very small, 2.5 % at span length 25 m, LM1 was used for all span lengths to ease the study. Considering shear force it can be seen that LM1 was

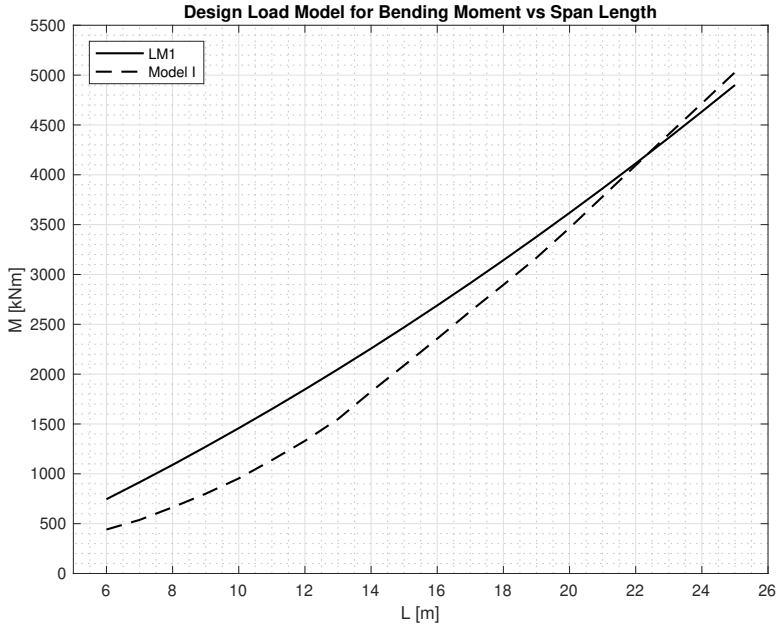

Figure 3.11 Design load model with respect to bending moment for varying span length.

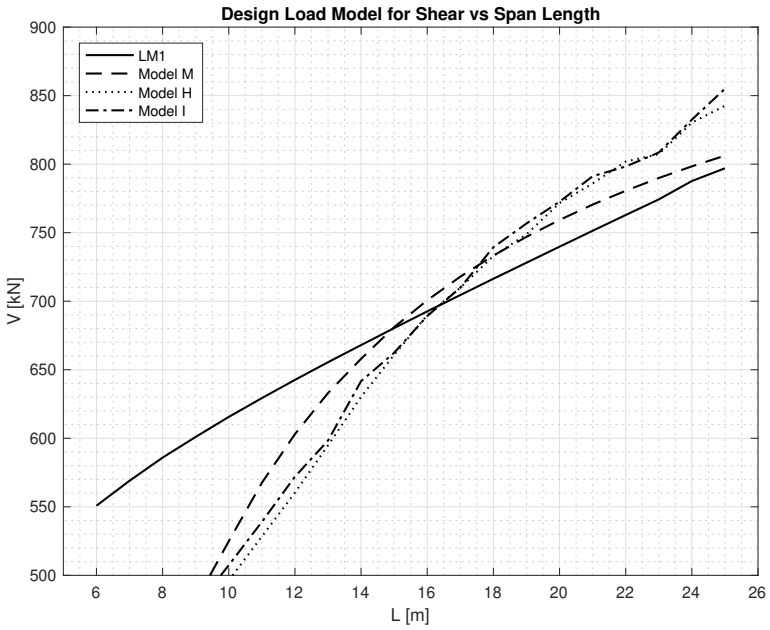

Figure 3.12 Design load model with respect to shear force for varying span length.

decisive up to a span length of around 16 meters. After that point, the design load model shifted between vehicle-model M, H and I. In this investigation vehicle-model I was used from span length 16-25 m since the difference between the three decisive models was small.

3.5.1.1 Placement of design loads

For maximum moment, the resultant of the concentrated loads from the load model should be placed with equal distance between the mid-span and the closest concentrated load (Ljungberg, no date). The principle is illustrated in the middle and the right Figure in Figure 3.13. For maximum shear force, point loads should be placed as close to the support as possible. The closest point load is normally placed $0.9d$ from the support (where d is the effective height). If the load is placed closer to the support, the load will transfer through arch action and no shear force develops.

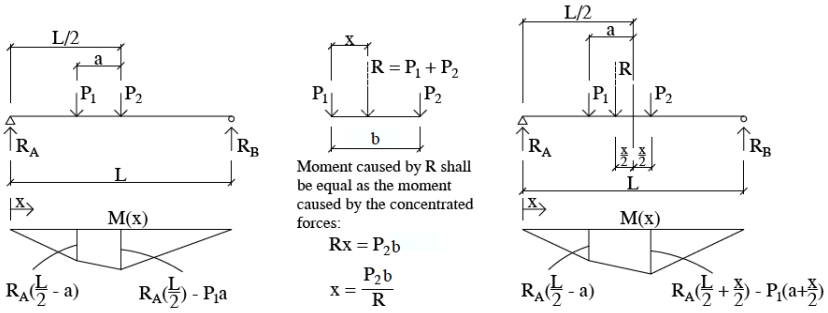

Figure 3.13 How concentrated loads normally are placed to obtain maximum moment (left) and how the concentrated loads should be placed in theory to obtain maximum moment (right) (Ljungberg, no date).

The worst placement with respect to moment for LM1 and vehicle model I can be seen in Figure 3.14 and 3.15. Please note that R stands for the resultant of the forces. The worst placement for shear force for the same models is shown in Figure 3.16 and 3.17.

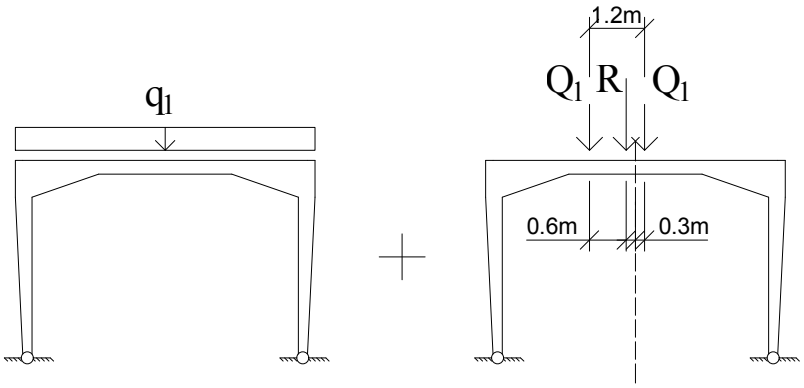

Figure 3.14 Placement of loads for maximum moment, LM1.

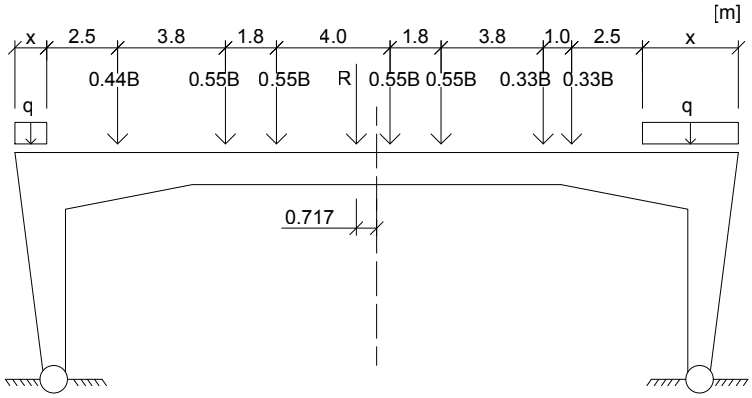

Figure 3.15 Placement of loads for maximum moment, vehicle-model I.

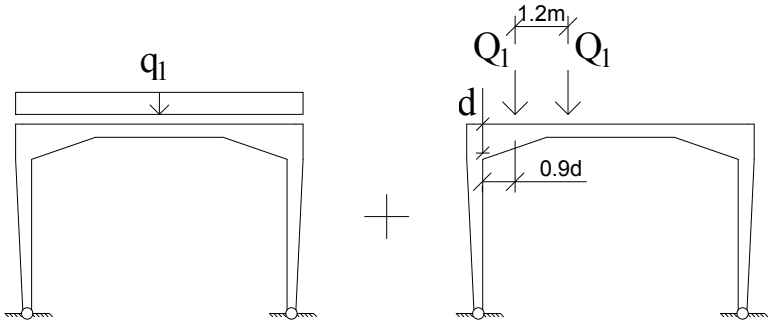

Figure 3.16 Placement of loads for maximum shear force, LM1.

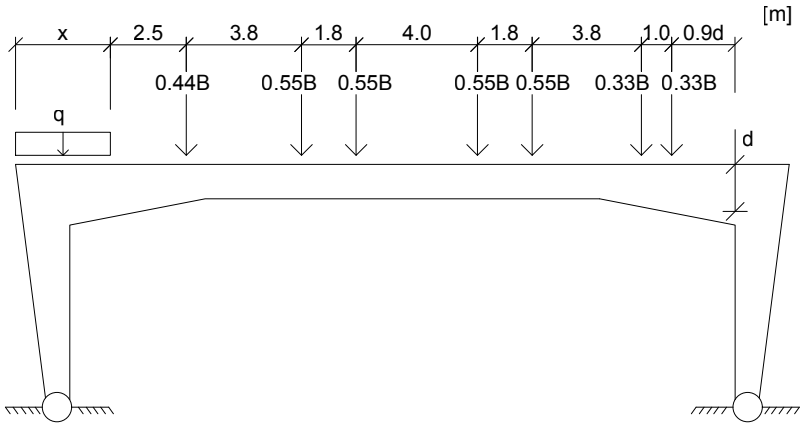

Figure 3.17 Placement of loads for maximum shear force, Vehicle-model I.

3.5.2 Critical sections

A structure is to be designed to resist the worst case scenario that may affect any section of the structure. This thesis used critical cross-sections to determine the worst case scenarios. Critical sections were predefined in order to limit the computational time of the optimization process. Critical sections with respect to bending moment and shear force for a slab frame bridge is illustrated by the left Figure in Figure 3.18.

Vehicle loads are movable loads. However, analyses were executed for static vehicle loads with predefined positions along the bridge deck. The loads were then successively moved to new positions until the worst load position was found.

Critical sections are sections in the frame that are subjected to high concentrations of internal forces and are therefore the sections that will obtain its load-bearing capacity first. In case of a slab frame bridge the critical sections are the corners between the frame legs and the bridge deck, the mid-span of the bridge deck and in the span of the frame legs. The boundary conditions between the frame legs and the connections do, however, affect the distribution of internal forces and in case of fixed connections one may also check the bending moment at the supports.

The critical sections have been determined by cutting the frame into sub-parts, as illustrated in the right Figure in Figure 3.18. It is important to note that the frame corners have been checked both in the x-direction (the vertical section in the longitudinal section of the bridge) and in the y-direction (the horizontal section in the longitudinal section of the bridge). Even though the design moment is equal for both sections due to the compatibility condition, the normal force varies which affects the design tensile force of the reinforcement. The capacity of the two sections may also vary depending on the reinforcement layout and the size of the cross-section.

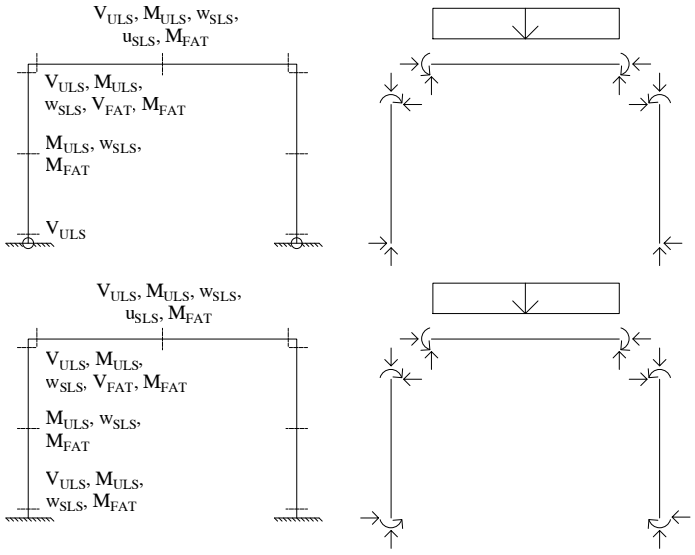

Figure 3.18 Critical sections and design checks that are controlled in each section. M: bending moment, V: shear force, w: crack width, u: deflection.

The positions where the design section forces were extracted in frame corners have been simplified. In the two-dimensional study, the design section forces were extracted in the corner of the system line, since the haunches were neglected from the study. However, in the three-dimensional numerical study the positions of the critical sections were determined following the haunches. For frames with right-angled haunches the design bending moment was extracted from the corner of the system line, whereas the design shear force was extracted at a distance that equals half the width of a wheel away from the start of the haunch. The design shear force in frame corners considering the frame leg have been extracted at the vertical distance of the system line where the haunch and frame leg connects. For frames with haunches with a length that equals a quarter of the span, the design bending moment was extracted from the corner of the system line whereas the design shear force was extracted at a distance of half the width of a wheel away from the inside of the frame leg, and in the position where the haunch and frame leg connects. All design section forces extracted in frame corners were checked against the sectional capacity with the actual thickness of the critical sections (the sections where the design shear force were extracted). A further explanation about the critical sections for the three-dimensional numerical study is given by section 5.3.1.

3.6 Optimization

The aim of the optimization was to minimize the environmental impact and the economic cost of the structure. According to section 2.9, the environmental impact of a concrete structure was minimized by optimizing the slenderness of each section. However, the increase in cost for very slender members was neglected since environmental aspect was evaluated as more important. The optimization objective was therefore to minimize the thickness of the structural parts. The optimization parameters were optimized by seeking the smallest possible values.

Contractors have different experience regarding constructability of slab frame bridges and the answers obtained from three different contractors (section 2.10) were different. Studying the answers in detail one may think that it is, from a constructability point of view, possible to mount several layers of reinforcement in a slender cross-section but that it is not preferable. Two of the contractors answered that the labour costs did not increase as the number of reinforcement layers increased, whereas the third contractor pointed out that the labour costs increases considerably. However, in the optimization, the increase in labour cost for several reinforcement layers was neglected, but a maximum number of reinforcement layers was used as a constraint.

3.6.1 Constraints

General structural constraint in the optimization were all ULS, SLS and fatigue limit state requirements according to EC as well as the Swedish Traffic Administration's requirements from the Swedish appendix for design of bridges.

As mentioned in Section 3.2, the input variables constituted constraints for the optimization. Besides those geometric constraints, there were additional constraints regarding minimum dimensions of the structural parts. Due to constructability, a minimum thickness of 300 *mm* was defined for any optimization parameter.

Structural constraints regarding reinforcement design were implemented to ease the optimization process. Reinforcement amounts were predefined to a "maximum" amount of what was practical with respect to constructability and was not necessary the required reinforcement amount for each section. However, the study did not aim for a complete design of the bridges but dimensions of the optimization parameters that can be used in the design.

The tensile reinforcement was predefined and limited to two layers of ϕ25 mm due to constructability. The tensile reinforcement was arranged in groups according to Figure 3.19, resulting in an equivalent spacing of s100 mm. In sections where shear reinforcement may be needed, the shear reinforcement have been predefined to 6ϕ10 s120 per unit width which is the maximum amount of shear reinforcement due to requirement on minimum spacing between stirrups and constructability. Frame legs were designed without any shear reinforcement due to practical difficulties in mounting and work costs (section 2.10). The reinforcement arrangement used in the analyses is presented in Figure 3.19.

The stopping criteria was in the study defined as a limit of the calculation time in the form of maximum iterations. The maximum number of iterations was set to 15.

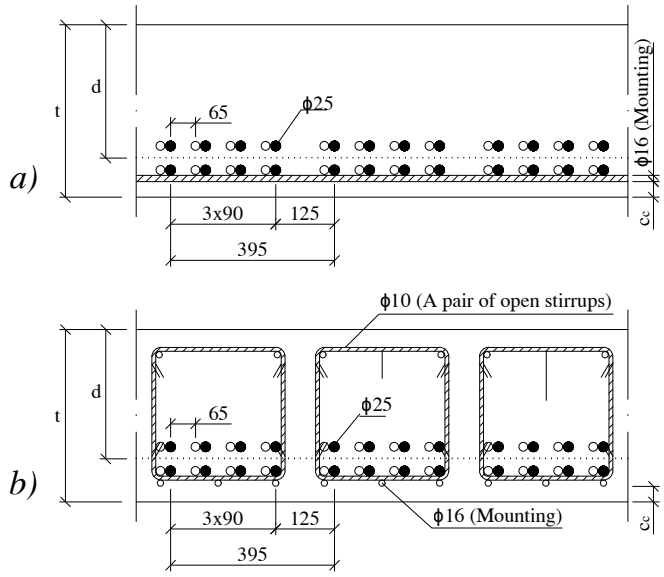

Figure 3.19 Reinforcement layout used in the preliminary design. a) In sections without shear reinforcement. b) In sections with shear reinforcement.

4

Analytical optimization of two-dimensional frames

The following chapter is a presentation of an analytical optimization of two-dimensional frames. The aim of the two-dimensional analyses was to generate values for the optimization parameters (the thickness of the bridge deck and frame legs, respectively) that could be used as start values in the numerical analyses (chapter 5) in order to reduce the computational time. Moreover, the analyses were performed to study the relation in results compared to the numerical analyses and how well the results corresponded to each other.

4.1 Geometry

In the two-dimensional analyses, some simplifications regarding the geometry of the bridge were made. The haunches were neglected from the geometry which means that constant thickness was assumed for each member. The frame legs were assumed to be extended to the bottom of the foundation slab where the boundary conditions were applied. Furthermore, a meter strip of the three meters wide Load field 1 was studied (Figure 2.7). Any effects of transverse force distribution was therefore neglected from the analyses. The geometry used in the 2D-analyses can be seen in Figure 4.1. The optimization parameters were limited to t_s and t_f since the haunches were neglected in the analyses.

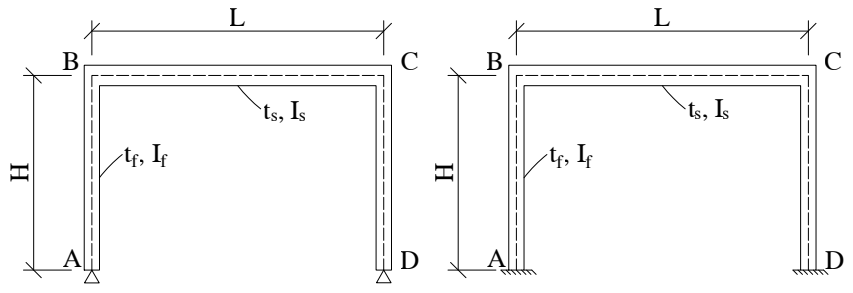

Figure 4.1 Two-dimensional models studied for a frame with pinned and fixed BC's, respectively.

4.2 Structural behaviour of a 2D frame

The moment distribution for a statically indeterminate structure can be both complicated and time-consuming to calculate. One way of solving this is to implement the *moment distribution method* developed by Hardy Cross in 1932. Expressions for moments in critical sections of a frame can be found in section 4.4, which is based on the moment distribution method, and has been used to study relations and understanding on how the optimization parameters affects the moment distribution. The expressions are valid under the assumptions that the frame is symmetric and that the moment of inertia of the frame walls and the bridge deck are constant along their lengths.

The moments in critical sections are highly dependent on the bending stiffness relation between the frame legs and the bridge deck. Forces are attracted towards stiffer regions so if the bending stiffness of the frame legs is increasing, the moment at the frame corners will increase as a result. Thus, the moment in span of the bridge deck slab will decrease in order to satisfy equilibrium condition.

The bending stiffness relation between the frame legs and the bridge deck is in the moment distribution method taken into account with a factor k:

$$k = \frac{I_s}{I_f}\frac{H}{L} \tag{4.1}$$

Where I_s and I_f is the second moment of area of the bridge deck and frame leg, respectively. Observe that the relation is valid only if the frame is symmetric along the longitudinal section.

The contribution to the second moment of area from the haunches can not be included directly into the formulas for the moment in critical sections as the equations only are valid for a member with constant cross-section. The influence from the haunches can, however, be taken into account afterwards.

4.3 Loads

The following loads were included in the two-dimensional analyses:

1. Self-weight of the bridge
2. Lateral earth pressure
3. Vertical traffic load
4. Surcharge load on one side
5. Surcharge load on both sides
6. Braking force

The representation of the loads can be found in Section 3.4. Characteristic values of all loads used in the study is presented in Appendix E. The combination of loads was

analysed in detail to make sure that the most unfavourable case was found. Since different loads are acting in different directions, both in the vertical and horizontal plane, it is unambiguous if a certain load give rise to a favourable or unfavourable effect in a certain section.

Some loads that normally need to be included in design were not taken into account in the two-dimensional analyses. Loads from the soil, embankment and surcharge on the wing walls were excluded. The two-dimensional analyses considered a meter-strip in the middle of the bridge and therefore the forces from the wing walls were not included. Temperature variations were not included in the two-dimensional analyses as well as shrinkage of the concrete. Differential settlements of the supports were not included.

4.4 Moment equations

Elementary-cases for a frame with pinned and fixed BC's were used to derive design moments for the frame (Wåhlin, 1947). Elementary-cases based on the moment distribution method for all relevant loads are presented in this section. The moments were superimposed with corresponding load combination factors in order to obtain design moments for each section of interest. The variables are defined in Figure 4.1. The stiffness relation factor k is given in expression (4.1).

Flexural moments in span were calculated with a linear elastic relation and the lower bound solution when moments in frame corners are known. The expressions in table 4.2 - 4.14 assumes a positive moment (tensile stresses on the inside of the frame). Hence, a negative moment symbolize tensile stresses on the outside of the frame.

4.4.1 Self-weight

Figure 4.2 shows a frame with different boundary conditions subjected to its self-weight and the bending moment distribution. Corner and support moments due to self-weight for frames with pinned and fixed BC's are presented in Table 4.1 and 4.2.

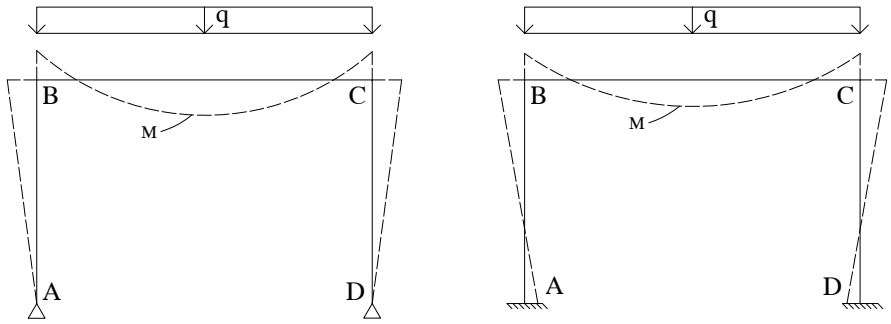

Figure 4.2 Self-weight acting on a frame with pinned and fixed BC's, respectively.

Table 4.1 Moment due to self-weight for a frame with pinned BC's (Wåhlin, 1947, p. 394).

Corner moment	Support moment
$M_B = -\frac{qL^2}{4(2k+3)}$	$M_A = 0$
$M_C = -\frac{qL^2}{4(2k+3)}$	$M_D = 0$

Table 4.2 Moment due to self-weight for a frame with fixed BC's (Wåhlin, 1947, p. 399).

Corner moment	Support moment
$M_B = -\frac{qL^2}{6(k+2)}$	$M_A = \frac{qL^2}{12(k+2)}$
$M_C = -\frac{qL^2}{6(k+2)}$	$M_D = \frac{qL^2}{12(k+2)}$

4.4.2 Earth pressure

The lateral earth pressure increases linearly with depth and results in negative moments in frame corners (tensile stresses on the outside of the frame corners). Since the frame legs are of equal length the magnitude of the lateral earth pressure is equal on both frame legs and, hence, the moments in frame corner are equal. The moment in the bridge deck is constant and equal to the corner moments. The moment distribution can be seen in Figure 4.3.

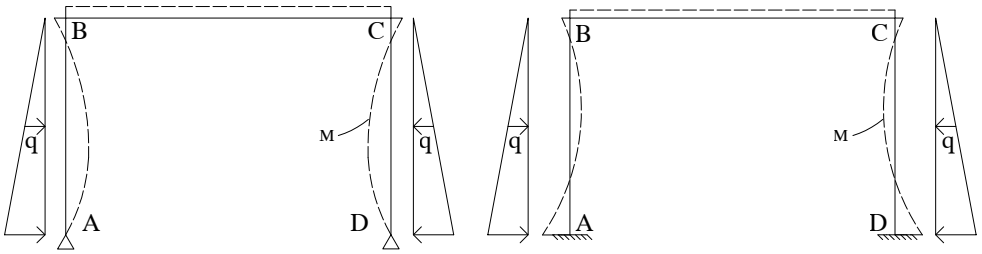

Figure 4.3 Triangular earth pressure acting on a frame with pinned and fixed BC's, respectively.

Table 4.3 Moment due to triangular earth pressure, pinned BC's (Wåhlin, 1947, p. 394).

Corner moment	Support moment
$M_B = -\frac{7qH^2}{60} \cdot \frac{k}{2k+3}$	$M_A = 0$
$M_C = -\frac{7qH^2}{60} \cdot \frac{k}{2k+3}$	$M_D = 0$

Table 4.4 Moment due to triangular earth pressure, fixed BC's (Wåhlin, 1947, p. 399).

Corner moment	Support moment
$M_B = -\frac{qH^2}{30} \cdot \frac{k}{k+2}$	$M_A = -\frac{qH^2}{60} \cdot \frac{3k+8}{k+2}$
$M_C = -\frac{qH^2}{30} \cdot \frac{k}{k+2}$	$M_D = -\frac{qH^2}{60} \cdot \frac{3k+8}{k+2}$

4.4.3 Vertical traffic load

The models used for vertical traffic load in the design was LM1 and vehicle model I, as presented in section 3.5.1. The load models consisted of concentrated loads and uniformly distributed loads of varying magnitude. Expressions for moments due to concentrated load and uniformly loads were superimposed to simulate the full load models. Moments from uniform distributed loads along the entire length of the bridge deck were the same as used for moments due to self-weight, which were presented in Table 4.1 - 4.2. In case of a uniformly distributed load that is not acting over the entire bridge deck the distributed load have been considered as an equivalent point load with the same magnitude as the total load from the distributed load. The load effect does not represent the real load case fully, but was assumed to be good enough. Corner and support moments from concentrated loads are presented in Tables 4.5 and 4.6. Figure 4.4 shows the bending moment distribution for a frame with pinned and fixed BC's, respectively.

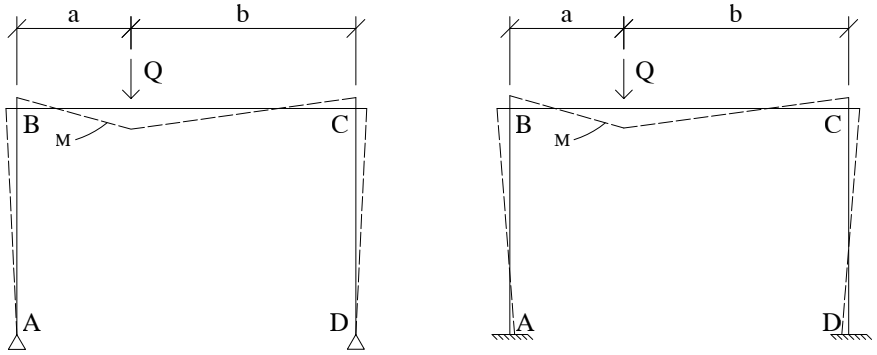

Figure 4.4 Concentrated load on a frame with pinned and fixed BC's, respectively.

Table 4.5 Moment due to axle-load. Frame with pinned BC's (Wåhlin, 1947, p. 394).

Corner moment	Support moment
$M_B = -\frac{3Qab}{2L(2k+3)}$	$M_A = 0$
$M_C = -\frac{3Qab}{2L(2k+3)}$	$M_D = 0$

Table 4.6 Moment due to axle-load. Frame with fixed BC's (Wåhlin, 1947, p. 400).

Corner moment	**Support moment**
$M_B = -\frac{Qab}{2L} \cdot \frac{13k+4-2\alpha(k+2)}{(k+2)(6k+1)}$	$M_A = \frac{Qab}{2L} \cdot \frac{5k-1+2\alpha(k+2)}{(k+2)(6k+1)}$
$M_C = -\frac{Qab}{2L} \cdot \frac{11k+2\alpha(k+2)}{(k+2)(6k+1)}$	$M_D = \frac{Qab}{2L} \cdot \frac{7k+3-2\alpha(k+2)}{(k+2)(6k+1)}$

Where $\alpha = \frac{a}{L}$

4.4.4 Surcharge load - one side

The load case with a surcharge load on one side was, as presented in section 3.4.2, divided in two loads; surcharge load and counteracting earth pressure. Expressions for corner moments and support moments are presented separately. Each moment was then superimposed to generate the action of the full load-case.

4.4.4.1 Surcharge load on one side

Figure 4.5 represents the bending moment distribution for a frame subjected to surcharge load on one frame leg. Expressions for corner moments and support moments due to surcharge load on one side is shown in Tables 4.7 and 4.8.

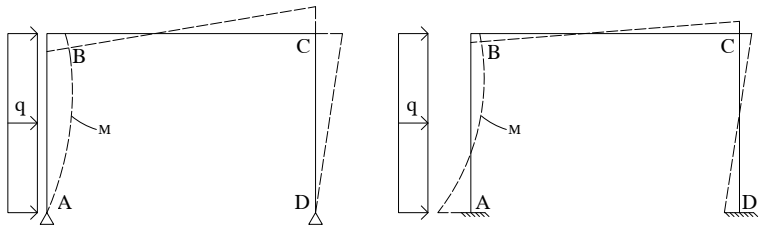

Figure 4.5 Surcharge load acting on one frame leg, pinned and fixed BC's, respectively.

Table 4.7 Moment due to surcharge load on one frame leg, pinned BC's (Wåhlin, 1947, p. 394).

Corner moment	Support moment
$M_B = \frac{3qH^2}{8} \cdot \frac{k+2}{2k+3}$	$M_A = 0$
$M_C = -\frac{qH^2}{8} \cdot \frac{5k+6}{2k+3}$	$M_D = 0$

Table 4.8 Moment due to surcharge load on one frame leg, fixed BC's (Wåhlin, 1947, p. 400).

Corner moment	Support moment
$M_B = \frac{qH^2}{24}\left(\frac{12k}{6k+1} - \frac{k}{k+2}\right)$	$M_A = -\frac{qH^2}{24}\left(12 - \frac{5k+9}{k+2} - \frac{12k}{6k+1}\right)$
$M_C = -\frac{qH^2}{24}\left(\frac{12k}{6k+1} + \frac{k}{k+2}\right)$	$M_D = \frac{qH^2}{24}\left(\frac{5k+9}{k+2} + \frac{12k}{6k+1}\right)$

4.4.4.2 Counteracting earth pressure

The elementary cases for a triangular shaped load on a frame has been derived from the *displacement method* presented in Algers, Forsby, and Tell (1959). The derived expressions for moments are presented in Tables 4.9 and 4.10. Figure 4.6 represents a frame subjected to a triangular shaped load and the bending moment distribution.

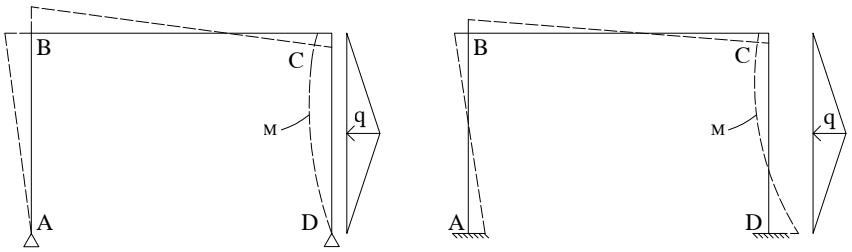

Figure 4.6 Counteracting triangular shaped load on a frame with pinned and fixed BC's, respectively.

Table 4.9 Moment due to counteracting triangular shaped load, pinned BC's.

Corner moment	Support moment
$M_B = -\frac{3qH^2}{64} \cdot \frac{7k+8}{2k+3}$	$M_A = 0$
$M_C = \frac{qH^2}{64} \cdot \frac{11k+24}{2k+3}$	$M_D = 0$

Table 4.10 Moment due to counteracting trapezoidal load, fixed BC's.

Corner moment	Support moment
$M_B = -\frac{qH^2}{192} \cdot \frac{72k^2+89k}{6k^2+13k+2}$	$M_A = \frac{qH^2}{192} \cdot \frac{72k^2+133k+33}{6k^2+13k+2}$
$M_C = \frac{qH^2}{192} \cdot \frac{12k^2+79k}{6k^2+13k+2}$	$M_D = -\frac{qH^2}{192} \cdot \frac{132k^2+323k+63}{6k^2+13k+2}$

4.4.5 Surcharge load on both frame legs

Corner moments and support moments due to surcharge load on both frame legs are presented in Tables 4.11 and 4.12. The surcharge loads were assumed to be of equal magnitude resulting in a symmetric moment distribution along the longitudinal section of the frame, $M_B = M_C$, and at supports, $M_A = M_D$ (Figure 4.7).

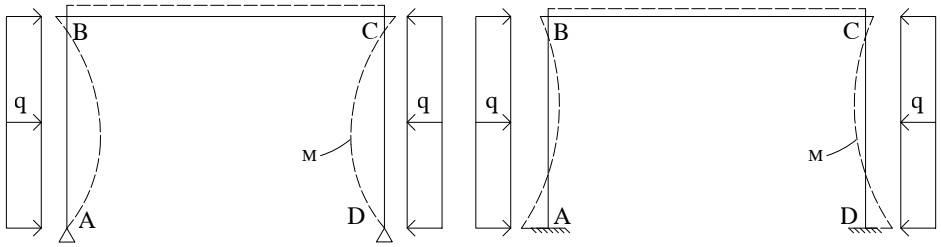

Figure 4.7 Load from embankment on two sides, pinned and fixed BC's, respectively.

Table 4.11 Moment due to load from embankment from two sides. Pinned BC's (Wåhlin, 1947, p. 394).

Corner moment	Support moment
$M_B = -\frac{qH^2}{4} \cdot \frac{k}{2k+3}$	$M_A = 0$
$M_C = -\frac{qH^2}{4} \cdot \frac{k}{2k+3}$	$M_D = 0$

Table 4.12 Moment due load from embankment from two sides. Fixed BC's (Wåhlin, 1947, p. 399).

Corner moment	Support moment
$M_B = -\frac{qH^2}{12} \cdot \frac{k}{k+2}$	$M_A = -\frac{qH^2}{12} \cdot \frac{k+3}{k+2}$
$M_C = -\frac{qH^2}{12} \cdot \frac{k}{k+2}$	$M_D = -\frac{qH^2}{12} \cdot \frac{k+3}{k+2}$

4.4.6 Braking force

The load case for braking force consists of two loads; braking force and counteracting trapezoidal load. The moments due to trapezoid load are presented in Table 4.9 and 4.10. Figure 4.8 shows the bending moment distribution caused by a concentrated horizontal load placed in a frame corner.

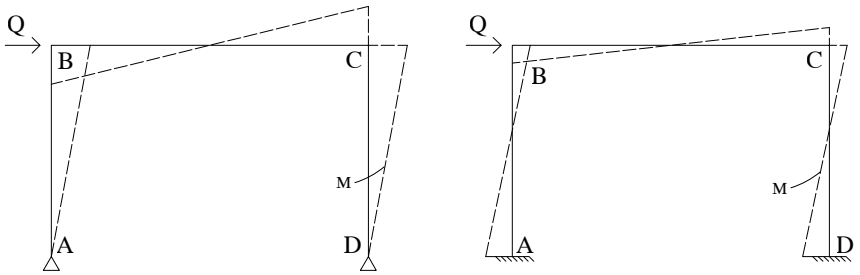

Figure 4.8 Braking force acting on a frame with pinned and fixed BC's, respectively.

Corner moments and support moments due to braking force are shown in Table 4.13 and 4.14.

Table 4.13 Moment due to braking force. Pinned BC's (Wåhlin, 1947, p. 394).

Corner moment	Support moment
$M_B = \frac{qH}{2}$	$M_A = 0$
$M_C = -\frac{qH}{2}$	$M_D = 0$

Table 4.14 Moment due to braking force. Fixed BC's (Wåhlin, 1947, p. 399).

Corner moment	Support moment
$M_B = \frac{qH}{2} \cdot \frac{3k}{6k+1}$	$M_A = -\frac{qH}{2} \cdot \frac{3k+1}{6k+1}$
$M_C = -\frac{qH}{2} \cdot \frac{3k}{6k+1}$	$M_D = \frac{qH}{2} \cdot \frac{3k+1}{6k+1}$

4.5 Analyses

Design moments and shear force in critical sections were used to evaluate the frames. Design checks according to EC regarding ULS (bending moment and shear force), SLS (crack widths) as well as fatigue design were taken into account. The equations used for each design check is presented in Appendix F. *Utilization ratios* (the fraction between load effect and sectional capacity) were evaluated for each design check.

Before any design could be performed, load effects were superimposed and summarized. At predefined span length of the bridge deck and height of the frame legs, thicknesses of the bridge deck and the frame legs were iterated until a utilization ratio of ≈ 95 % was reached in any control. Arrangement of reinforcement is given in section 3.6.1. Analyses were performed for frames with heights of 4 m, 6 m and 8 m with span lengths in the range 6 m - 25 m.

4.6 Results

Thicknesses of the frame legs and the bridge deck have been plotted against the span length and is marked with black dots. Trend lines based on the set of data illustrates the trend of how the parameters varies with the span length. To give an estimation over the prediction interval, the mean value of the standard error (Mean(Δ)) is presented for each trend line. $t \pm$ Mean(Δ) and $t \pm 2$Mean(Δ) represents the 68 % and 95 % prediction of the parameter (confidence limits), respectively.

Figure 4.9 shows the notations of the optimization parameters. Figure 4.10 to 4.12 represent the thicknesses of the frame legs and the bridge deck in case of pinned connection to the foundation and Figure 4.13 to 4.15 for fixed connection.

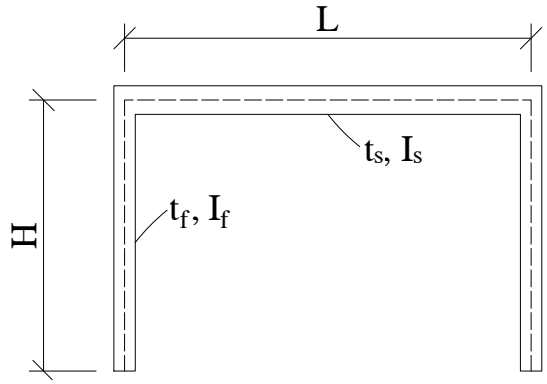

Figure 4.9 Notations of optimization parameters in the 2D-optimization.

Thickness of the frame leg at the level of the foundation slab (t_{f1}) and in frame corner (t_{f2}), respectively, as a function of the span length for slab frame bridges with 13-25 m spans and fixed BC's. Results from numerical optimization of three-dimensional frames (scatter plots) are compared to trend lines for different bridge heights (H).

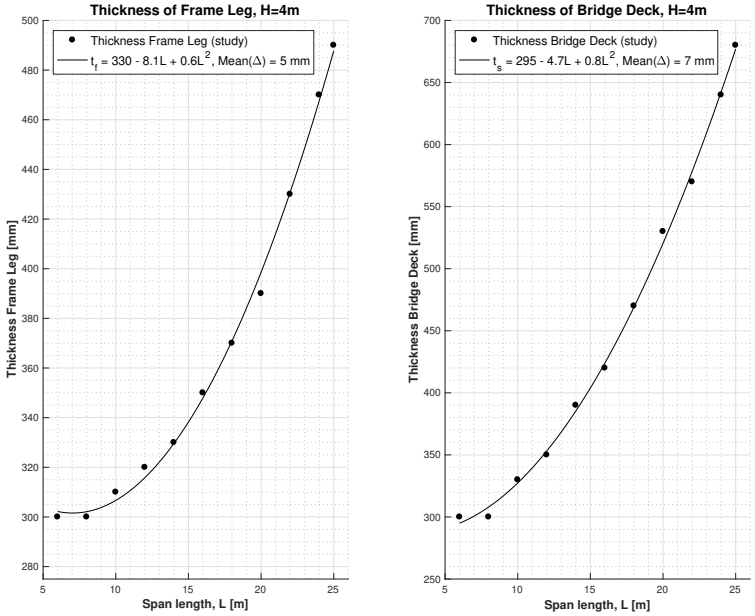

Figure 4.10 Thickness of frame leg and bridge deck, respectively, as a function of span length, for a frame height of H = 4 m and with pinned BC's. Results determined through analytical optimization of two-dimensional frames (scatter plots) are compared to trend lines.

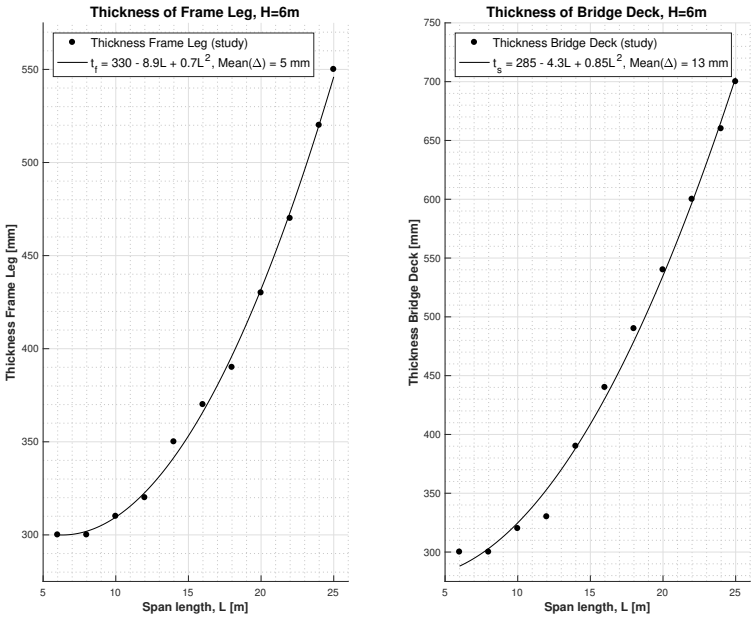

Figure 4.11 Thickness of frame leg and bridge deck, respectively, as a function of span length, for a frame height of H = 6 m and with pinned BC's. Results determined through analytical optimization of two-dimensional frames (scatter plots) are compared to trend lines.

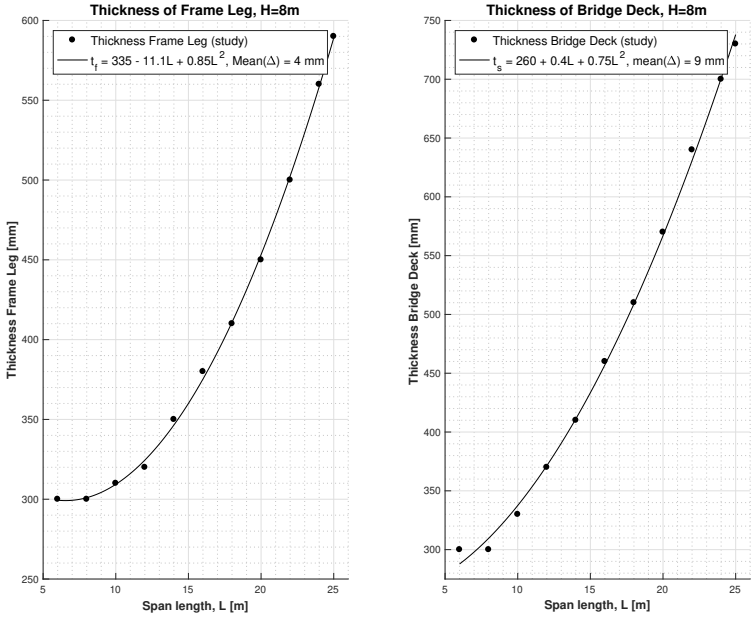

Figure 4.12 Thickness of frame leg and bridge deck, respectively, as a function of span length, for a frame height of H = 8 m and with pinned BC's. Results determined through analytical optimization of two-dimensional frames (scatter plots) are compared to trend lines.

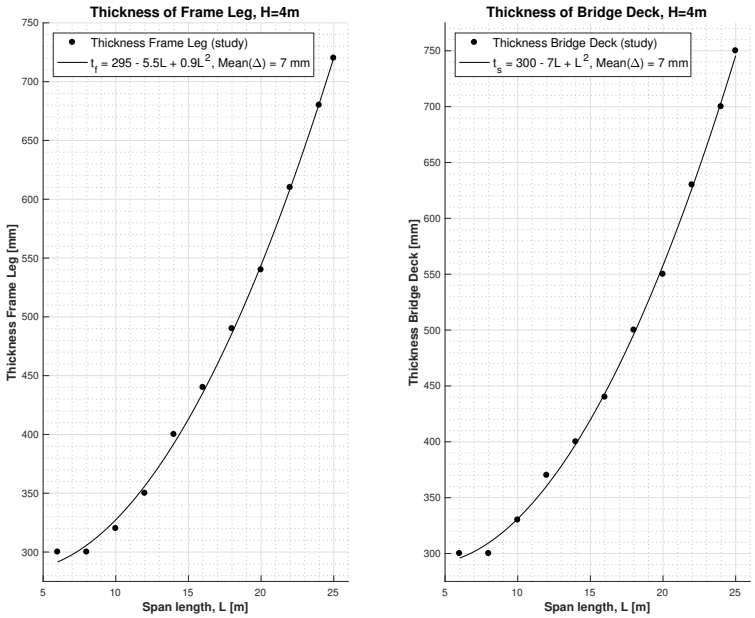

Figure 4.13 Thickness of frame leg and bridge deck, respectively, as a function of span length, for a frame height of H = 4 m and with fixed BC's. Results determined through analytical optimization of two-dimensional frames (scatter plots) are compared to trend lines.

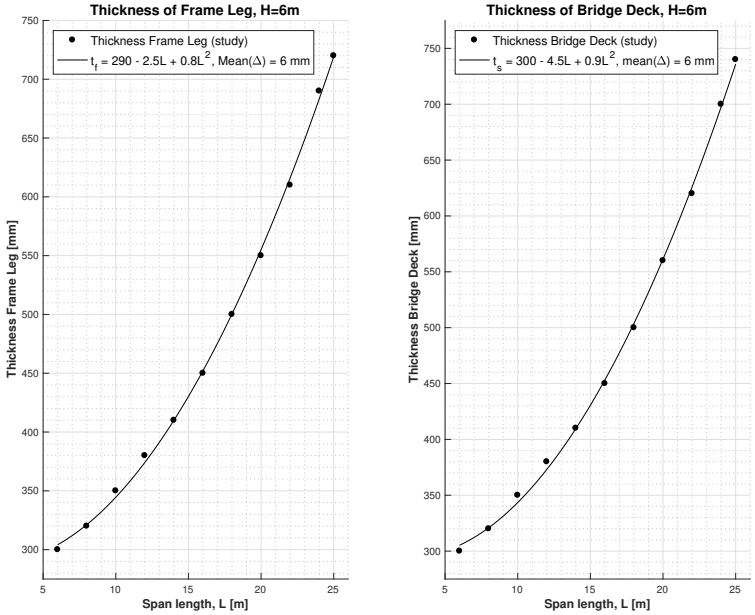

Figure 4.14 Thickness of frame leg and bridge deck, respectively, as a function of span length, for a frame height of H = 6 m and with fixed BC's. Results determined through analytical optimization of two-dimensional frames (scatter plots) are compared to trend lines.

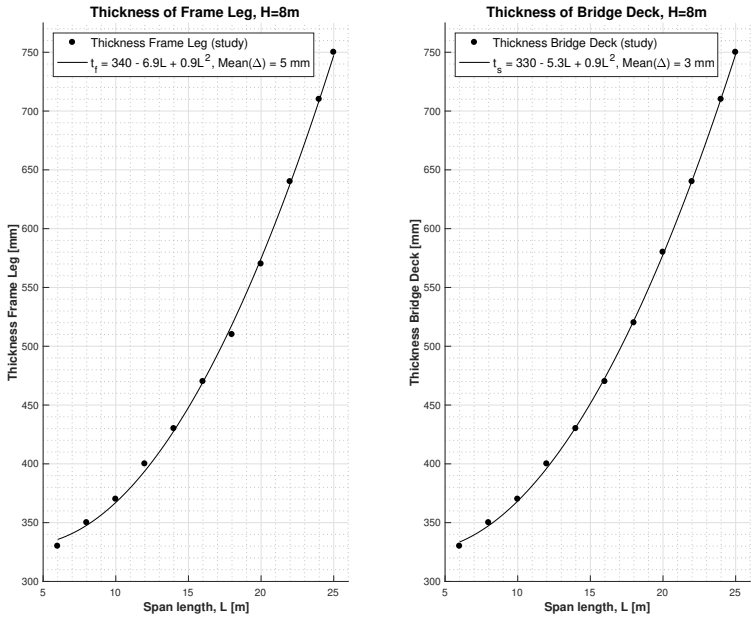

Figure 4.15 Thickness of frame leg and bridge deck, respectively, as a function of span length, for a frame height of H = 8 m and with fixed BC's. Results determined through analytical optimization of two-dimensional frames (scatter plots) are compared to trend lines.

4.7 Discussion

It is important to note that the results presented in section 4.6 do not represent the final values of the parameters. There are several factors that have not been taken into account to ease the calculations and to reduce the working hours in the two-dimensional optimization process. Haunches were ignored since the moment equations becomes invalid for varying cross-section. The overall stiffness of the frame has been overestimated since the calculated thicknesses have been assumed along the whole member when in reality it would have been more efficient to strengthen the member only in local areas (the critical sections) by using haunches. Another aspect that did affect the results was the exemption of 3D effects. Concentrated loads placed on top of the bridge deck tends to be spread in the transverse direction, as described in section 2.1.1. Moreover, any influence of temperature has been neglected in the analyses. In case of an expansion of the bridge deck due to temperature, an additional passive earth pressure is induced in the soil behind the frame legs. The effect is similar to the braking force, where the additional passive earth pressure depends on the expansion of the bridge deck. However, these simplifications are judged to have a minor influence on the frame dimensions.

One can clearly observe a quadratic behaviour on how the thicknesses varies with the span length. Each case has been described with a polynomial of second degree. The differences in thicknesses between the bridge deck and the frame legs are small for short spans but increases when the span length increases. Studying the trend lines it is possible to observe that the linear term in the equations is dominating the thickness for short spans while the quadratic term in the equations is dominating for large spans. This phenomena can be explained by the design process. For short span bridges the bending moments are smaller and it is possible to compensate the short effective height (d) with a larger amount of reinforcement. At a particular span length, the tensile capacity of the reinforcement is reached and to increase the moment capacity the effective height must be increased.

It is possible to conclude that the bending moment is the decisive factor for the thickness of the structural parts and thus the quadratic behaviour of the trend lines. Other design checks, such as fatigue, crack widths and shear can be controlled by different reinforcement layouts. As a final remark the deflection criteria have not been checked and it is possible that the deflection governs the final design for longer spans.

5

Numerical optimization of three-dimensional frames

The optimization parameters were in this chapter designed by using Python ("Python.org", 2020) and BRIGADE/Plus (Scanscot Technology AB, 2018). Python was used as programming language to define geometry, loads and load-combinations, and design checks whereas the finite element software BRIGADE/Plus was used to perform finite element analyses and to extract and evaluate results obtained from BRIGADE/-Plus. By constructing the finite element model with Python-code, the input variables and optimization variables, or anything else in the model, could easily be changed. Coding the model enabled the optimization parameters to be updated automatically by iterating a range of thickness values until an optimized thickness was found for each member of the frame.

BRIGADE/Plus performed the finite element analyses, performed load combinations and returned section forces where the most unfavourable load effects for each cross-section were summarized.

5.1 General Python script for optimization

The models were built with the programming language Python and were then imported to BRIGADE/Plus. The principle was that Python contained information about the model and BRIGADE/Plus executed the analyses. Internal forces and displacements were then extracted from BRIGADE/Plus to Python where load effects in a certain section were checked against the capacity of the section. The working tree is shown in Figure 5.1.

The principle used to update the thickness of the section was the following. For each design check that was performed an utilization ratio, μ, was computed. If the utilization ratio was within a certain range, $0.90 \leq \mu \leq 0.97$ (with the aim of obtaining 0.94), the input thickness was returned. If the utilization ratio was higher or lower than this range a new thickness was computed and the model was updated accordingly.

$$t_{new} = t_{old}\frac{\mu}{0.94} \tag{5.1}$$

The linear thickness relation in expression (5.1) holds for all design checks except

for deflection and fatigue checks, since these checks depend on the moment of inertia rather than the thickness directly. However, the same approach can be implemented:

$$I_{new} = I_{old}\frac{\mu}{0.94} \tag{5.2}$$

For which the updated thickness can be solved:

$$t_{new} = \sqrt[3]{t_{old}^3\frac{\mu}{0.94}} \tag{5.3}$$

For each design check the thickness of the investigated section was stored in a vector. The final value of the thickness that was used in the upcoming iteration was the largest value that was stored in the vector. This process continued until each thickness of the sections converged, see Figure 5.1. The optimization technique *memorization* was implemented to reduce computational time, by keeping track of which calculations that have been made with certain input. If the calculations ended up in a loop hole, where the solutions jumped between two different values which neither one is converged, this have been captured by memorization. At that point, the algorithm for updating thicknesses was changed. This have been done by defining a new guess manually to make the update smaller. In this thesis the manual new guess, to avoid loop hole problems, was the old thickness plus/minus an additional 10 mm, depending on if the thickness needs to increase or decrease (equation (5.1) or (5.3)).

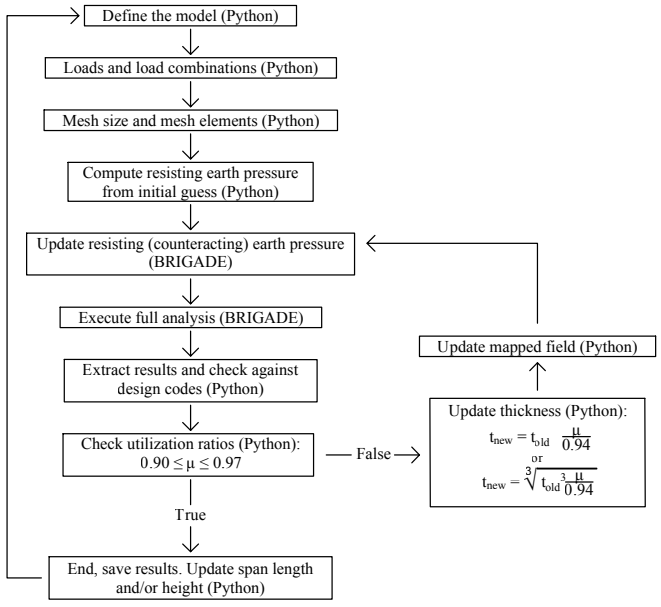

Figure 5.1 Working tree implemented in Python and BRIGADE/Plus for optimization of slab frame bridges.

With respect to analysis complexity it is important to think of what kind of results that are of interest and what numerical model that is representative. As described

in section 5.2.3, a linear elastic model is effective with respect to computational time and is suitable for design in ultimate limit state and was therefore chosen.

In the model complexity level one may investigate how the bridge can be modelled to reduce the computational time but still describe the behaviour in an appropriate way. Shell elements are effective with respect to computational time and due to the less complexity in meshing and were therefore been chosen. A mesh convergence study was also performed to found out for which mesh size the results converged, and where finer mesh does not affected the results to greater extent.

5.2 Model in BRIGADE/Plus

The finite element software BRIGADE/Plus was used to compute internal forces and deflections based on the codes from Python. There are tools available in BRIGADE/Plus that were used to get combined load effects from load combinations, here referred to as *load-envelopes*. The load combinations can be defined manually or generated from the BRIGADE/Plus library (Scanscot Technology AB, 2018).

5.2.1 Geometry of structural model

One notable difference from the 2D-analyses was the influence of haunches. Geometrical variations affects the moment of inertia throughout the member and thus the centre of gravity lines. In Sweden, the National Board of Housing (Boverket) states in the document BBK 04 (Boverket, 2004, p. 153-154) the maximum change of height that should be accounted for. The maximum change of height that should be used in the analyses is 3:1 for vertical members and 1:3 for horizontal members.

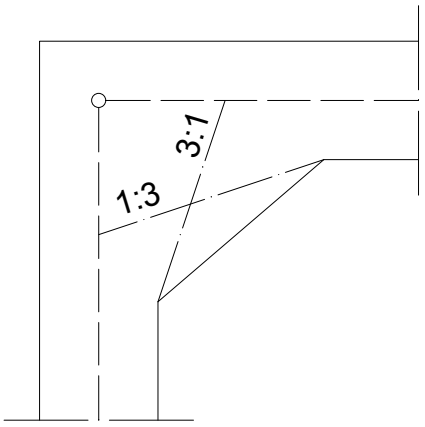

Figure 5.2 Maximum slope of geometrical changes that can be accounted for (Boverket, 2004, p. 153-154).

Four-noded quadratic shell elements with equal size along the entire structure were used in the analyses and the shell thickness was described with the analytical *mapped field* in BRIGADE/Plus. The mid-plane of the shell elements followed the system lines of the frame, see Figure 5.3(a), and the shell thickness was described symmetric around the mid-plane for each element (Figure 5.3(b)). This is because mapped fields can only extend the thickness symmetric around the element mid-planes. The members were then assembled (Figure 5.3(c)).

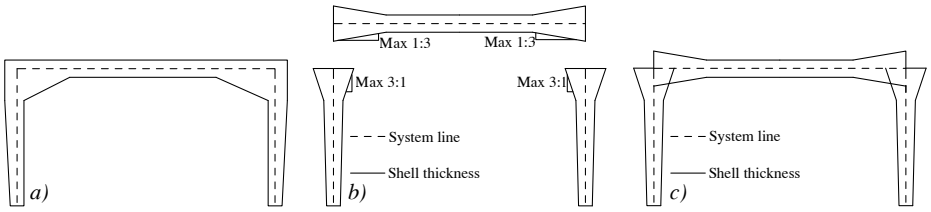

Figure 5.3 How the geometry of bridge has been modelled. a) Illustration of the system line b) Modification of geometrical changes c) The structural members are assembled.

In accordance with Figure 2.7, two load fields were to be included since the width of the bridge was 6m. Since the magnitude of the traffic load was different for the two load fields (Figure 2.8) the effect of a transverse force distribution was of importance.

5.2.2 Boundary conditions

It was more realistic to prescribe a certain boundary condition at the bottom of the foundation slab rather than at the connection between the frame legs and the foundation slab. The foundation slab was not included in the model but spring connections have been used between the frame legs and the soil by using a point to ground connection, with an offset of 600 mm below the frame legs, to account for the thickness of the foundation slab (Figure 5.4). The spring was given a finite large stiffness in all translational and rotational degrees of freedoms that represented a fixed connection. A similar approach was used for a pinned connection but with a finite small stiffness for the rotation around the axis perpendicular to the longitudinal axis of the bridge. The boundary conditions modelled in BRIGADE/Plus are illustrated in Figure 5.5

5.2.3 Material model

A linear elastic material model was used with material parameters presented in Appendix F. According to the theory presented in section 2.3.1 the effect of temperature and shrinkage in the transverse direction can be excluded in the linear elastic analyses. This was achieved by defining the thermal expansion coefficient a zero value in the transverse direction of the bridge.

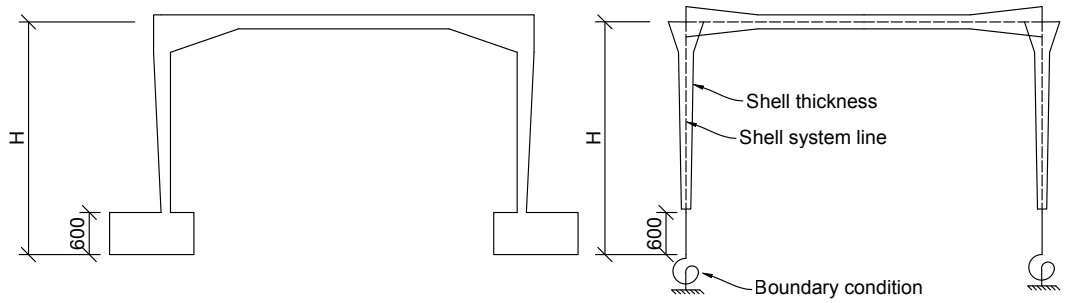

Figure 5.4 Left: The actual slab frame bridge of investigation. Right: How the slab frame bridges has been modelled.

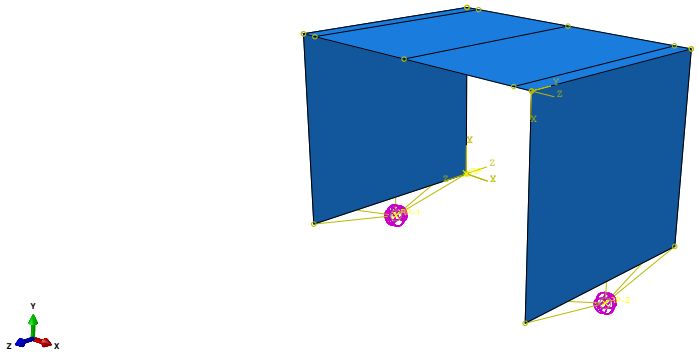

Figure 5.5 Boundary conditions modelled in BRIGADE/Plus.

5.2.4 Loads

Loads that were taken into account in the analyses were permanent loads such as self-weight, paving, creep, shrinkage, lateral earth pressure and differential settlements. Variable loads that were included was the vertical traffic load, surcharge load and the acceleration/braking force. Since the loads are of different types they were applied to the model in different ways. A short description on how the loads were applied is given below. A further explanation on how the different load modules are working is given in the BRIGADE/Plus User's manual (Scanscot Technology AB, 2018, p. 289-298). All loads were defined in a step which was specific for each load. The characteristic values of all loads used is presented in Appendix E.

5.2.4.1 Self-weight and paving

The self-weight of the bridge was applied as a gravity load. The magnitude was given by the shell thickness which was defined by analytical *mapped field*. Paving was defined as a uniform *pressure load* acting on the bridge deck.

5.2.4.2 Earth pressure

Earth pressure was applied as a pressure load with mapped field to generate the linear increase of load with depth, as illustrated in Figure 5.6.

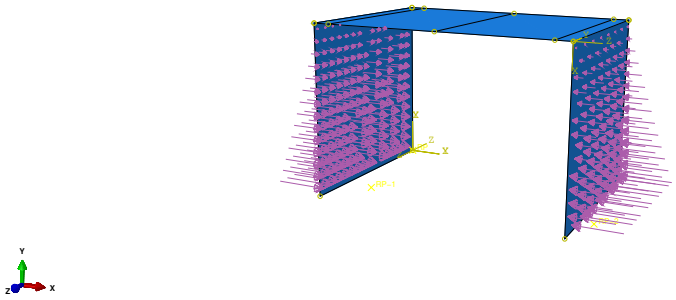

Figure 5.6 Earth pressure applied in BRIGADE/Plus.

5.2.4.3 Shrinkage and temperature

Both shrinkage and temperature was applied as *predefined temperature fields* on the entire model. The two load-cases with uniform temperature variation were defined as constant through the shell thickness while the cases with temperature gradient was defined with points through the shell thickness.

The load-case with uniform high temperature included a counteracting earth pressure on both frame legs. The counteracting earth pressure has a triangular shape and was applied in the same way as for the surcharge load.

5.2.4.4 Differential settlements

The differential settlements were applied as *prescribed displacement* of the boundary conditions.

5.2.4.5 Loads from wing walls

Loads from wing walls were applied as line loads using *shell edge loads* with three different components; bending moment and forces in the transverse and longitudinal direction of the bridge. Self-weight from wing walls was applied as *shell edge traction*, see Figure 5.7.

5.2.4.6 Surcharge

Surcharge load was applied as a uniform pressure on the frame legs. The counteracting earth pressure was applied as a pressure load with mapped field for the

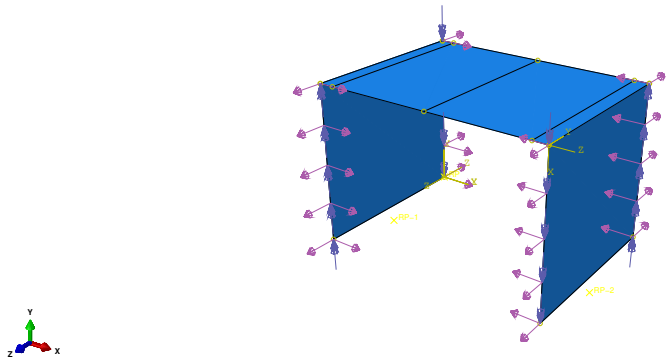

Figure 5.7 Equivalent forces from wing walls modelled in BRIGADE/Plus.

triangular shape.

5.2.4.7 Vertical traffic load

Since the bridge was 6 meters wide, there was space for two traffic lanes, see Figure 2.8. The uniformly distributed loads in LM1 and vehicle model I was applied with mapped fields for each traffic lane, see Figure 5.8. The concentrated loads were applied in reference points with an offset from the shell. The reference points were connected to the shell element with ties which distributed the load slightly.

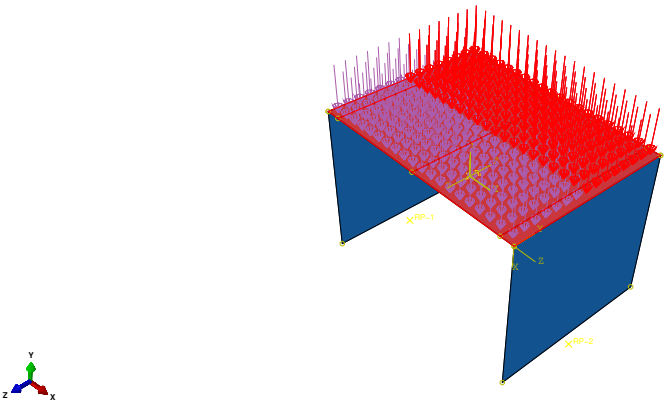

Figure 5.8 Uniformly distributed load in LM1 applied in BRIGADE/Plus.

5.2.4.8 Braking force

Braking force was applied as a *surface traction* distributed on the entire bridge deck. Moment due to eccentricity from the upper surface of the bridge deck and the system line was not included.

Counteracting earth pressure was applied as a pressure load with mapped field, just as for the counteracting earth pressure due to surcharge.

5.2.5 Load combination

Load combination was performed with the built in module *load combination* (Scanscot Technology AB, 2018, p. 346-349). The design load combinations presented in Section 3.5 was defined and produced in BRIGADE/Plus, which then created envelops of the final load combinations. The envelops contains maximum and minimum values of each section force in each node in the model with corresponding values. The effect of each variable load was evaluated for each node to determine if it was favourable or unfavourable and to determine which variable load that was dominant for each node.

5.2.6 Mesh convergence study

To find an appropriate mesh size that is valid for all combinations of span length and height of the frame legs, a mesh convergence study was performed. It was made for a frame with $L = 6\ m$ and $H = 4\ m$ (the smallest frame). Convergence was evaluated by analysing the deflection caused by a concentrated load applied in the middle of the bridge. To avoid singularity problems, the point where the deflection was evaluated was not directly below the placement of the load. If convergence occurs for this specific case, the mesh size can be used for all geometrical combinations since the number of mesh elements will increase tremendously for bridges with larger dimensions.

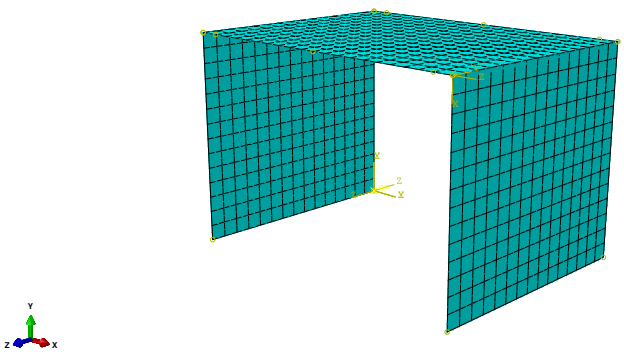

Figure 5.9 Final Mesh determined from convergence study.

Normally, a convergence study can be performed to decide what error that gives sufficiently reliably values in percent, compared to the converged solution. In this paper the converged solution was found to correspond to a mesh size of 50 mm. According to Figure 5.10 a mesh size of 400 mm gave sufficiently reliably values. That corresponded to an error compared to the converged solution of $\approx 1.8\%$. The final mesh can be seen in Figure 5.9.

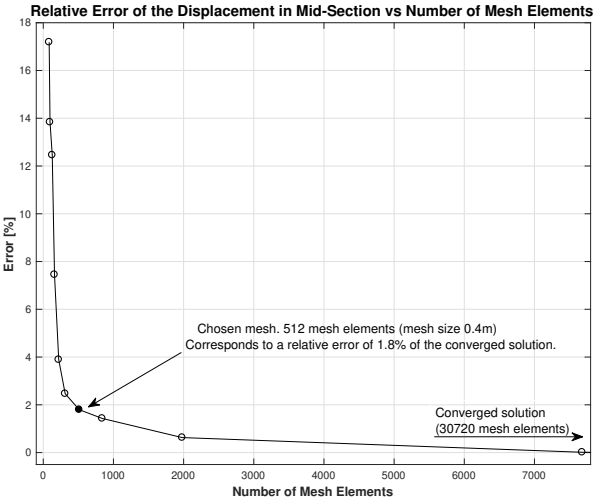

Figure 5.10 Convergence study and how the relative error varies with increased number of mesh elements compared to the converged solution.

5.2.7 Verification of the FE-model

In addition to the mesh convergence study, the reliability of the load effects computed from the FE-analysis were studied.

To see if the analytical mapped field containing the shell thickness has been implemented correctly and hence the self-weight of the bridge, the deflection in mid-span caused by the self-weight have been checked.

For a given span width of $L = 10\ m$, frame height $H = 4\ m$ and corresponding thicknesses $t_s = 330\ mm$ and $t_f = 310\ mm$, following deflection was obtained (Figure 5.11, pinned boundary conditions).

The deflection caused by the self-weight was superimposed together with the bending moment in frame corner in an analytical verification, as illustrated in equation 5.4.

$$u(\frac{L}{2}) = \frac{5qL^4}{384EI} - 2\frac{ML^2}{16EI} \tag{5.4}$$

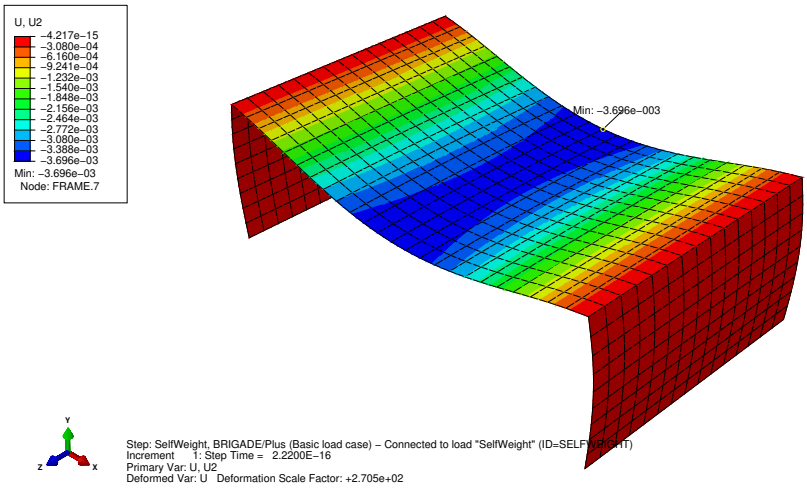

Figure 5.11 Deflection caused by self-weight of the bridge. $L = 10$ m, $H = 4$ m.

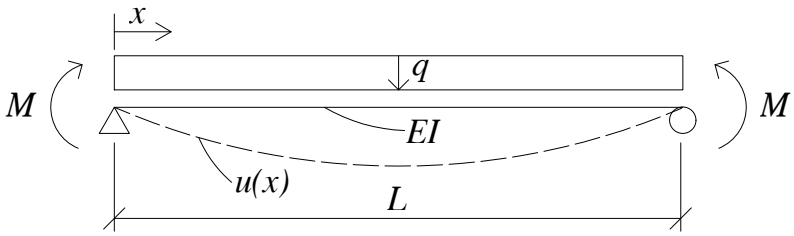

Figure 5.12 Model for verification of deflection in mid-span caused by the self-weight of the bridge.

Where $q = 8.25\ kN/m$, $M = 56.83\ kNm$, $E = 34\ GPa$ and $I = 2.995 \cdot 10^{-}3\ m^4$. Equation (5.4) gives an deflection in mid-span of 3.57 mm and from Figure 5.11 the deflection in mid-span is 3.696 mm. The difference in deflection between the numerical and analytical solution may be explained by the influence from the deformation of the frame legs, since the rotational stiffness in frame corner makes the deck slab partially fixed. The mesh size did also contain an error of 2 % compared to the analytical solution.

Design forces and load-envelopes were checked and verified with another numerical programs. The differences is small and may be explained by the way the model is built up and how the load envelopes summarizes the internal forces in BRIGADE/-Plus.

5.3 Post-processing

Section forces were extracted from load-envelopes in BRIGADE/Plus for relevant load combinations. Paths along the width of the bridge was defined for each critical section to extract results. The section forces were extracted 0.8 meters from the edge of the heaviest loaded traffic lane. This represents the third node in the paths

since mesh elements with a size of 0.4 meters were used. In this way, local effects at the boundary were avoided.

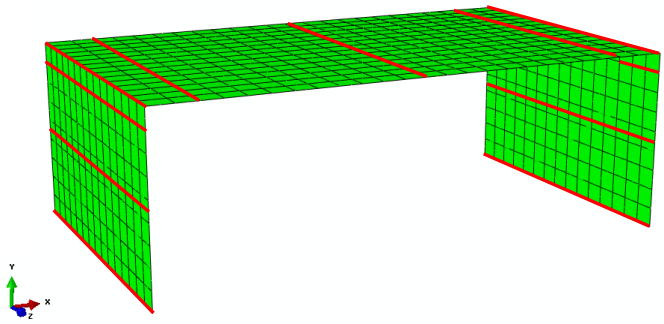

Figure 5.13 Paths in BRIGADE/Plus for extracting results in critical sections.

BRIGADE/Plus evaluates three different sectional moment components, SM1, SM2 and SM3, where SM1 and SM2 are the bending moment in the longitudinal and transverse direction, respectively, and SM3 is the torsional moment. The design bending moment, design shear force and corresponding normal forces was summarized according to the theory presented in section 2.3.2. With the notations from BRIGADE/Plus, design bending moment and normal force were determined according to Equations 5.5 and 5.6.

$$M = SM1 \pm |SM3| \tag{5.5}$$

$$N = SF1 \pm |SF3| \tag{5.6}$$

In BRIGADE/Plus the shear force in the longitudinal (x-direction) and in the transverse direction (z-direction) are named SF4 and SF5, respectively. The design shear force, with the notation used in BRIGADE/Plus, was calculated as presented in Equation 5.7.

$$V = \sqrt{SF4_x^2 + SF5_z^2} \tag{5.7}$$

5.3.1 Sectional design

Design section forces were used to evaluate each critical section and to determine if the requirements in EC (CEN, 2004) were fulfilled. The shear force capacity with shear reinforcement was evaluated in the bridge deck in a section with haunches, the exact position varied depending on the geometry of the haunch. For span up to 12 meters, the shear force capacity was evaluated at a section with the distance of half the width of a wheel from the beginning of the haunch. For longer spans, the shear force was evaluated at a section of the same distance but from the end of the haunch. The critical sections for shear force with shear reinforcement can be seen

in Figure 5.14. Usually the shear force is evaluated at a distance of $0.9d$ from the haunch as stated in section 3.5.1.1. The critical section was approximated as the distance of half the width of a wheel, since the exact position of the critical section is dependent on the thickness of the bridge deck. Furthermore, the shear capacity without shear reinforcement was evaluated in mid-span of the bridge deck as well as in middle and bottom of the frame legs and in a position where the haunch connect with the frame legs.

The bending moment capacity was evaluated for each critical section. The position where the sectional capacity in the frame corner was evaluated was the same as for critical shear force in the bridge deck, depending on the type of haunch used. The bending moment capacity in the frame legs was evaluated where the frame legs were connected to the foundation slab, the middle and in a section where the haunch connected to the frame leg. Yielding of reinforcement was controlled in order to secure a ductile fracture. When the reinforcement did not reached yielding, the configuration of the cross-section is unacceptable and a larger thickness was required. In this case, the output from the design check was a new thickness which was 10 mm larger than the current thickness.

Fatigue was checked for the concrete in compression and for the reinforcement in tension in each section. The section with shear reinforcement was checked for fatigue in the shear reinforcement. Crack widths were controlled for each section. Maximum allowed crack width varied depending on the exposure class of each section. Deflection was evaluated in the section of the mid span of the bridge deck.

Utilization ratios for each design check was determined for every relevant section. The utilization ratio was then used to predict the required thickness for a optimized structure as explained in section 5.1.

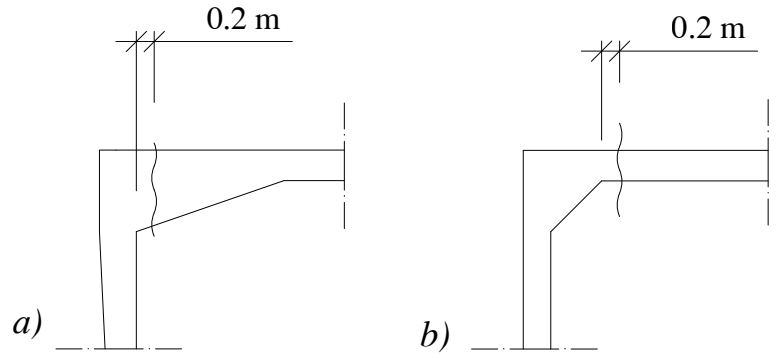

Figure 5.14 Critical sections in the bridge deck for shear force.

The sections where the the different design checks were evaluated is presented schematically by Figure 3.18. All equations used for the design checks can be found in Appendix F.

5.4 Case Study - Carbon Dioxide Impact

An analysis of total environmental impact was performed, to enable a comparison of the environmental impact of several existing bridges compared to what the environmental impact would be if they were designed with optimized dimensions. SRA present statistics over dimensions from slab frame bridges that has been designed and constructed in Sweden, which were used for the comparison (Vägverket, 1998, p. 3-5). Several bridges and their cross-sectional dimensions of the bridge decks are summarized and can be seen in Table 5.1. It should be noted that there were no information given about the dimensions or the height of the frame legs, if the cross-section of the frame legs was kept constant along the height or if it is varying. The height of the frame legs have therefore been assumed to 6 m, and the boundary conditions as pinned. The dimensions of the frame legs for the existing bridges were evaluated in the design program to obtain 90 % utilization ratio for shear force in critical sections of the frame legs. The frame legs were assumed unreinforced for shear force. A minimum thickness of 400 mm of the frame legs was assumed for the existing bridges, which is a bit larger than for the optimization. In addition to the bridges presented by SRA, two other bridges recently designed by a Swedish consulting company, was used for comparison. The dimensions can be seen in Table 5.2. For these bridges the reinforcement layout was known and is presented in Appendix H, along with the used dimensions and reinforcement layouts for the Bridges in Table 5.1. Results from the optimization study in terms of required thicknesses for varying span lengths were used as input in comparison to the existing bridges.

Table 5.1 Thickness in mid-span and end of haunch of designed slab frame bridges (Vägverket, 1998, p. 3-5).

Bridge	L [m]	t_s/t_{sh} [mm]
L 814	6.0	350/850
Y 1283	10.0	450/950
Z 1060	14.5	550/750
Y 1217	18.0	730/930

Table 5.2 Thickness of bridge deck and frame leg of recently designed slab frame bridges.

Bridge	L [m]	H [m]	t_s/t_{sh} [mm]	t_{f1}/t_{f2} [mm]
A	11.5	8.4	600/1100	550/550
B	13.6	5.7	666/866	600/600

Evaluation of total carbon impact of the bridges was performed according to the theory presented in Section 2.9, where the total volume of concrete and reinforcement steel was multiplied with their corresponding EMC-value. EMC-values used in the analyses are presented in Table 2.7.

Required reinforcement amount was calculated based on section forces generated by BRIGADE/Plus in the optimization program. Since the vertical traffic load was placed at critical positions instead of evaluated as the envelope of moving vehicles, some assumptions regarding curtailment of reinforcement and extension of shear reinforcement was made. The tensile reinforcement generated in mid-span, was assumed to be extended $L/4$ to each side. One fourth of the reinforcement amount was assumed to continue to the corner. Similarly for the tensile reinforcement in frame corners, where the reinforcement bars were extended $L/4$ from the corner to the bridge deck and $H/2$ from the corner to the frame leg. The other areas of the bridge were assumed to be reinforced with one fourth of the tensile reinforcement amount in frame corners. The reinforcement amount on the inside of the frame leg was assumed to extend $H/4$ on both sides from the middle of the frame legs while one fourth of the reinforcement is extended to the frame corner and the bottom of the frame legs. When shear reinforcement was needed the amount required at the corner of the bridge deck was assumed to extend approximately $L/8$ in to the bridge deck.

6
Results

In this section results from the numerical optimization are presented. The notations for the parameters in different sections follows the notations presented in Figure 6.1. The results are divided into different graphs depending on the geometrical constraints and BC's. Following the constraints, results are divided into different graphs depending on span length; 6 $m \leq L \leq 12$ m (with prescribed dimensions of haunches and constant thickness of the frame legs along the height) and 13 $m \leq L \leq 25$ m (with a design of haunches and a linear variation in thickness along the height of the frame legs).

Figure 6.2 - 6.3 shows the required thickness of the deck slab (t_s) and the frame legs (t_{sh}) with pinned BC's to the soil, respectively. Figure 6.4 - 6.5 shows the required thickness of the deck slab in span (t_s) and in frame corner (t_{sh}), the thickness of the frame legs at frame corner (t_{f2}) and at the connection to the foundation slab (t_{f1}). Pinned connections. Results for frames with fixed BC's are given in Figure 6.6 - 6.9.

All graphs are plotted as a function of the span length with a height of the frame leg given by the figures. All graphs contain the values of each parameter obtained from the numerical optimization (represented by the scatter plots) and trend lines. Equations for each trend line with corresponding mean value of the standard error are given below each graph. $t \pm \bar{\Delta}$ and $t \pm 2\bar{\Delta}$ represents the confidence limits for 68 % and 95 % prediction of the parameter, respectively.

All data points with decisive design check and corresponding utilization ratios can be found in Appendix G.

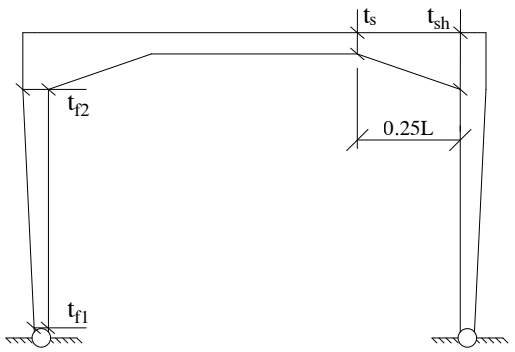

Figure 6.1 Notations used for the optimization parameters.

6.1 Frame with pinned BC's

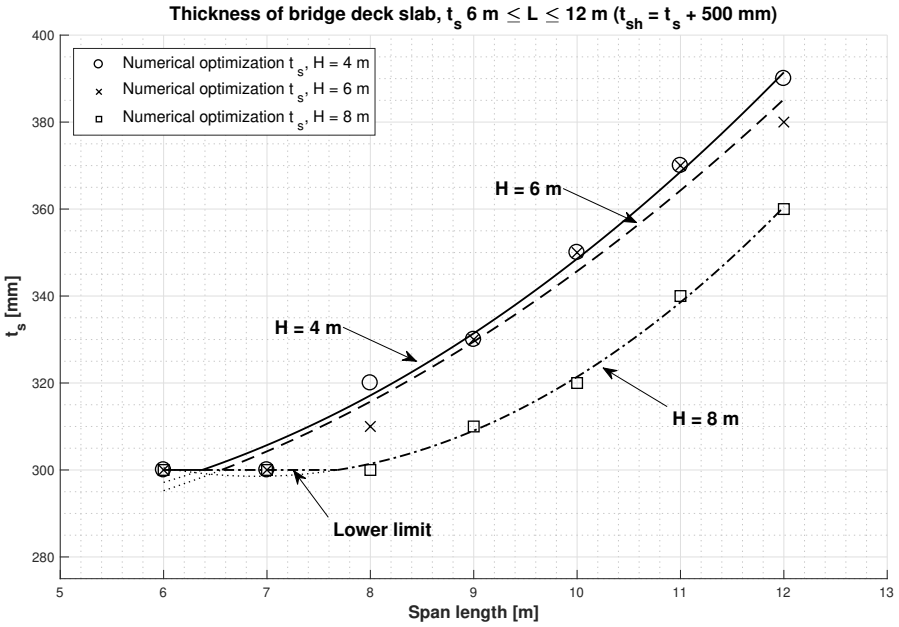

Figure 6.2 Thickness of the bridge deck slab (t_s) as a function of the span length, for slab frame bridges with 6-12 m spans and pinned BC's. Results from numerical optimization of three-dimensional frames (scatter plots) are compared to trend lines for different bridge heights (H). The thickness at the end of the haunch (t_{sh}) is obtained by adding 500 mm to the thickness required for the bridge deck slab.

The equations to the trend lines, and their mean value of the standard errors, were determined to:

$$t_s^{H\,=\,4\ m} = \begin{cases} 300\ mm,\ \bar{\Delta} = 0\ mm & 6\ m \leq L \leq 6.4\ m \\ 305 - 10L + 1.43L^2\ [mm],\ \bar{\Delta} = 4\ mm & 6.4\ m\ < L \leq 12\ m \end{cases}$$

$$t_s^{H\,=\,6\ m} = \begin{cases} 300\ mm,\ \bar{\Delta} = 0\ mm & 6\ m \leq L \leq 6.6\ m \\ 290 - 6.5L + 1.2L^2\ [mm],\ \bar{\Delta} = 7\ mm & 6.6\ m\ < L \leq 12\ m \end{cases}$$

$$t_s^{H\,=\,8\ m} = \begin{cases} 300\ mm,\ \bar{\Delta} = 0\ mm & 6\ m \leq L \leq 7.7\ m \\ 410 - 33L + 2.4L^2\ [mm],\ \bar{\Delta} = 2\ mm & 7.7\ m\ < L \leq 12\ m \end{cases}$$

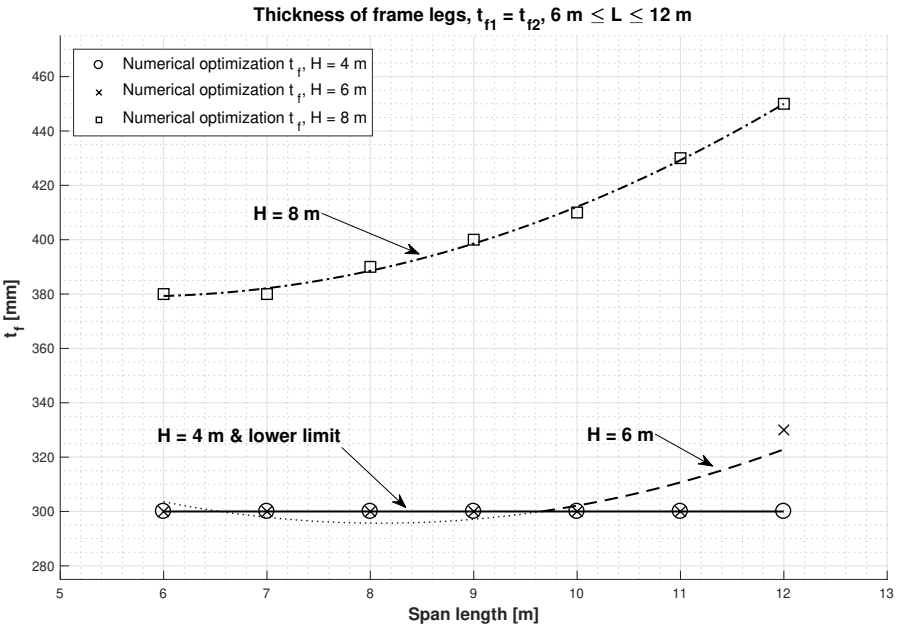

Figure 6.3 Thickness of the frame leg (t_f) as a function of the span length, where $t_f = t_{f1} = t_{f2}$, for slab frame bridges with 6-12 m spans and pinned BC's. Results from numerical optimization of three-dimensional frames (scatter plots) are compared to trend lines for different bridge heights (H).

The equations to the trend lines, and their mean value of the standard errors, were determined to:

$$t_f^{H\,=\,4\ m} = 300\ mm,\ \bar{\Delta} = 0\ mm \qquad 6\ m \leq L \leq 12\ m$$

$$t_f^{H\,=\,6\ m} = \begin{cases} 300\ mm,\ \bar{\Delta} = 0\ mm & 6\ m \leq L \leq 9.7\ m \\ 420 - 30L + 1.8L^2\ [mm],\ \bar{\Delta} = 9\ mm & 9.7\ m\ < L \leq 12\ m \end{cases}$$

$$t_f^{H\,=\,8\ m} = 435 - 20.4L + 1.78L^2\ [mm],\ \bar{\Delta} = 2\ mm \qquad 6\ m\ \leq L \leq 12\ m$$

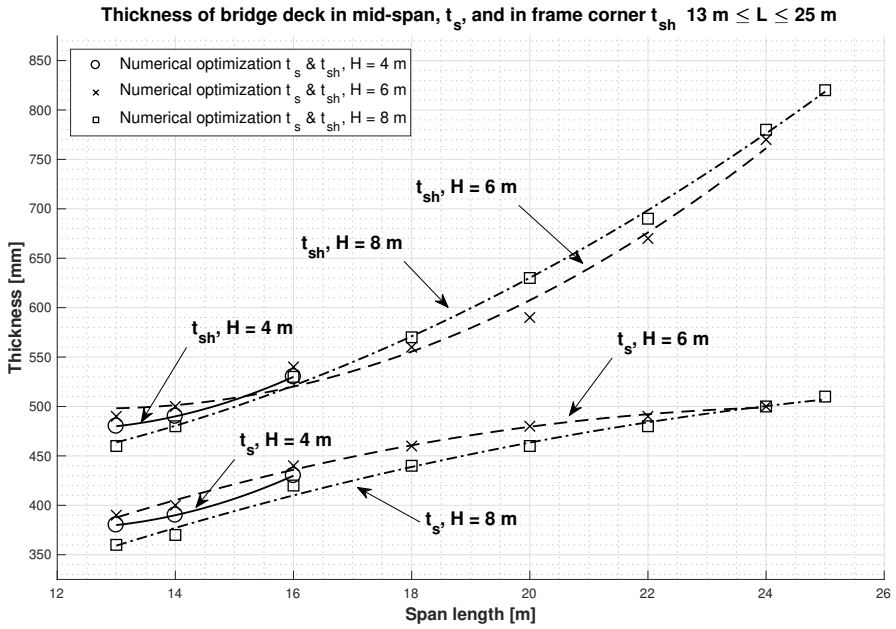

Figure 6.4 Thickness of the bridge deck slab (t_s) and at the end of the haunch (t_{sh}), respectively, as a function of the span length, for slab frame bridges with 13-25 m spans and pinned BC's. Results from numerical optimization of three-dimensional frames (scatter plots) are compared to trend lines for different bridge heights (H).

The equations to the trend lines, and their mean value of the standard errors, were determined to:

$$t_s^{H\,=\,4\ m} = 855 - 80L + 3.33L^2\ [mm],\ \bar{\Delta} = 0\ mm \qquad 13\ m\ \leq L \leq 16\ m$$

$$t_s^{H\,=\,6\ m} = 22 + 37.9L - 0.75L^2\ [mm],\ \bar{\Delta} = 4\ mm \qquad 13\ m\ \leq L \leq 24\ m$$

$$t_s^{H\,=\,8\ m} = 32 + 32L - 0.51L^2\ [mm],\ \bar{\Delta} = 7\ mm \qquad 13\ m\ \leq L \leq 25\ m$$

$$t_{sh}^{H\,=\,4\ m} = 955 - 80L + 3.33L^2\ [mm],\ \bar{\Delta} = 0\ mm \qquad 13\ m\ \leq L \leq 16\ m$$

$$t_{sh}^{H\,=\,6\ m} = 835 - 53L + 2.1L^2\ [mm],\ \bar{\Delta} = 18\ mm \qquad 13\ m\ \leq L \leq 24\ m$$

$$t_{sh}^{H\,=\,8\ m} = 455 - 14.4L + 1.16L^2\ [mm],\ \bar{\Delta} = 7\ mm \qquad 13\ m\ \leq L \leq 25\ m$$

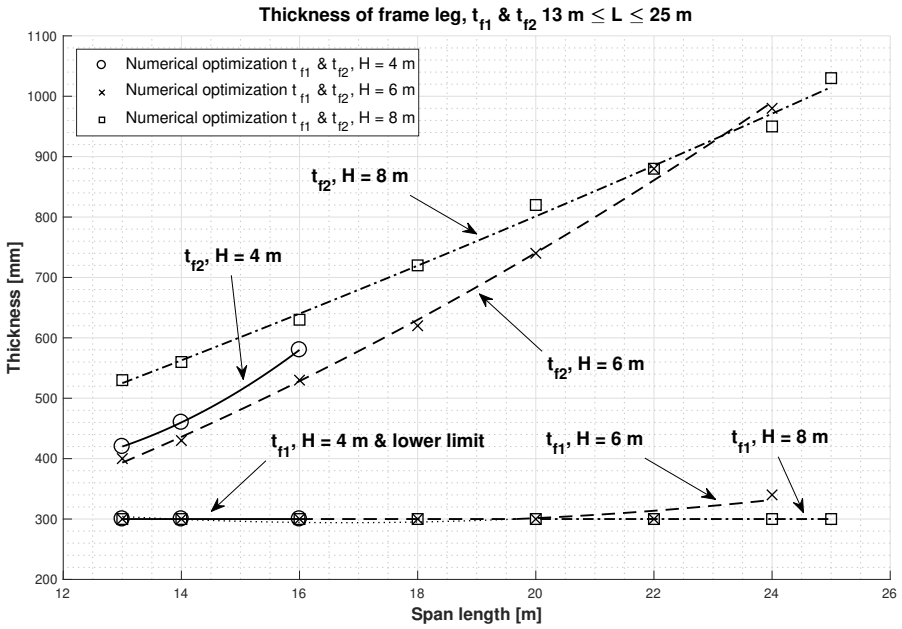

Figure 6.5 Thickness of the frame leg at the level of the foundation slab (t_{f1}) and in frame corner (t_{f2}), respectively, as a function of the span length for slab frame bridges with 13-25 m spans and pinned BC's. Results from numerical optimization of three-dimensional frames (scatter plots) are compared to trend lines for different bridge heights (H).

The equations to the trend lines, and their mean value of the standard errors, were determined to:

$$t_{f1}^{H\,=\,4\ m} = 300\ mm,\ \bar{\Delta} = 0\ mm \qquad 13\ m\ \leq L \leq 16\ m$$

$$t_{f1}^{H\,=\,6\ m} = \begin{cases} 300\ mm,\ \bar{\Delta} = 0\ mm & 13\ m \leq L \leq 20\ m \\ 495 - 24.2L + 0.72L^2\ [mm],\ \bar{\Delta} = 5\ mm & 20\ m\ < L \leq 24\ m \end{cases}$$

$$t_{f1}^{H\,=\,8\ m} = 300\ mm,\ \bar{\Delta} = 0\ mm \qquad 13\ m\ \leq L \leq 25\ m$$

$$t_{f2}^{H\,=\,4\ m} = 1110 - 140L + 6.7L^2\ [mm],\ \bar{\Delta} = 0\ mm \qquad 13\ m\ \leq L \leq 16\ m$$

$$t_{f2}^{H\,=\,6\ m} = 50 + 11.3L + 1.16L^2\ [mm],\ \bar{\Delta} = 15\ mm \qquad 13\ m\ \leq L \leq 24\ m$$

$$t_{f2}^{H\,=\,8\ m} = -11 + 40.84L\ [mm],\ \bar{\Delta} = 16\ mm \qquad 13\ m\ \leq L \leq 25\ m$$

6.2 Frame with fixed BC's

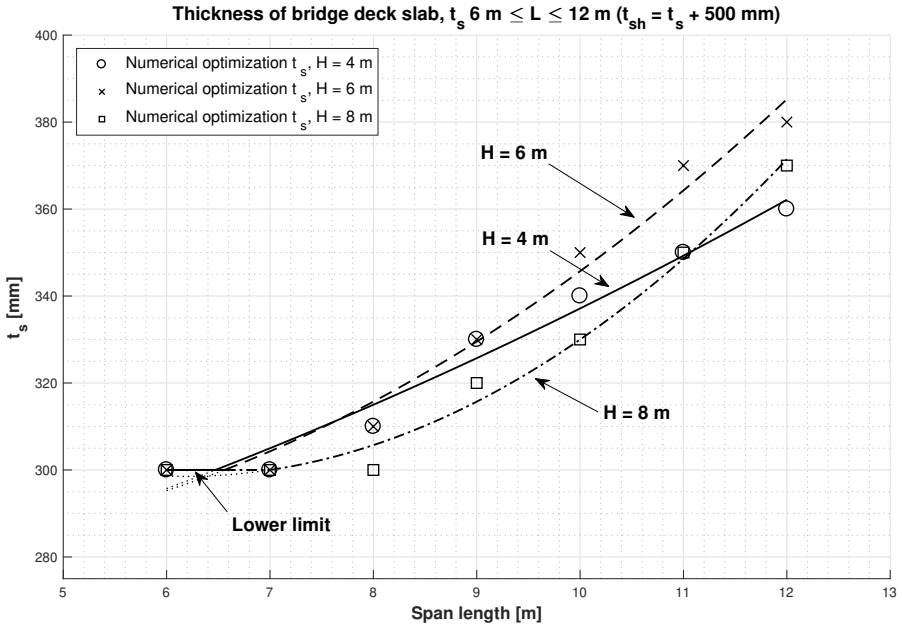

Figure 6.6 Thickness of the bridge deck slab (t_s) as a function of the span length, for slab frame bridges with 6-12 m spans and fixed BC's. Results from numerical optimization of three-dimensional frames (scatter plots) are compared to trend lines for different bridge heights (H). The thickness at the end of the haunch (t_{sh}) is obtained by adding 500 mm to the thickness required for the bridge deck slab.

The equations to the trend lines, and their mean value of the standard errors, were determined to:

$$t_s^{H\,=\,4\ m} = \begin{cases} 300\ mm,\ \bar{\Delta} = 0\ mm & 6\ m \leq L \leq 6.5\ m \\ 255 + 4.64L + 0.36L^2\ [mm],\ \bar{\Delta} = 6\ mm & 6.5\ m\ < L \leq 12\ m \end{cases}$$

$$t_s^{H\,=\,6\ m} = \begin{cases} 300\ mm,\ \bar{\Delta} = 0\ mm & 6\ m \leq L \leq 6.6\ m \\ 290 - 6.4L + 1.2L^2\ [mm],\ \bar{\Delta} = 7\ mm & 6.6\ m\ < L \leq 12\ m \end{cases}$$

$$t_s^{H\,=\,8\ m} = \begin{cases} 300\ mm,\ \bar{\Delta} = 0\ mm & 6\ m \leq L \leq 7\ m \\ 380 - 26.4L + 2.14L^2\ [mm],\ \bar{\Delta} = 4\ mm & 7\ m\ < L \leq 12\ m \end{cases}$$

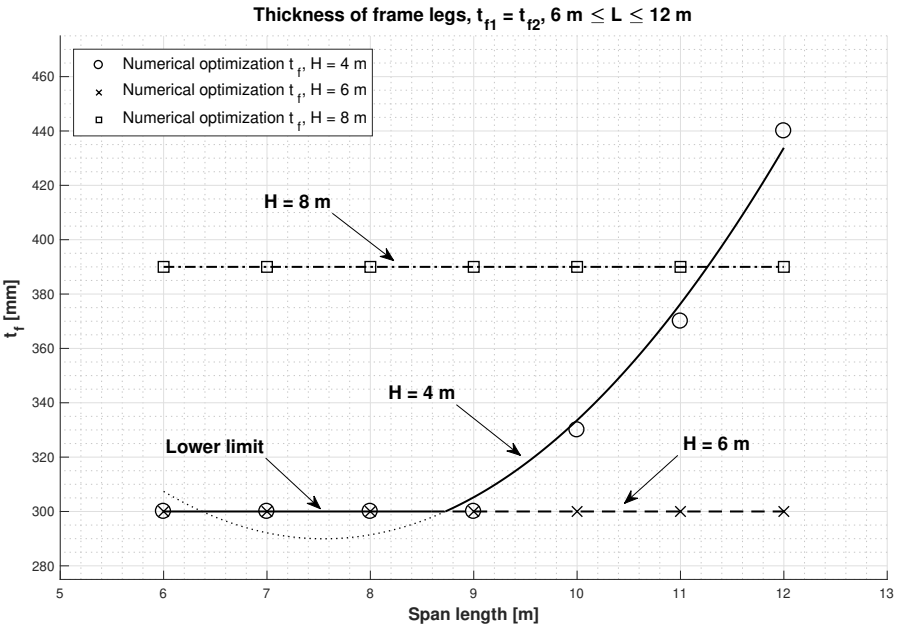

Figure 6.7 Thickness of the frame leg (t_f) as a function of the span length, where $t_f = t_{f1} = t_{f2}$, for slab frame bridges with 6-12 m spans and fixed BC's. Results from numerical optimization of three-dimensional frames (scatter plots) are compared to trend lines for different bridge heights (H).

The equations to the trend lines, and their mean value of the standard errors, were determined to:

$$t_f^{H\,=\,4\ m} = \begin{cases} 300\ mm,\ \bar{\Delta} = 0\ mm & 6\ m \leq L \leq 8.7\ m \\ 705 + -110L + 7.3L^2\ [mm],\ \bar{\Delta} = 10\ mm & 8.7\ m\ < L \leq 12\ m \end{cases}$$

$$t_f^{H\,=\,6\ m} = 300\ mm,\ \bar{\Delta} = 0\ mm \qquad 6\ m\ \leq L \leq 12\ m$$

$$t_f^{H\,=\,8\ m} = 390\ mm,\ \bar{\Delta} = 0\ mm \qquad 6\ m\ \leq L \leq 12\ m$$

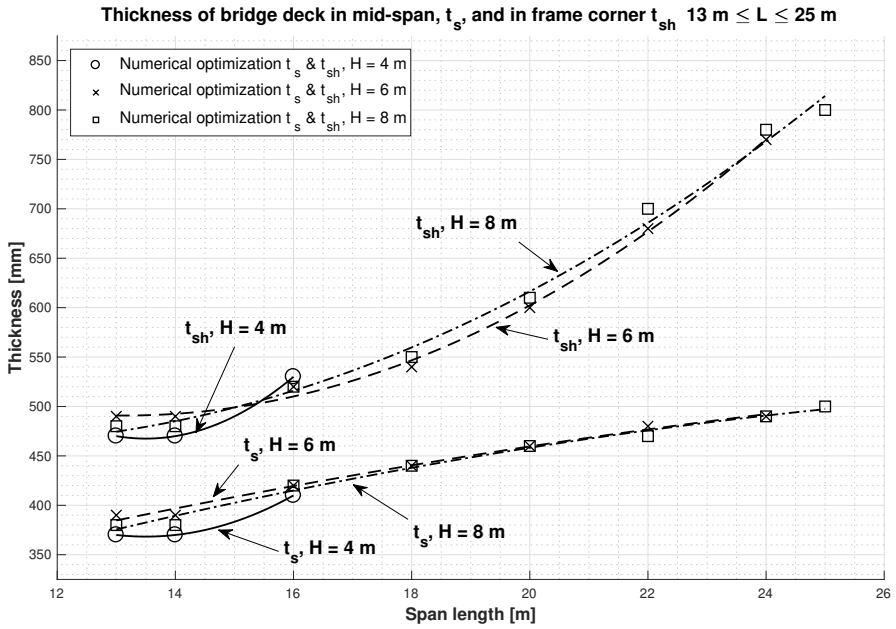

Figure 6.8 Thickness of the bridge deck slab (t_s) and at the end of the haunch (t_{sh}), respectively, as a function of the span length, for slab frame bridges with 13-25 m spans and fixed BC's. Results from numerical optimization of three-dimensional frames (scatter plots) are compared to trend lines for different bridge heights (H).

The equations to the trend lines, and their mean value of the standard errors, were determined to:

$$t_s^{H\,=\,4\ m} = 1585 - 180L + 6.67L^2\ [mm],\ \bar{\Delta} = 0\ mm \qquad 13\ m\ \leq L \leq 16\ m$$

$$t_s^{H\,=\,6\ m} = 185 + 18.3L - 0.23L^2\ [mm],\ \bar{\Delta} = 6\ mm \qquad 13\ m\ \leq L \leq 24\ m$$

$$t_s^{H\,=\,8\ m} = 135 + 22.8L - 0.33L^2\ [mm],\ \bar{\Delta} = 7\ mm \qquad 13\ m\ \leq L \leq 25\ m$$

$$t_{sh}^{H\,=\,4\ m} = 2290 - 270L + 10L^2\ [mm],\ \bar{\Delta} = 0\ mm \qquad 13\ m\ \leq L \leq 16\ m$$

$$t_{sh}^{H\,=\,6\ m} = 900 - 62.4L + 2.4L^2\ [mm],\ \bar{\Delta} = 8\ mm \qquad 13\ m\ \leq L \leq 24\ m$$

$$t_{sh}^{H\,=\,8\ m} = 630 - 33.8L + 1.6L^2\ [mm],\ \bar{\Delta} = 14\ mm \qquad 13\ m\ \leq L \leq 25\ m$$

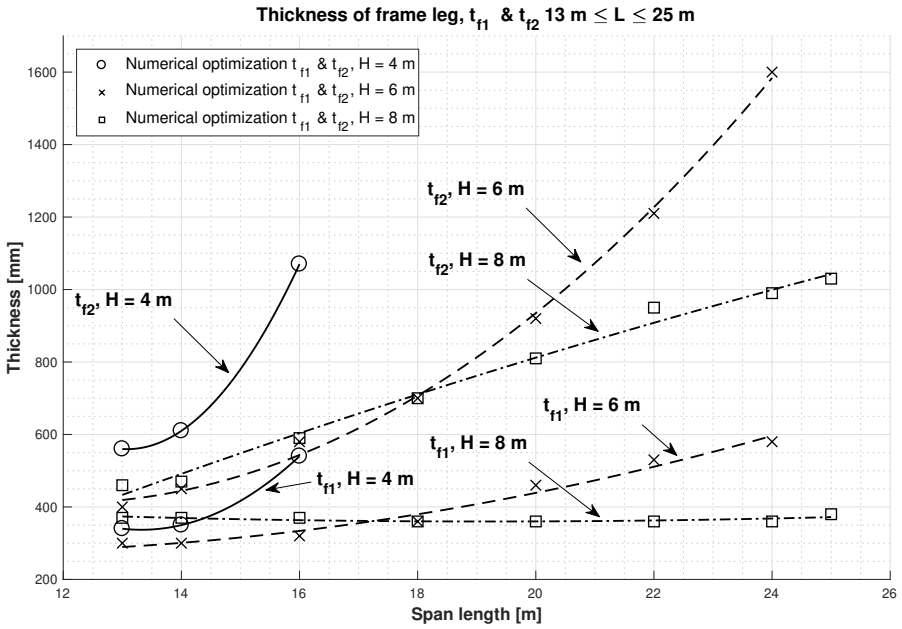

Figure 6.9 Thickness of the frame leg at the level of the foundation slab (t_{f1}) and in frame corner (t_{f2}), respectively, as a function of the span length for slab frame bridges with 13-25 m spans and fixed BC's. Results from numerical optimization of three-dimensional frames (scatter plots) are compared to trend lines for different bridge heights (H).

The equations to the trend lines, and their mean value of the standard errors, were determined to:

$$t_{f1}^{H\,=\,4\ m} = 5365 - 755L + 28.3L^2\ [mm],\ \bar{\Delta} = 0\ mm \qquad 13\ m\ \leq L \leq 16\ m$$

$$t_{f1}^{H\,=\,6\ m} = 435 - 32.64L + 1.63L^2\ [mm],\ \bar{\Delta} = 6\ mm \qquad 13\ m\ \leq L \leq 24\ m$$

$$t_{f1}^{H\,=\,8\ m} = 490 - 13.8L + 0.36L^2\ [mm],\ \bar{\Delta} = 7\ mm \qquad 13\ m\ \leq L \leq 25\ m$$

$$t_{f2}^{H\,=\,4\ m} = 10830 - 1570L + 60L^2\ [mm],\ \bar{\Delta} = 0\ mm \qquad 13\ m\ \leq L \leq 16\ m$$

$$t_{f2}^{H\,=\,6\ m} = 1555 - 192L + 8.1L^2\ [mm],\ \bar{\Delta} = 30\ mm \qquad 13\ m\ \leq L \leq 24\ m$$

$$t_{f2}^{H\,=\,8\ m} = -445 + 76.1L - 0.66L^2\ [mm],\ \bar{\Delta} = 30\ mm \qquad 13\ m\ \leq L \leq 25\ m$$

6.3 Environmental impact

As presented in Section 5.4, a comparison regarding environmental impact between several existing bridges and optimized bridge design was performed. The environmental impacts of the existing designs was evaluated and compared to potential environmental impacts of designs according to the results from the optimization study. The results are presented in Table 6.1. The calculations, including used dimensions and required reinforcement amounts can be found in Appendix H.

Table 6.1 Environmental impact of existing slab frame bridges and optimized design.

Bridge	L [m]	CO_2-eq *(Existing)*	CO_2-eq *(Optimization)*	Difference
L 814	6.0	14454 kg	11648 kg	19.4 %
Y 1283	10.0	19918 kg	15201 kg	23.7 %
Z 1060	14.5	30011 kg	23490 kg	21.7 %
Y 1217	18.0	42200 kg	32013 kg	24.1 %
A	11.5	34664 kg	25200 kg	27.3 %
B	13.6	35010 kg	21315 kg	39.1 %

7
Discussion

It is obvious that there is a potential in optimizing the cross-section from a structural point of view and there are several reasons for this.

7.1 General discussion about results

From the stiffness relation presented in equation (4.1), higher frame legs result in weaker frames which means that the span moment would be larger compared to a frame with shorter frame legs. With this argument the thickness of the deck slab would increase, which also applies in the analytical optimization, since more internal forces were attracted to the slab. However, in the numerical optimization this was not true to the same extent. The numerical optimization accounted for geometrical changes of the structural members, haunches, which enabled the frame to be stiffened locally in areas with high stress concentrations. When studying the results for different span lengths it is therefore important to studying the overall geometry of the frame and not only how a certain parameter may vary with an increased span length.

The massive frame legs for longer spans, in combination with the haunches, resulted in smaller slab thickness due to the increased rotational stiffness in the corners (and hence a larger bending moment in frame corners and smaller bending moment in span). The decisive design check for the frame legs in most cases was the shear capacity of the cross-sections without shear reinforcement (i.e. the frame legs). This was governed by the constraint for the optimization due to constructability. One can clearly see how the trend lines for the thickness of the frame legs increased slightly exponential for frames with pinned BC's, and to some extent for fixed BC's. This is reasonable since the capacity for shear failure varies slightly exponential, see Figure 7.1.

If shear reinforcement would have been used in the frame legs, it is obvious that the frame legs could have been more optimized with respect to slenderness. On the other hand, the internal force distribution would have been affected since the rotational stiffness of the frame corner would have changed, which might have affected the thickness of the bridge deck.

There are several constraints that affected the results. The constraint regarding the minimum allowed thickness of 300 mm affected the utilization ratios, and smaller

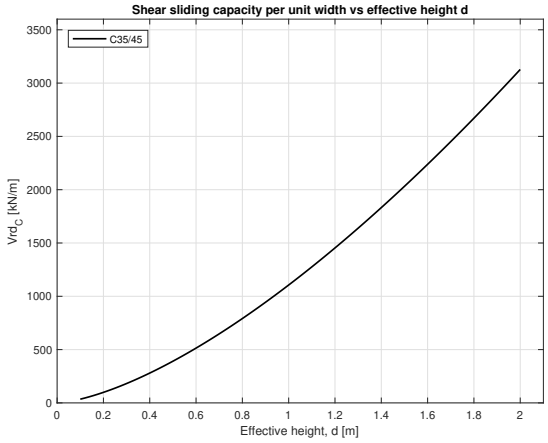

Figure 7.1 Concrete capacity against shear failure per unit width vs the effective height (d), for cross-sections without shear reinforcement.

dimensions might have been found without this constraint. The geometric constraints regarding haunches affected the internal force distribution. For frames with span lengths up to 12 m, right-angled triangular shaped haunches were used where the cathetus was prescribed to 500 mm. The haunches gave a large contribution to the capacity of the section and there is a potential in optimizing the haunch itself, or even investigate whether or not it should be used. According to a bridge engineer at WSP bridge department[1], the right-angled triangular shaped haunches may not be necessary, and are therefore neglected in some design cases in practice. The haunches with a length of a quarter of the span length may be designed as a parabola, to follow the bending moment curve and utilize more of the cross-section. This is, however, something that may be investigated in a future project.

Comparing the results between frames with pinned BC's to frames with fixed BC's one can see that the differences in thickness in mid-span of the bridge deck is small whereas the difference is a bit larger for the frame legs. The BC's did not affect the fundamental bending moment for each load in the frame corners considerably, and the bending moment was the decisive design check (in most of the cases) for the bridge deck. On the other hand, there is a larger difference in shear force in the frame legs for a frame with pinned and fixed BC's, respectively. This can be explained by studying the internal forces in the frame legs. The bending moment at the boundary for the frame with fixed BC's gives an additional contribution to the shear force.

The results from the comparison of carbon dioxide emissions for existing bridges showed that there is great potential in reducing the environmental impact of future slab frame bridges. The results showed a difference in carbon impact of 20-40 % compared to previous design. Considering the extent of slab frame bridges in Sweden, this reduction could have a large effect on the environmental impact of the infrastructure industry. Considering the infrastructure sector's goal regarding

[1](personal communication, 13 May 2020

reduction of carbon dioxide with 50 % by the year 2030, the reduction presented from the results could be a considerable part of that goal.

7.2 Comparison of optimization parameters between analytical and numerical analyses

The analytical two-dimensional study was performed to obtain an understanding of how slab frame bridges performed when studying the geometrical relations between the frame legs and the deck slab. Small changes in stiffness of the members affected the internal force distribution. Furthermore, the bending moment in frame corner increased with increased span length and decreased with an increased height of the frame.

The analytical optimization of two-dimensional frames was also performed to serve the three-dimensional finite element model with values of the optimization parameters that were close to the solution achieved from the numerical analyses, in that way the computational time decreased. This worked well for shorter span lengths where differences in the results were small. For longer span lengths the numerical model did have problems with convergence. It is possible that the initial guess of the parameters affected the optimization process and might forced the stiffness distribution in a certain way already at the first iteration. There are, however, considerable differences between the results obtained from the analytical and the numerical analyses. The results obtained from the numerical analyses demonstrates frames which are more optimized compared to the results from the analytical study. The differences may be explained by an amount of inequalities between the different studies but the two major reasons are:

- **Haunches**: Any influence of haunches have been neglected in the analytical analyses. Hence, a different force distribution is obtained and the optimization parameters are affected thereof. The critical design check in the two-dimensional study for longer spans was the check of bending moment in the frame corner of the bridge deck. This means that the thicknesses obtained by the analytical solution represents the required thickness in frame corners, and not the thickness in span.
- **Transverse force distribution**: In the analytical analyses, a meter "strip" of load field 1 was investigated. The model assumed a pure one-way behaviour whereas in the numerical analyses two load fields with different magnitude of the traffic loads have been taken into account, resulting in a transverse force distribution.

The effect of transverse force distribution has been investigated. A two-dimensional (strip) model has been analysed in Frame Analysis with a one-way behavior (model name Strip), and two different three-dimensional BRIGADE/Plus models. The BRIGADE/Plus models were modelled with a one-way and two-way behavior, respectively. The model with a one-way behavior (model name B1) was subjected

to loads of equal magnitude in both load fields whereas the model with a two-way behavior was subjected to different magnitude of the loads in the two load fields (model name B2). The differences in bending moments in frame corners and mid-span are given in percentage and are summarized in Table 7.2 and 7.1.

Table 7.1 Difference in bending moments between the BRIGADE/Plus model with one-way behaviour (B1) compared to the two-dimensional frame model (Strip).

L [m]	H [m]	Difference, span [%]	Difference, corner [%]
6	6	8.3	4.8
12	6	4.2	3.9
18	6	2.6	4.2
24	6	1.8	5.0

Table 7.2 Difference in bending moments between the BRIGADE/Plus model with a two-way behavior (B2) compared to the two-dimensional frame model (Strip).

L [m]	H [m]	Difference, span [%]	Difference, corner [%]
6	6	1.3	4.6
12	6	-9.8	-10.3
18	6	-15.7	-15.9
24	6	-18.6	-19.6

The values in Table 7.1 indicates that the differences in bending moments in the longitudinal section of the bridge increases with an increased span length. The notable difference may be explained by the compatibility condition of the deflection. If the slab is divided into strips along the longitudinal and transverse direction of the bridge and that the load is unevenly distributed (like in the numerical analyses) the deflection of the different strips must be dependent on each other, to fulfil the compatibility condition. Hence, the load is spread in the transverse direction of the bridge. Since the deflection does not depend linearly on the span length the amount of load that is spread in the transverse direction of the bridge increases exponentially.

7.3 Comparison between optimized parameters and existing slab frame bridges

When comparing the results with currently used suggestion of dimensions (Vägverket, 1996, p. 42), shown in Figure 7.2, a large difference can be seen.

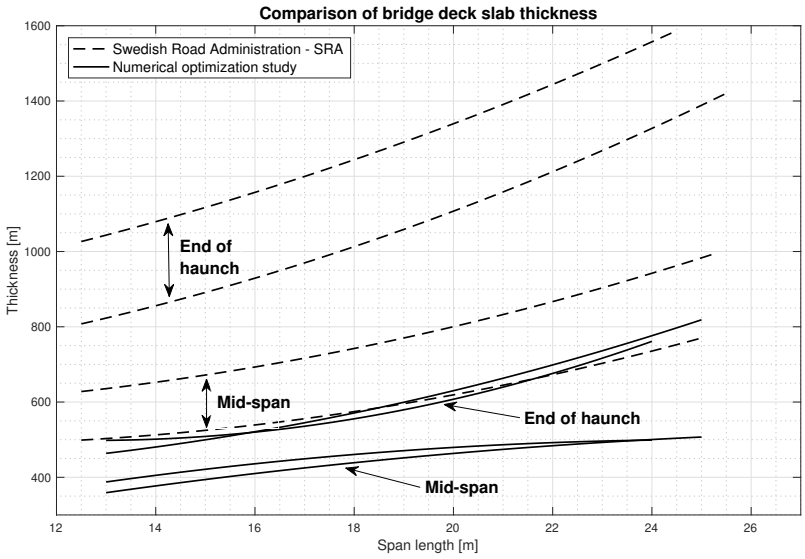

Figure 7.2 Old recommendations of thickness for the bridge deck (Vägverket, 1996, p. 42) and trend lines from optimization study.

The methodology SRA (Swedish Transport Administration) applied when developing the graphs are based on statistics from existing slab frame bridges. Consequently, the graphs do not represent optimized cross-sections with respect to slenderness and reinforcement amount. Vägverket (1996, p. 42) point out that the designer should be careful with optimizing the slenderness of the cross-section since the slab frame bridges in most cases already are heavily reinforced. One may argue that the graphs are based on this advice, and that the aim was to increase the height of the cross-section to decrease the reinforcement amount, rather than slenderness. Moreover, if the designers in the past implemented two-dimensional analytical analyses when designing slab frame bridges this does also affect the parameters and so also the background to the statistics presented by SRA.

The results from the numerical optimization study were compared with previously constructed bridges according to the statistics presented in Section 5.4, and the differences turned out to be significant. Table 7.3 shows statistics of the slab thickness in mid-span and adjacent to the frame corners from SRA (Vägverket, 1998, p. 3-5) and from the optimization study.
It can clearly be seen that there is a great potential in optimizing slab frame bridges. The comparison study indicates that the difference in thickness increases with an increased span length. Again, SRA does not explain or give any information about

Table 7.3 Comparison of thickness in mid-span and end of haunch between designed slab frame bridges (Vägverket, 1998, p. 3-5) and optimized thickness.

Bridge	L [m]	t_s/t_{sh} [mm] (SRA)	t_s/t_{sh} [mm] (Optimization study)	Difference span/end of haunch [%]
L 814	6.0	350/850	300/800	14.3/5.9
Y 1283	10.0	450/950	350/850	22.2/10.5
Z 1060	14.5	550/750	410/510	25.5/32.0
Y 1217	18.0	730/930	460/560	37.0/40.0

the full design. The design of the frame legs are not published, but are of great interest in order to study the differences fully. The results obtained from the optimization study are based on several constraints. Shear reinforcement was assumed in the haunch, which (in most cases) eliminates problems with shear and, hence, the decisive check is the moment capacity of the section. By assuming a large amount of reinforcement the effective height can be reduced and thus the thickness of the cross-section.

The large differences in thickness between the results and existing bridges were validated by studying a case study performed by Solat Yavari, Pacoste, and Karoumi (2014) where the optimization potential of slab frame bridges is presented. According to Solat Yavari et al. (2014), the reduction in thickness for the structural parts of a slab frame bridges could be reduced with 40-50 % using the method of *pattern search optimization*, compared to an existing bridge. The optimized dimensions of the bridge would result in a 20 % reduction in production cost. However it is not stated if any constraint regarding minimum thickness due to constructability was implemented in the case study.

The results from the comparison of environmental impact presented in Section 6.3 indicates that there is also a great potential in reduction of carbon dioxide of slab frame bridges. As for the comparison of thicknesses, the reduction increases with longer spans. Again, it should be noted that due to lack of information about the bridges presented by SRA, assumptions regarding dimensions and height of frame legs has been made which will influence the actual percentage reduction. In addition to those assumptions, several assumptions and simplifications regarding reinforcement layout and curtailment has been implemented which results in uncertainties regarding actual reinforcement amount. However, the difference in environmental impact was larger for the two bridges where the geometry of the frame legs is known, which might indicate that the assumptions used for the other bridges are conservative.

7.4 Simplification and potential source of error

It is important to discuss potential sources of errors, but also to investigate the reactions of the results from experienced bridge engineers. When practicing engineers

make a design of slab frame bridges it is common that they use their experience to determine preliminary dimensions of the structural members, or by using the recommendations from the SRA. Some engineers does also maximize the slab thickness in a preliminary stage. By doing this the engineer eliminates the risk that the section heights need to be increased later on in the project, causing increased efforts and increased costs compared to the plan. Hence, the results obtained in this report might show surprisingly large potential for carbon reduction since the effective height is compensated by the reinforcement amount.

The results have also been discussed with a bridge engineer at WSP in Stockholm[2]. The engineer confirms the reliability of the results and that the optimization parameters follows his experience. The bridge engineer does also give information about the recommendations of dimensions given by the SRA. The recommendations are based on statistics of designed slab frame bridges and are not optimized in any terms of slenderness. However, potential sources of errors that might have affected the results are:

- **Edge beams**: Edge beams have been neglected in the study. When edge beams are integrated with the superstructure the effect of transverse force distribution increases which, locally, would have affected the internal force distribution.
- **Loads excluded**: Loads such as pore water pressure, low and high ground water level have been discussed with the supervisors of the project and has been neglected to ease the time spent on building the numerical model.
- **Vertical traffic load**: The placement of the vertical traffic loads have been predefined according to the theory of how to place the loads on the bridge deck to obtain maximum load effects. However, the ignorance of moving the vehicle loads leads to uncertainties if the maximum load effects are found, and in a full design moving the vertical traffic load is preferable. Moreover, the simplification affects the total reinforcement amount calculated in the comparison study about carbon dioxide impact since moving vehicle loads is important in the design of curtailment of the reinforcement.
- **Constraints**: The constraints have been defined after discussions with the supervisors and the answers from the interview regarding constructability. It is worth mentioning that it is hard to predict the constraints without practical experience of constructing slab frame bridges, so the interview with practicing contractors have been highly appreciated. However, a potential source of error is if the respondents interpreted the questions correctly.

The shear capacity was only evaluated in two sections of the bridge deck; at the mid-span and in the haunch. The shear force in mid-span was usually small and therefore no shear reinforcement was assumed. In the section for maximum shear force, near the support, the capacity was calculated with shear reinforcement. It is not stated how far into the bridge deck it is viable to have shear reinforcement due to cost and constructability. Potentially there exists a section outside the haunch

[2](personal communication, 13 May 2020)

were shear reinforcement is not wanted but where the shear force is rather large. This might result in another section that can be decisive for the slab thickness which have not been studied in the project.

The comparison study related to the carbon dioxide impact clearly showed how the total CO_2 - equivalents decreased when the concrete volume decreased (i.e., the total cement content), even though the reinforcement amount increased. However, the carbon dioxide impact from reinforcement varied dependent on what type of reinforcement that was used (Table 2.4). Thus, using recycled reinforcement is preferable. Some assumptions when calculating the CO_2 - equivalents were made, as presented in section 5.4, and it is therefore more reasonable to look at the general trend of CO_2 - equivalents (decreased environmental impact for slender, heavy reinforced cross-sections), rather than the actual values of the environmental impact.

The costs decreased with increased slenderness to a certain limit, where the reinforcement cost governed the total costs. The cost of reinforcement is flexible and depends on the market situation. The small increase in costs for very slender cross-section has been neglected since the environmental advantages of slender cross-section was considered to be more important.

7.5 Optimization algorithm

The optimization algorithm used in the study was based on that the design checks that generated the highest utilization ratio decided what thickness that should be used in the next iteration. This resulted in that the design check that was decisive in the first iteration decided the following iterations and therefore the outcome of the optimization. This means that far from every possible combination was tested since the very first iteration limited the search and decided in which direction the optimization turned out. Other optimization algorithms such as pattern search methods or genetic algorithm would evaluate many more combination of the optimization parameters and might generate other results that still has fulfilled the constraints of utilization ratios. These optimization algorithm is however more computationally heavy.

The optimization objective used in the study was based on the comparison of optimal cross-section presented in section 2.9. The comparison showed that the environmental impact decreases with decreased thickness. However, it is not certain that the absolute optimized dimensions and ratios of concrete and reinforcement was generated by using this optimization objective. As presented in figure 2.13, there might be a combination of reinforcement and concrete that results in minimum environmental impact which was not reached in this optimization. An alternative approach would have been to evaluate the total environmental impact at the end of each iteration. In that case the optimization objective would be to minimize the total EMC-value directly. In this study, the optimization objective was simplified to minimized thickness in order to save computational time and ease the complexity in the optimization.

Another approach could be to perform a full-scale parameter study, where a large number of combinations of the thicknesses of the structural parts is tested. The results from every combination would be evaluated afterwards and the combination that results in the smallest EMC-value and cost but still fulfills design requirements could be located. However, this method is very computationally heavy and generates a large amount of data that needs to be analyzed.

8

Conclusion

The project indicates that there is a considerable possibility of optimizing slab frame bridges with respect to investment costs and environmental impact. In general, one can conclude that the environmental impact and investment costs decreases with increased slenderness of the cross-section and that it is more favourable to decrease the thickness of the structural members and compensate with reinforcement. However, the report does also indicate that the investment and labour cost might increase for very slender cross-sections, and that this depends on the material cost related to the reinforcement amount.

In case of designing slab frame bridges, the report shows differences in the design depending on which method that is applied. An analytical two-dimensional representation of a frame, where a strip in the longitudinal section of the bridge was investigated, results in optimization parameters that are conservative. A three-dimensional numerical model, on the other hand, is preferable to use in order to take transverse force distribution into account. In addition, the geometry of the bridge can be defined easily and, hence, a more reliable stiffness distribution of the frame is used.

The optimization method implemented tends to affect the optimization process. The frame is sensitive to changes in stiffness and when a design check starts to be critical in a certain section the optimization parameter is updated accordingly. This results in a section that in the upcoming iteration is stiffer and therefore attracts a larger portion of internal forces, and the optimization parameter does have to be updated again.

The results from the optimization are intended to be used in a preliminary stage of a project. A final, detailed design might therefore differ from the results presented.

It can be concluded that use of dimensions according to old recommendations presented by SRA, Vägverket (1996, p. 42), will not result in an optimized design, nor with respect to carbon dioxide emissions or with respect to costs. The potential effect in reduction of carbon emission by implementing optimization in design is great.

8.1 Further studies

The thesis evokes several aspects of the study that would be interesting and necessary to investigate further:

- The total potential of reduction of environmental impact of slab frame bridges needs further investigation in order to obtain an absolute optimized structure with respect to environmental impact. For instance choices regarding exponent class and strength class of concrete and their effect on the environmental impact of the structure can be implemented in the optimization.
- The optimal ratio between concrete and reinforcement needs to be investigated further. Effects of concrete classes and types of concrete can be implemented in this investigation and thereby finding optimized combination for different conditions and requirements on the concrete.
- Since this thesis is limited to straight slab frame bridges, the graphs needs to be complemented with additional results for skewed slab frame bridges to cover any type of geometry of the road. Skewed slab frame bridges will result in larger moment in the corners with obtuse angle, which will influence the required thicknesses.
- Investigate how the preliminary design of slab frame bridges affects by implementing alternative optimization methods, such as a full scale parametric study, compared to the results obtained in this report.

References

AB Svenska Byggtjänst, & Cementa AB. (1994). *Betonghandboken - Material* (2nd edition). Stockholm: AB Svensk Byggtjänst.

Algers, B., Forsby, L., & Tell, W. (1959). *Bygg - Handbok för hus-, väg- och vattenbyggnad* (3rd edition). Stockholm: Byggmästarens förlag.

Almén, R. (2016). Division of Structural Engineering Investigation of cracking due to restraint forces in Swedish concrete slab frame bridges Utredning om sprickor orsakade av tvångskrafter i svenska betongplattrambroar.

Behrooz, H., & Hinton, E. (1999). *Homogenization and Structural Topology Optimization: Theory, Practice and Software*. doi:10.1007/978-1-4471-0891-7

Betonginitiativet. (2018). *Betonginitiativet – Färdplan för klimatneutral betong*.

Bhatti, M. A. (2000). *Practical Optimization Methods*. doi:10.1016/b978-0-12-805322-5.00006-x

Boverket. (no date). Miljöpåverkan ökar från byggsektorn. Retrieved from https://www.boverket.se/sv/om-boverket/publicerat-av-boverket/nyheter/miljopaverkan-okar-fran-byggsektorn/

Boverket. (2004). Boverkets handbok om betongkonstruktioner, BBK 04, 273.

Celsa Steel Service AS. (2015). *Environmental Product Declaration - Steel reinforcement products for concrete*.

Cementa AB. (2014a). *Environmental Product Declaration - Portland Cement CEM I 42.5 N-SR3/MH/LA*.

Cementa AB. (2014b). *Environmental Product Declaration - Portland Fly Ash Cement CEM II/A-V 42.5 N*.

CEN. (2002). *EN 1990 Eurocode - Basis of structural design*. CEN European Committee for Standardization. Brussels.

CEN. (2003a). *EN 1991-1-5 Eurocode 1: Actions on Structures - Part 1.5: General actions - Thermal actions*. CEN European Committee for Standardization. Brussels.

CEN. (2003b). *EN 1991-2 Eurocode 1: Actions on structures - Part 2: Traffic loads on bridges*. CEN European Committee for Stardardization. Brussels.

CEN. (2004). *EN 1992 Eurocode - Design of concrete structures* (technical report Number 138227). CEN European Committee for Standardization. Brussels.

Chalouhi, E. K. (2019). *Optimal design solutions of concrete bridges considering environmental impact and investment cost*. KTH Architecture and the Built Environment. Stockholm, Sweden.

Difs, J., & Karlsson, F. (2015). Preliminärdimensionering av plattrambroar med parallelliserade FEM-analyser enligt SBD, 60.

Ecoinvent. (2019). Ecoinvent 3.6 Database. Retrieved from https://www.ecoinvent.org/database/ecoinvent-36/ecoinvent-36.html

Engström, B. (2014). Design and analysis of slabs and flat slabs, 78.

Fossilfritt Sverige. (2018). *Färdplan för fossilfri konkurrenskraft Bygg- och anläggningssektorn*.

Francisco, M., Revollar, S., Vega, P., & Lamanna, R. (2005). *A comparative study of deterministic and stochastic optimization methods for Integrated Design of processes*. doi:10.3182/20050703-6-cz-1902.00917

Geoff, H., & Craig, J. (2008). *Embodied Carbon - The Inventory of Carbon and Energy*. The University of Bath. doi:10.1680/ener.2008.161.2.87

Göransson, O., & Nilsson, A. (2017). *Totalkostnadsanalys av armeringshantering*. Tekniska Högskolan vid Linköpings Universitet.

Gould, N. I. M., & Leyffer, S. (2003). An Introduction to Algorithms for Nonlinear Optimization, 109–197. doi:10.1007/978-3-642-55692-0{_}4

Johansson, M., Plos, M., & Pacoste, C. (2012). *Recommendations for finite element analysis for the design of reinforced concrete slabs*. Stockholm.

Lee, J. (2004). A First Course In Combinatorial Optimization. *36*.

Ljungberg, T. (no date). *Brobyggnad*, Stockholms Tekniska Institut.

Mathisen, K. M. (2012). Solution Methods for Nonlinear Finite Element Analysis (NFEA). Trondheim: Norwegian University of Science and Technology.

Norcem AS. (2013). *Environmental Product Declaration - CEM I , Anleggsement (CEM I 52 , 5N), Industrisement (52 , 5R) og Standardsement (CEM I 42 , 5R)*.

Norcem AS. (2014). *Environmental Product Decleration - CEM II , Anleggsement FA (CEM II / A-V) and Standardsement FA (CEM II / B-M)*.

Pucher, A. (1958). *Einflußfelder elastischer Platten* (Zweite Auf). Wien: Springer-Verlag.

Python.org. (2020). Retrieved from https://www.python.org

Scanscot Technology AB. (2018). BRIGADE Plus - User's Manual. Stockholm: Scanscot Technology AB.

Sioshansi, R., & Conejo, A. J. (2017). Optimization in Engineering: Models and Algorithms. *Springer Optimization and Its Applications*, *120*, 422. doi:10.1007/978-3-319-56769-3

Solat Yavari, M. (2017). *Slab Frame Bridges - Structural Optimization Considering Investment Cost and Environmental Impacts* (Doctoral dissertation, KTH Royal Institute of Technology).

Solat Yavari, M., Pacoste, C., & Karoumi, R. (2014). *Structural optimization of concrete slab frame bridges using heuristic algorithms*. Stockholm, Sweden.

Trafikverket. (2008). *Kodförteckning och beskrivning av Brotyper*. doi:10.1007/s11947-009-0181-3

Trafikverket. (2016). Råd Brobyggande - TDOK 2016:0203. *3*, 33.

Trafikverket. (2019a). Modell - Klimatkalkyl. Retrieved from http://webapp.trafikverket.se/Klimatkalkyl/Modell

Trafikverket. (2019b). *TDOK 2016:0204 - Krav Brobyggande*.

Transportstyrelsen. (2018). *TSFS 2018:57 -Transportstyrelsens föreskrifter och allmänna råd om tillämpning av eurokoder*.

Vägverket. (1996). Broprojektering - En Handbok.

Vägverket. (1998). *Brotyper - Statistik om broar byggda enligt BRO 94*. Avdelningen för bro och tunnel. Borlänge.

Venkataraman, S., & Haftka, R. T. (2004). Structural optimization complexity: What has Moore's law done for us? *Structural and Multidisciplinary Optimization*, *28*(6), 375–387. doi:10.1007/s00158-004-0415-y

Wåhlin, E. (1947). *Bygg - I Allmänna Grunder*. Stockholm: Tidskriften Byggmästaren.

Wynn, D. C., Eckert, C. M., & Clarkson, P. J. (2007). *Modelling Iteration in Engineering Design*. University of Cambridge. Cambridge.

Yavari, M. S., Pacoste, C., & Karoumi, R. (2016). Structural Optimization of Concrete Slab Frame Bridges Considering Investment Cost. *Journal of Civil Engineering and Architecture*, *10*(9), 982–994. doi:10.17265/1934-7359/2016.09.002

Zangeneh Kamali, A., Johansson, M., & Svedholm, C. (2013). *Effects of restrained thermal strains in transversal direction of concrete slab frame bridges*. KTH Stockholm. Stockholm.

Zielinski, K., & Laur, R. (2008). *Stopping Criteria for Differential Evolution in Constrained Single-Objective Optimization*. Bremen.

A

Interview regarding Constructability

Interview 1:

- **Påverkas arbetskostnaden för armeringsläggning / kg armering av tvärsnittets slankhet? Förutsätt samma armeringsmängd och armeringsutformning. Se bild.**

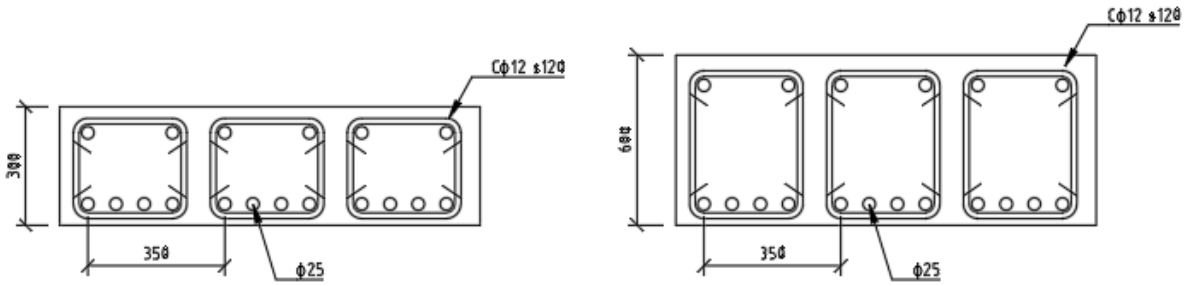

Svar: *Ingen större påverkan mellan figurerna ovan.*

- **Ser ni någon begränsning i tvärsnittets slankhet på en platta kan vara med två lager armering med hänsyn till byggbarhet? (Exempelvis plattjocklek 300mm) Förutsätt att konstruktören har gjort en teoretisk genomförbar armeringsutformning.**

Svar: *400 mm låter genomförbart.*

- **Ser ni en begränsning i antal lager armering i en plattrambro med avseende på byggbarhet?**

Svar: *Upp till 3 lager funkar men det är ju sällan så många lager behövs*.

- **Hur påverkas arbetskostnaden för armeringsläggning för lager 3 jämfört med lager 2? Se bild.**
  Säg att arbetskostnad för lager två är 1000 kr/ timme.

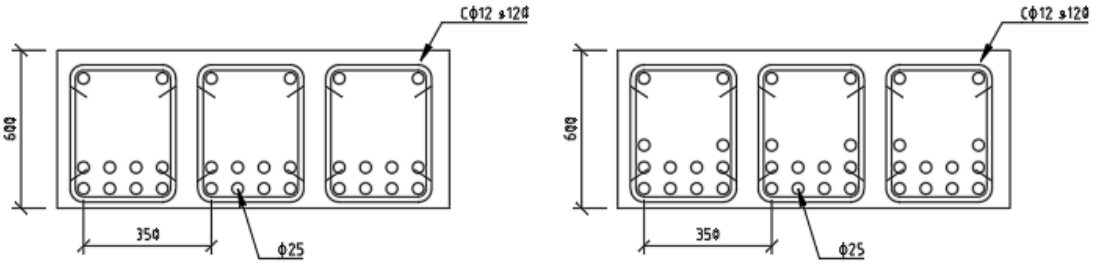

Svar: *Ungefär samma*

- **Hur är er övergripande inställning till skjuvarmering i ramben på en plattrambro? Om skjuvarmering i ramben anses problematisk; varför?**

  Svar: *Skjuvarmering utförd som dubbla C-järn brukar funka men skönt att slippa.*

  En fördel är om man får ”häftsvetsa” byglarna i monteringsjärn och kan förtillverkas som korgar(balkar).

Interview 2:

- **Påverkas arbetskostnaden för armeringsläggning / kg armering av tvärsnittets slankhet? Förutsätt samma armeringsmängd och armeringsutformning. Se bild.**

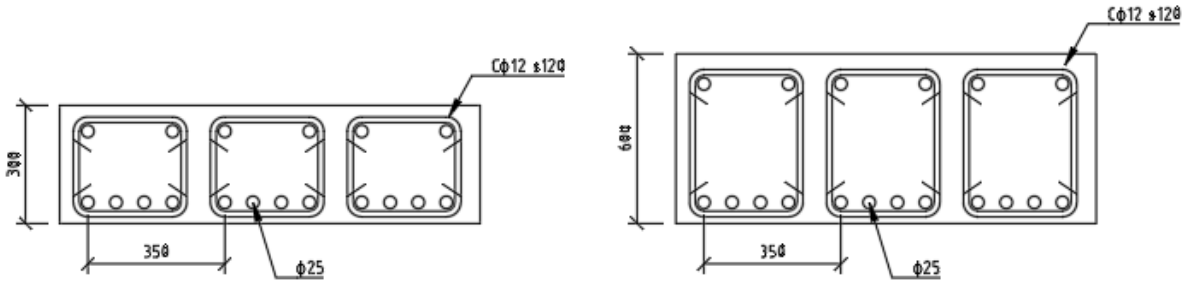

Svar: *Ingen större skillnad.*

- **Ser ni någon begränsning i tvärsnittets slankhet på en platta kan vara med två lager armering med hänsyn till byggbarhet? (Exempelvis plattjocklek 300mm) Förutsätt att konstruktören har gjort en teoretisk genomförbar armeringsutformning.**

Svar: *Ju tunnare platta desto svårare att få till överkantsarmeringen*

- **Ser ni en begränsning i antal lager armering i en plattrambro med avseende på byggbarhet?**

Svar: *Inte direkt om man följer övriga rekommendationer om avstånd mellan stänger o.s.v*

- **Hur påverkas arbetskostnaden för armeringsläggning för lager 3 jämfört med lager 2? Se bild.**
Säg att arbetskostnad för lager två är 1000 kr/ timme.

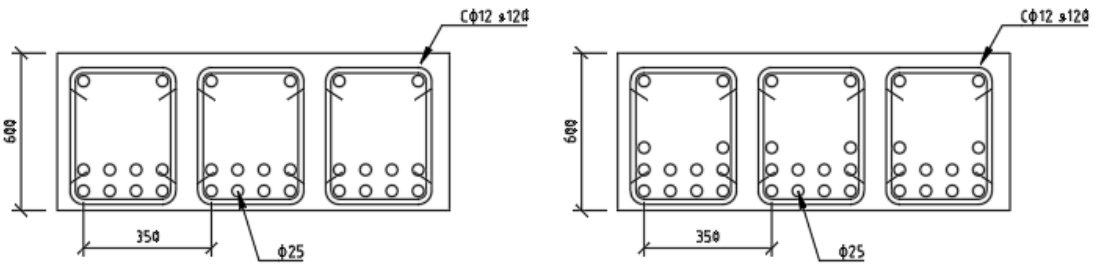

Svar: *Väldigt svårt att bedöma. Ingen större extra kostnad tror jag.*

- **Hur är er övergripande inställning till skjuvarmering i ramben på en plattrambro? Om skjuvarmering i ramben anses problematisk; varför?**

  Svar: *Skjuvarmering är alltid besvärlig och kostar ganska mycket oavsett var den sitter. Gör man det som N-byglar skall all armering träs i. Gör man dubbla c-byglar är det svårt att få den i rätt läge.*

Interview 3:

- **Påverkas arbetskostnaden för armeringsläggning / kg armering av tvärsnittets slankhet? Förutsätt samma armeringsmängd och armeringsutformning. Se bild.**

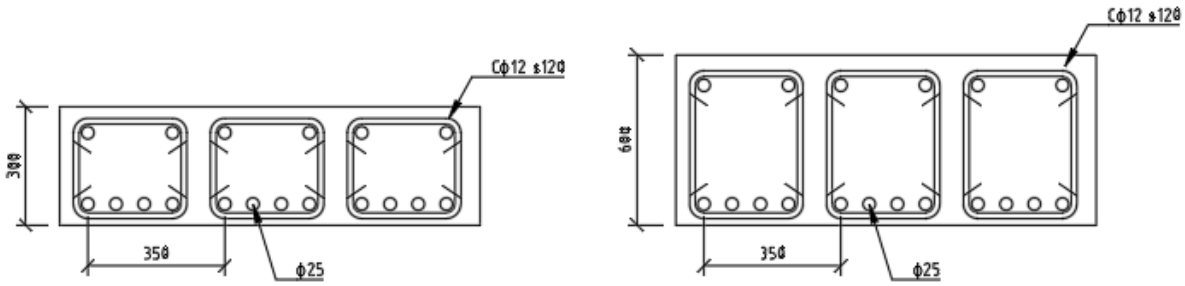

Svar: *Om man utgår helt från figuren d.v.s exakt lika armering med bara en förändring av d.v.s tvärsnittsmåttet så är det samma timkostnad/kg armering.*

- **Ser ni någon begränsning i tvärsnittets slankhet på en platta kan vara med två lager armering med hänsyn till byggbarhet? (Exempelvis plattjocklek 300mm) Förutsätt att konstruktören har gjort en teoretisk genomförbar armeringsutformning.**

Svar: *Med två lager armering förmodar jag att ni menar två lager armering i respektive sida.*

Om man utgår från att minsta armeringsdiameter är 16 mm. Vidare täckskikt ca 40 mm så innebär det att det undre lagret hamnar så långt in i ett 300 mm tvärsnitt att armeringen knappast blir verksam. Av denna anledning bör tvärsnittet ha minst 400 mm tvärsnittsmått för att fungera rent konstruktivt.

Detta stämmer även med avseende på byggbarhet.

- **Ser ni en begränsning i antal lager armering i en plattrambro med avseende på byggbarhet?**

Svar: *Med avseende på såväl byggbarhet som arbetskostnad per kg armering så skall man så långt möjligt sträva efter att ha ett lager. I särskilt påkända delar som över stöd, hörn eller i fältmitt kan två lager lokalt förekomma. Detta är enligt mitt synsätt en ganska optimal armeringsutformning med tanke på byggbarhet.*

- **Hur påverkas arbetskostnaden för armeringsläggning för lager 3 jämfört med lager 2? Se bild.**
  Säg att arbetskostnad för lager två är 1000 kr/ timme.

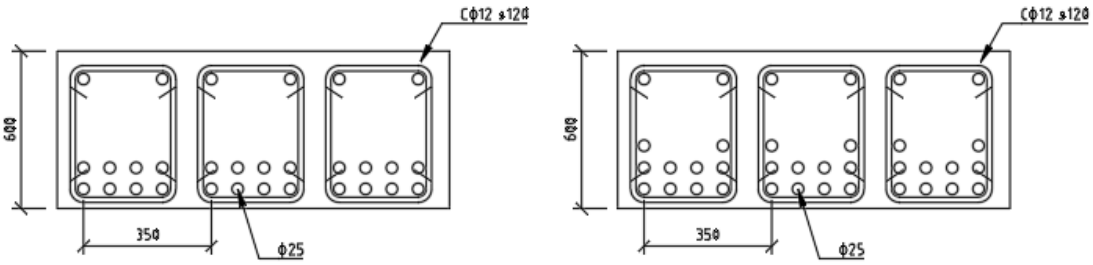

Svar: *Komplexiteten i armeringslängden ökar med antalet lager. Min uppfattning är att arbetskostnaden för lager 3 fördubblas.*

- **Hur är er övergripande inställning till skjuvarmering i ramben på en plattrambro? Om skjuvarmering i ramben anses problematisk; varför?**

Svar: *Min uppfattning är att skjuvarmering så långt möjligt skall undvikas i såväl platta som ramben. Den gör att man tappar mycket i byggbarhet, varvid arbetskostnaden stiger.*

Anledningen är att skjuvarmeringen är svår att få på plats även om man använder mötande C-byglar som på bilden. Problemen är att få de mötande schenklarna på plats eftersom det skall vara en omlottskarv där stängerna ligger intill varandra. Detta är svårare att få på plats i ett ramben än i en platta.

I plattan går det vanligen inte att undvika helt utan det finns åtminstone i stödsnitt.

I ramben där man kan dra nytta av normalkraftens positiva effekt på tvärkraftskapaciteten finns goda möjligheter att undvika skjuvarmering om man väljer en rimlig konstruktionstjocklek.

B

Vehicle models presented by Swedish Transport Agency

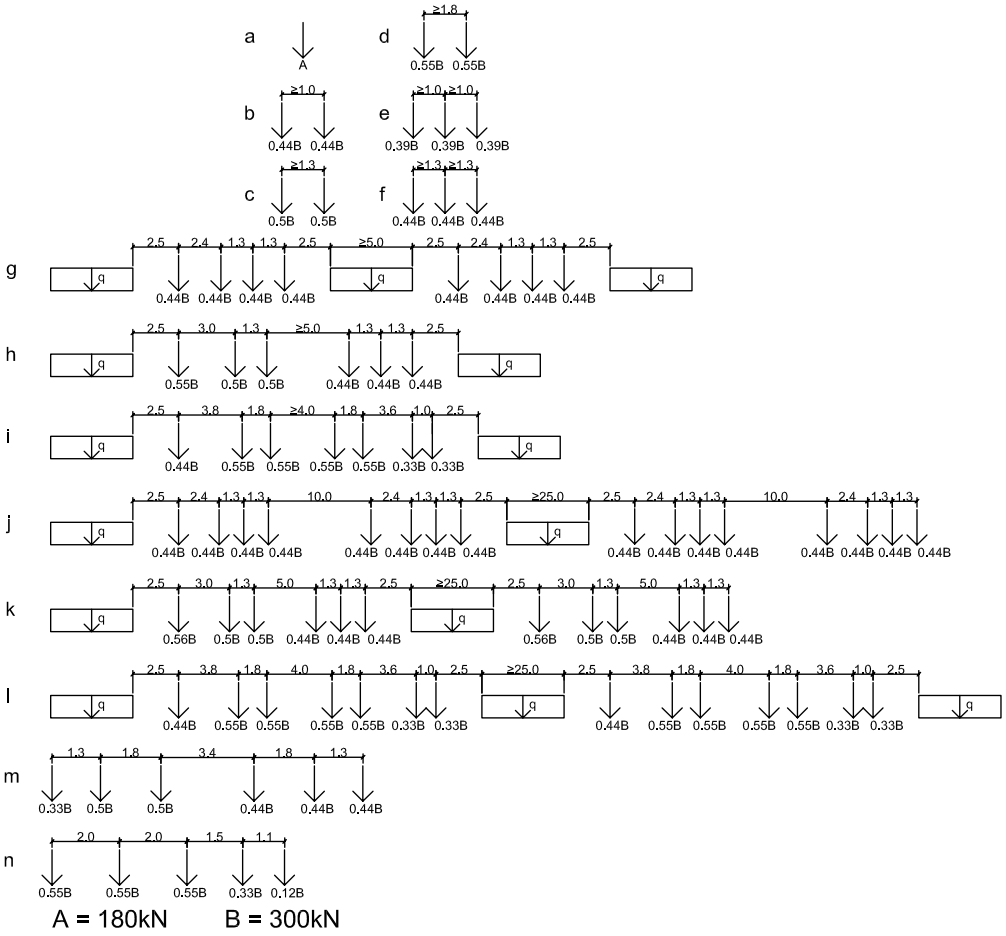
a
A
d
≥1.8
0.55B 0.55B
b
≥1.0
0.44B 0.44B
e
≥1.0 ≥1.0
0.39B 0.39B 0.39B
c
≥1.3
0.5B 0.5B
f
≥1.3 ≥1.3
0.44B 0.44B 0.44B
g
2.5 2.4 1.3 1.3 2.5 ≥5.0 2.5 2.4 1.3 1.3 2.5
q
0.44B 0.44B 0.44B 0.44B 0.44B 0.44B 0.44B 0.44B
h
2.5 3.0 1.3 ≥5.0 1.3 1.3 2.5
q
0.55B 0.5B 0.5B 0.44B 0.44B 0.44B
i
2.5 3.8 1.8 ≥4.0 1.8 3.6 1.0 2.5
q
0.44B 0.55B 0.55B 0.55B 0.55B 0.33B 0.33B
j
2.5 2.4 1.3 1.3 10.0 2.4 1.3 1.3 2.5 ≥25.0 2.5 2.4 1.3 1.3 10.0 2.4 1.3 1.3
q
0.44B 0.44B 0.44B 0.44B 0.44B 0.44B 0.44B 0.44B 0.44B 0.44B 0.44B 0.44B 0.44B 0.44B 0.44B 0.44B
k
2.5 3.0 1.3 5.0 1.3 1.3 2.5 ≥25.0 2.5 3.0 1.3 5.0 1.3 1.3
q
0.56B 0.5B 0.5B 0.44B 0.44B 0.44B 0.56B 0.5B 0.5B 0.44B 0.44B 0.44B
l
2.5 3.8 1.8 4.0 1.8 3.6 1.0 2.5 ≥25.0 2.5 3.8 1.8 4.0 1.8 3.6 1.0 2.5
q
0.44B 0.55B 0.55B 0.55B 0.55B 0.33B 0.33B 0.44B 0.55B 0.55B 0.55B 0.55B 0.33B 0.33B
m
1.3 1.8 3.4 1.8 1.3
0.33B 0.5B 0.5B 0.44B 0.44B 0.44B
n
2.0 2.0 1.5 1.1
0.55B 0.55B 0.55B 0.33B 0.12B
A = 180kN
B = 300kN

C

Comparison of vertical traffic load in 2D-models and 3D-models

Comparison study between modeling in 2D and 3D - Bending moments caused by traffic loading (LM1)

H = 6m, L = 6m

2D Frame Analyses:

Traffic lane 1, w=3m , No influence of transverse load distribution

Q=270/3m = 90kN/m

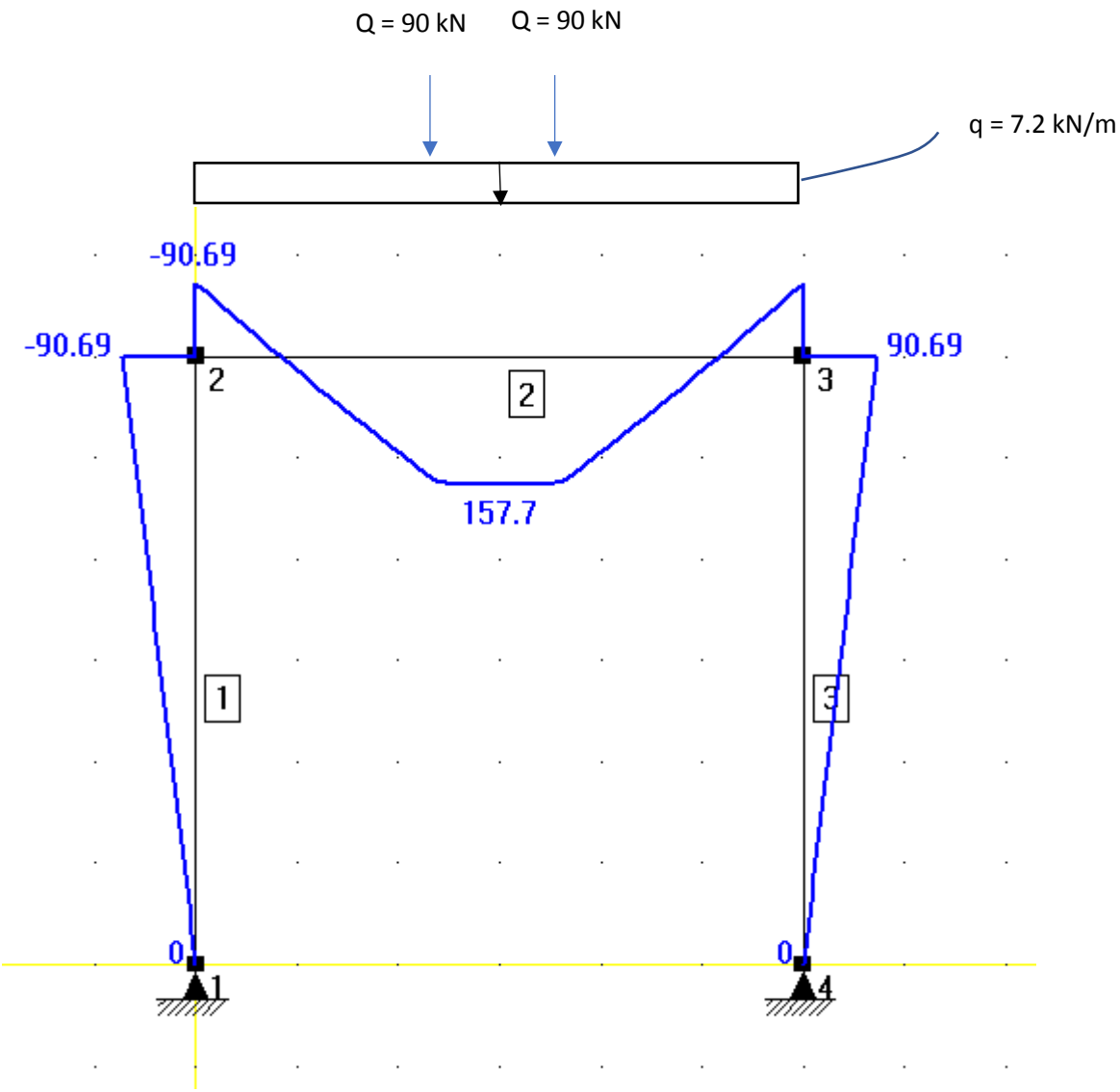

Brigade plus:

Traffic lane 1, w=3m, Q=270/2 kN, q=7.2 kN/m^2

Traffic lane 2, w=3m, Q=180/2 kN, q=2.5 kN/m^2

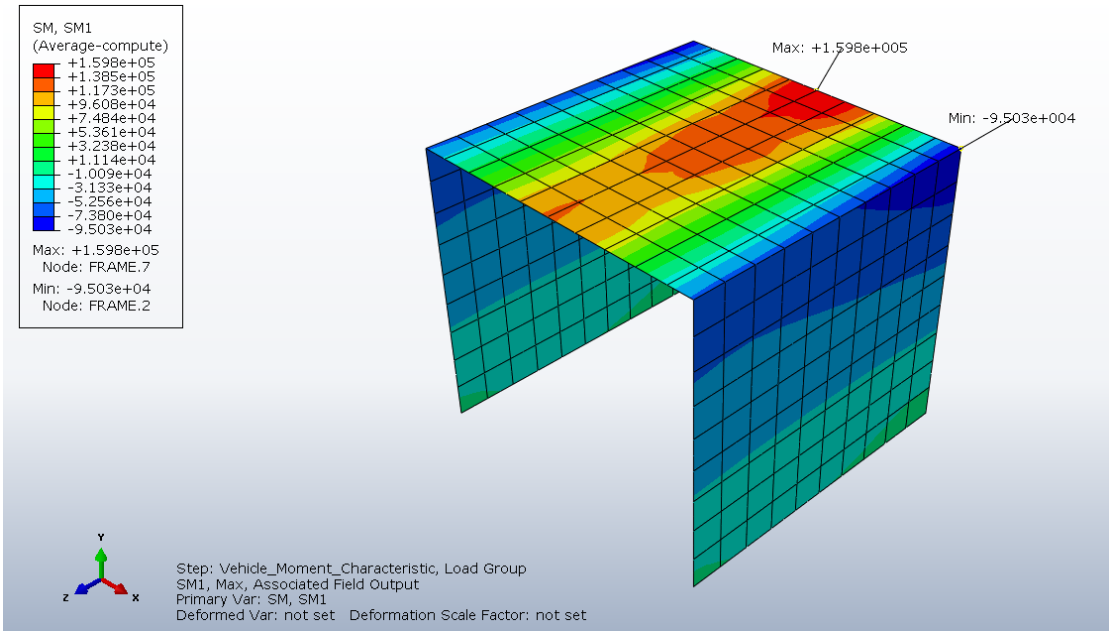

Difference field moment compared to frame analyses: 1,33 %

Difference in corner moment compared to frame analyses: 4,78%

Brigade plus:

Traffic lane 1, w=3m, Q=270/2 kN, q=7.2 kN/m2

Traffic lane 2, w=3m, Q=270/2, , q=7.2 kN/m2

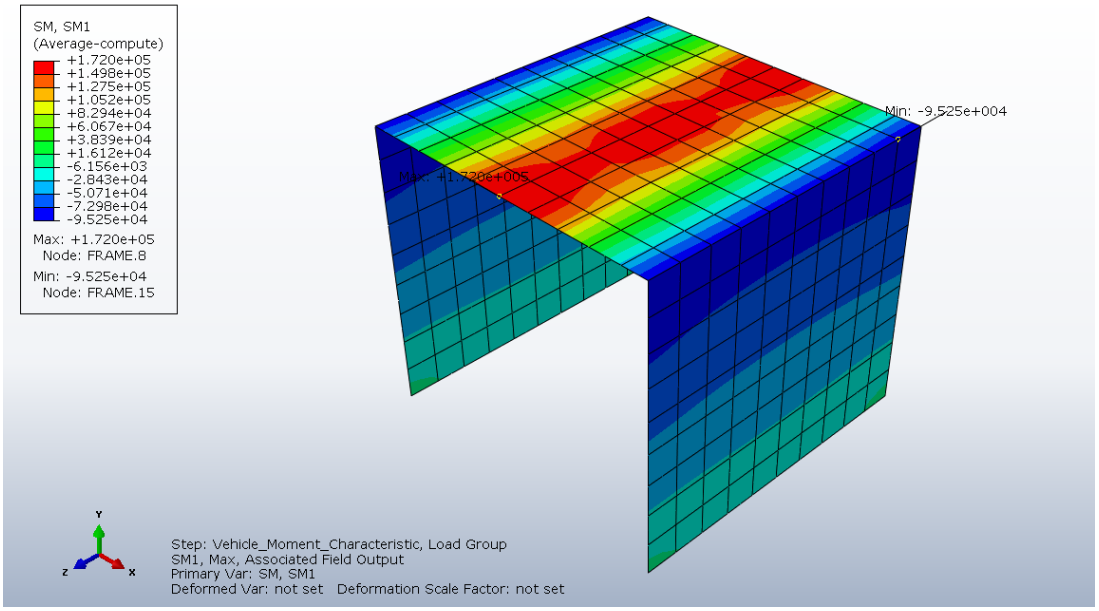

Difference field moment compared to frame analyses: 9.06 %

Difference in corner moment compared to frame analyses: 5,02%

H=6m, L= 12m

2D Frame Analyses:

Traffic lane 1, w=3m , No influence of transverse load distribution

Q=270/3m = 90kN/m

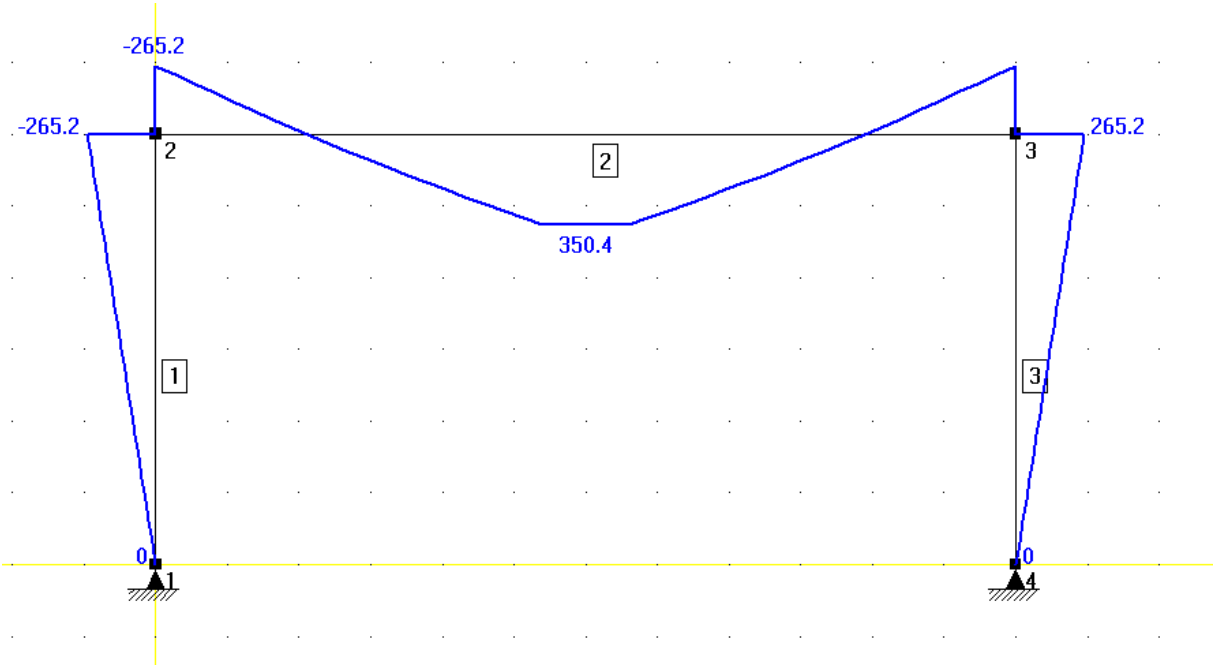

Brigade plus:

Traffic lane 1, w=3m, Q=270/2 kN, q=7.2 kN/m2

Traffic lane 2, w=3m, Q=180/2 kN, q=2.5 kN/m2

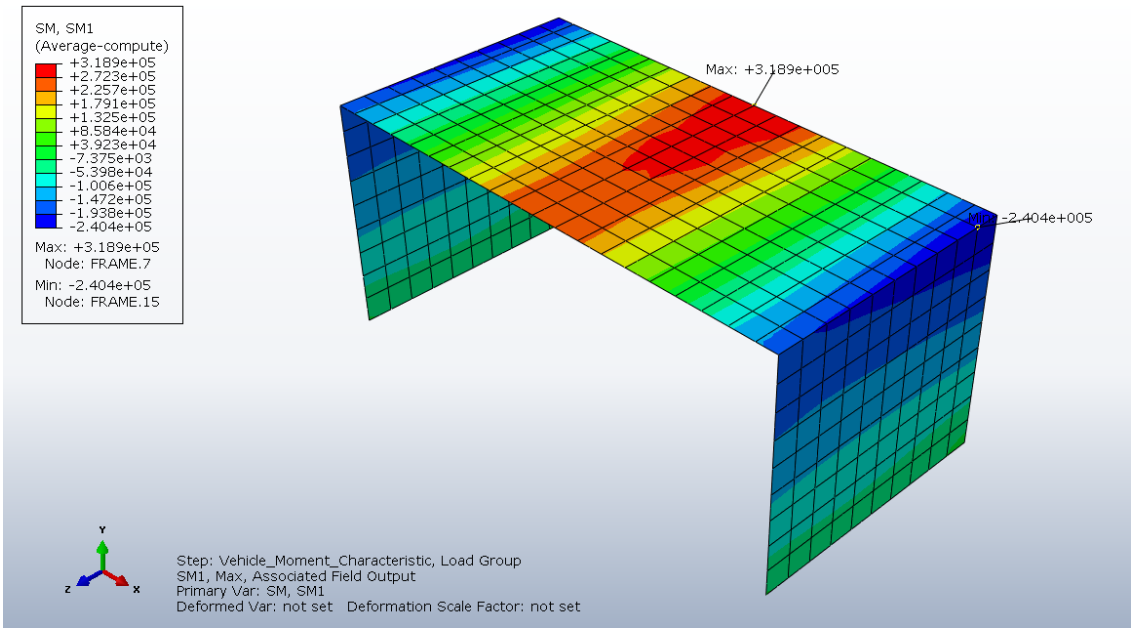

Difference field moment compared to frame analyses: 10.2 %

Difference in corner moment compared to frame analyses: 10.31%

Brigade plus:

Traffic lane 1, w=3m, Q=270/2 kN, q=7.2 kN/m2

Traffic lane 2, w=3m, Q=270/2, , q=7.2 kN/m2

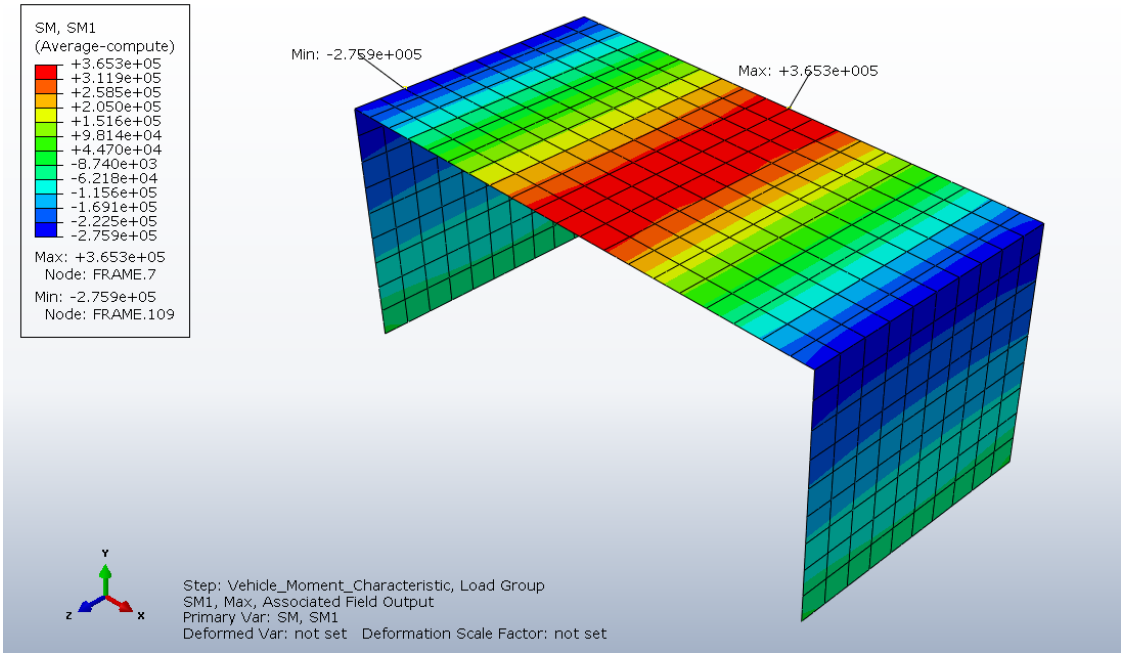

Difference field moment compared to frame analyses: 4,2 %

Difference in corner moment compared to frame analyses: 3,8%

H=6m, L= 18m

2D Frame Analyses:

Traffic lane 1, w=3m , No influence of transverse load distribution

Q=270/3m = 90kN/m

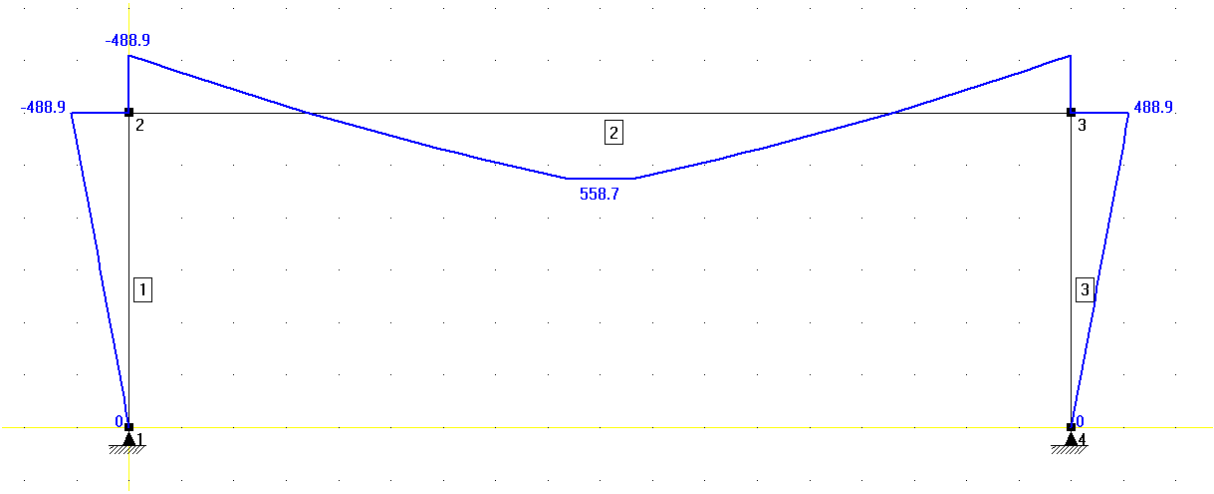

Brigade plus:

Traffic lane 1, w=3m, Q=270/2 kN, q=7.2 kN/m2

Traffic lane 2, w=3m, Q=180/2 kN, q=2.5 kN/m2

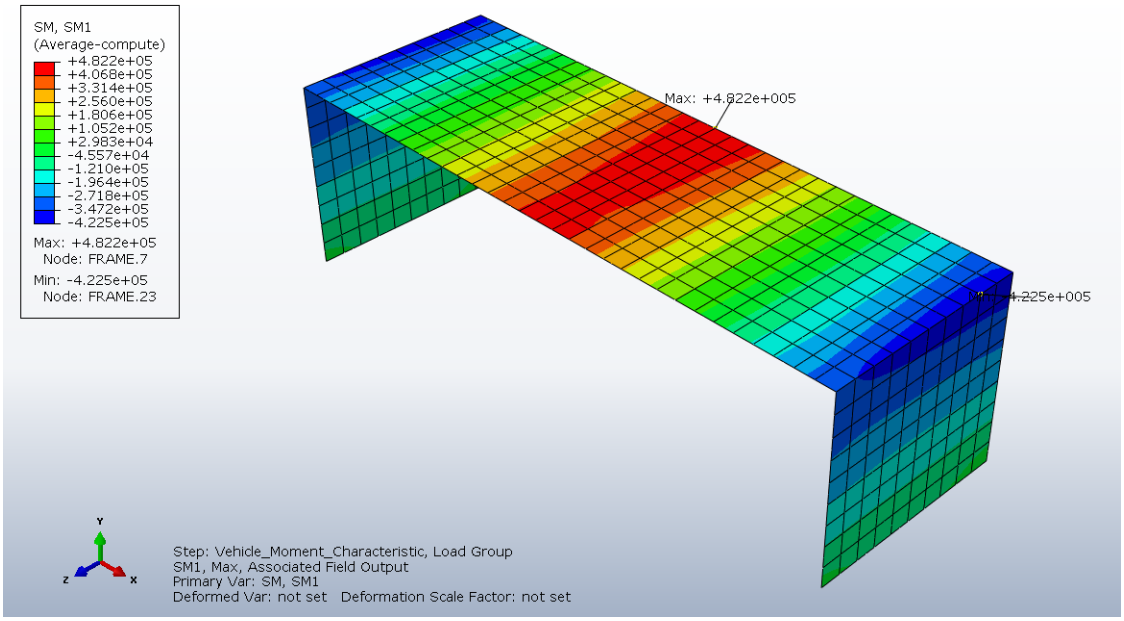

Difference field moment compared to frame analyses: 15,8 %

Difference in corner moment compared to frame analyses: 15.7%

Brigade plus:

Traffic lane 1, w=3m, Q=270/2 kN, q=7.2 kN/m2

Traffic lane 2, w=3m, Q=270/2, , q=7.2 kN/m2

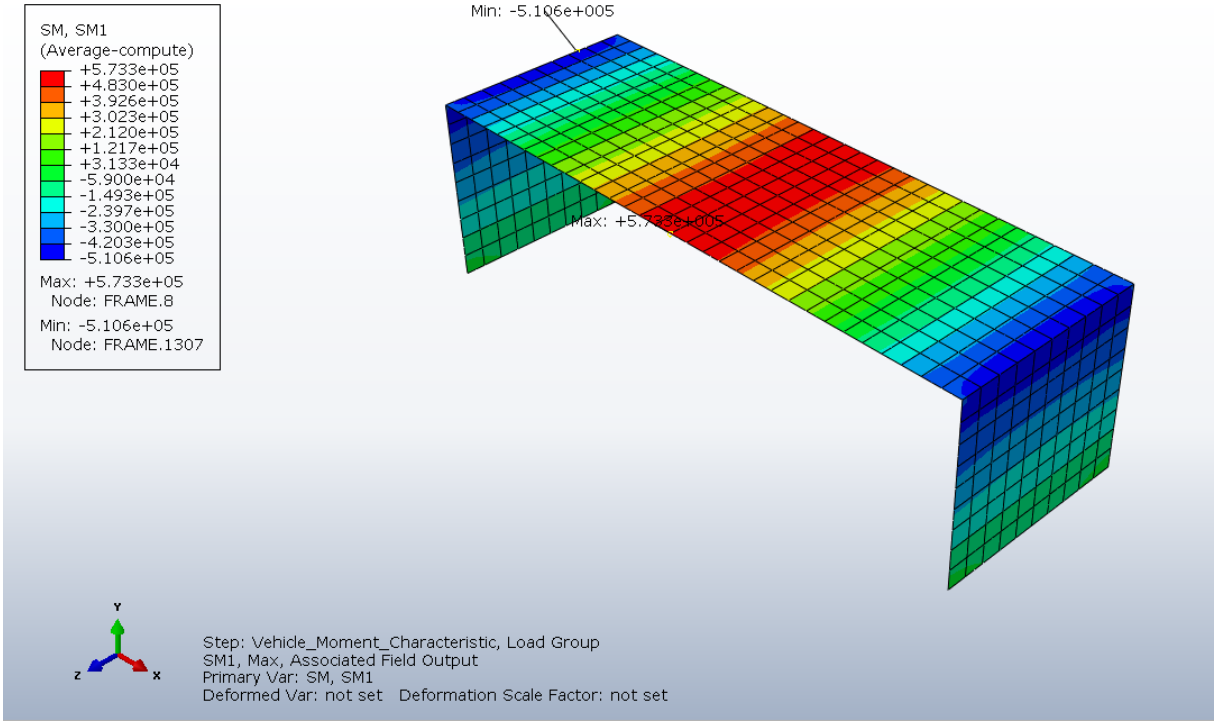

Difference field moment compared to frame analyses: 2.6 %

Difference in corner moment compared to frame analyses: 4.4%

H=6m, L=24m

2D Frame Analyses:

Traffic lane 1, w=3m , No influence of transverse load distribution

Q=270/3m = 90kN/m

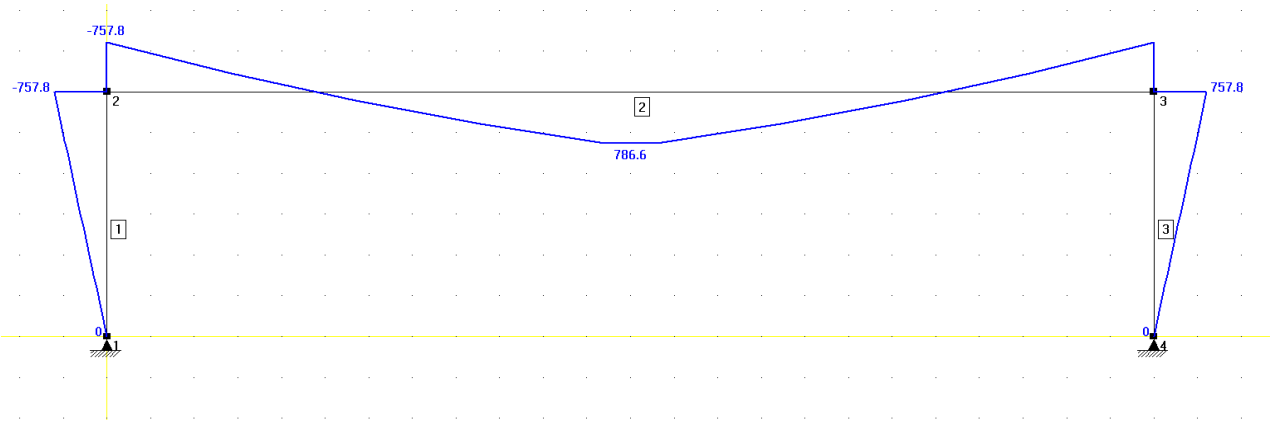

Brigade plus:

Traffic lane 1, w=3m, Q=270/2 kN, q=7.2 kN/m2

Traffic lane 2, w=3m, Q=180/2 kN, q=2.5 kN/m2

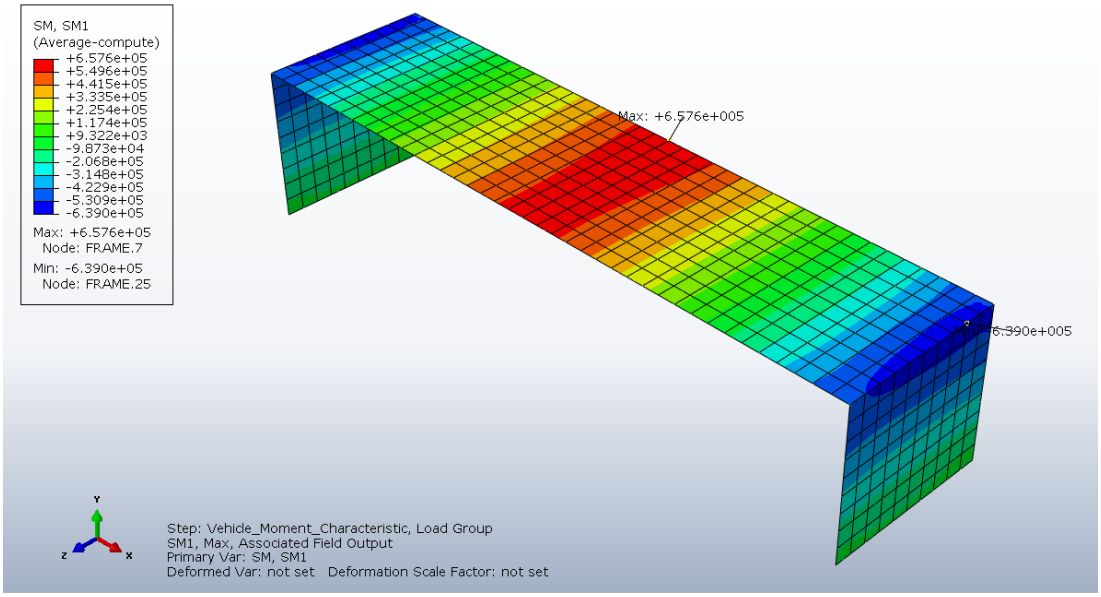

Difference field moment compared to frame analyses: 19,6%

Difference in corner moment compared to frame analyses: 18.6%

Brigade plus:

Traffic lane 1, w=3m, Q=270/2 kN, q=7.2 kN/m2

Traffic lane 2, w=3m, Q=270/2, , q=7.2 kN/m2

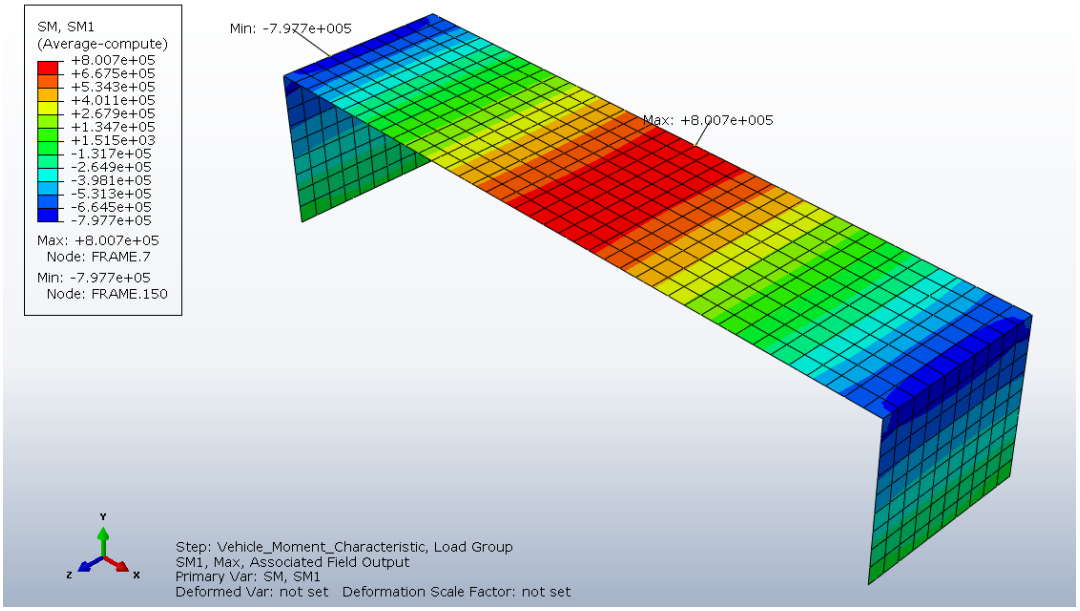

Difference field moment compared to frame analyses: 1,7%

Difference in corner moment compared to frame analyses: 5,2%

H=4m, L=24m

2D Frame Analyses:

Traffic lane 1, w=3m , No influence of transverse load distribution

Q=270/3m = 90kN/m

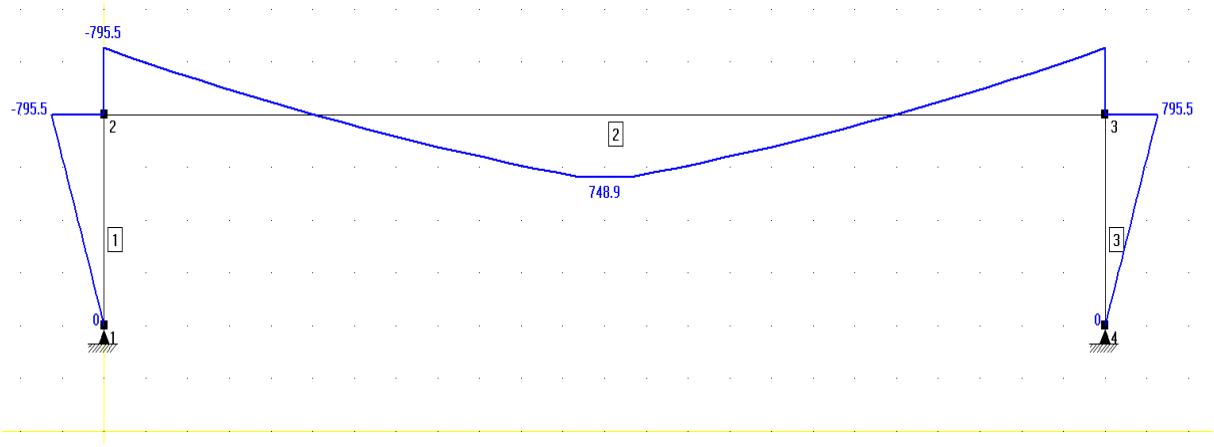

Brigade plus:

Traffic lane 1, w=3m, Q=270/2 kN, q=7.2 kN/m2

Traffic lane 2, w=3m, Q=180/2 kN, q=2.5 kN/m2

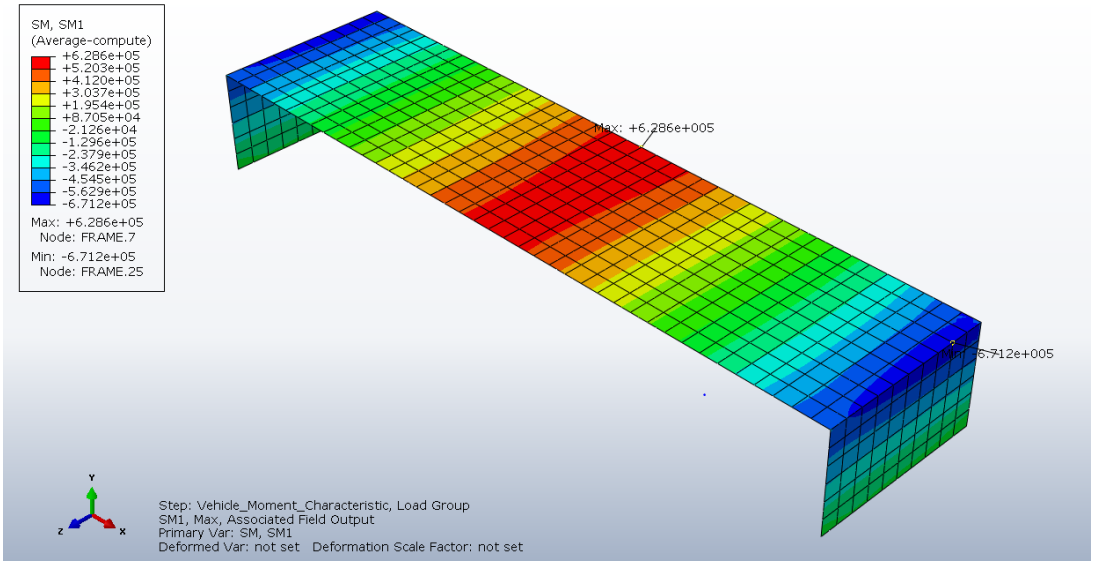

Difference field moment compared to frame analyses: 19.1%

Difference in corner moment compared to frame analyses: 18,5%

Brigade plus:

Traffic lane 1, w=3m, Q=270/2 kN, q=7.2 kN/m2

Traffic lane 2, w=3m, Q=270/2, , q=7.2 kN/m2

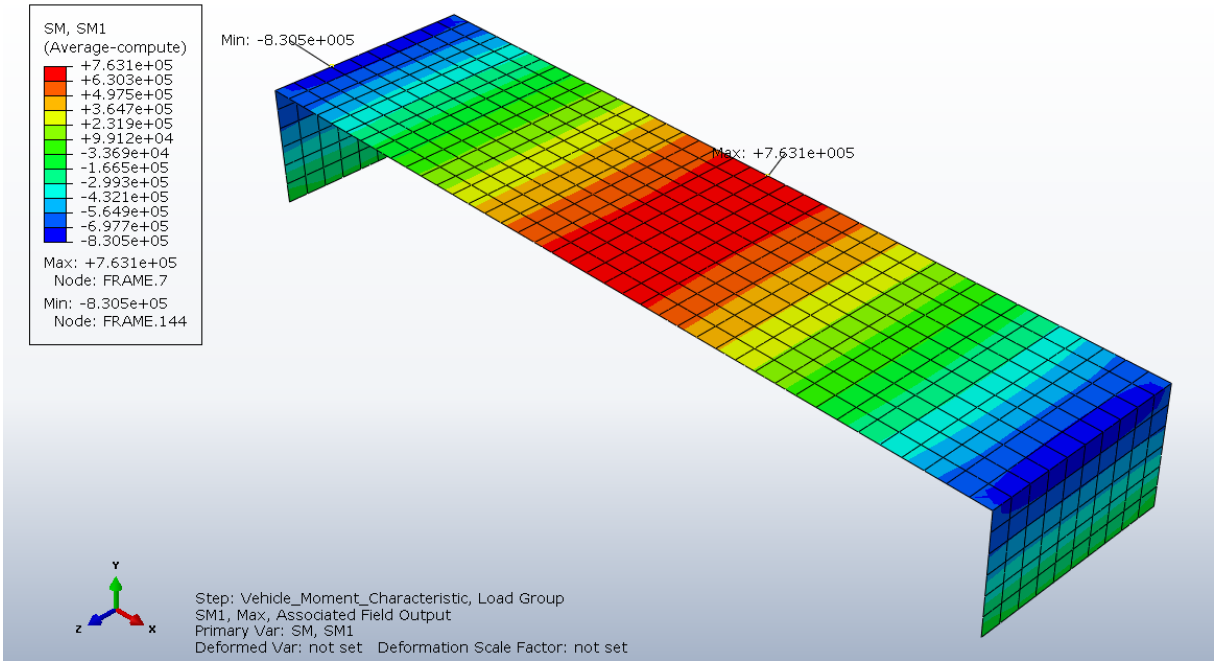

Difference field moment compared to frame analyses: 1,9%

Difference in corner moment compared to frame analyses: 4,4%

H=8m, L= 24m

2D Frame Analyses:

Traffic lane 1, w=3m , No influence of transverse load distribution

Q=270/3m = 90kN/m

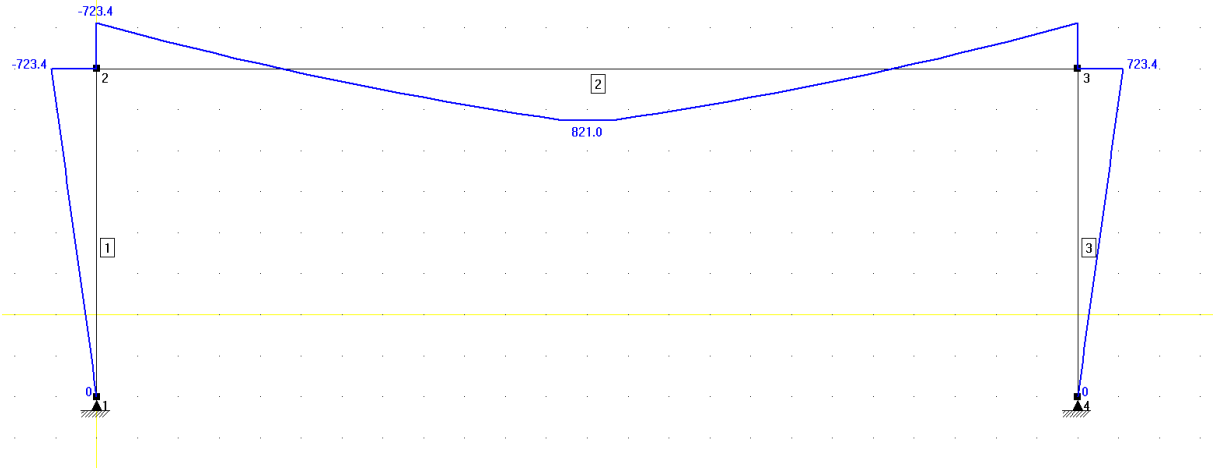

Brigade plus:

Traffic lane 1, w=3m, Q=270/2 kN, q=7.2 kN/m2

Traffic lane 2, w=3m, Q=180/2 kN, q=2.5 kN/m2

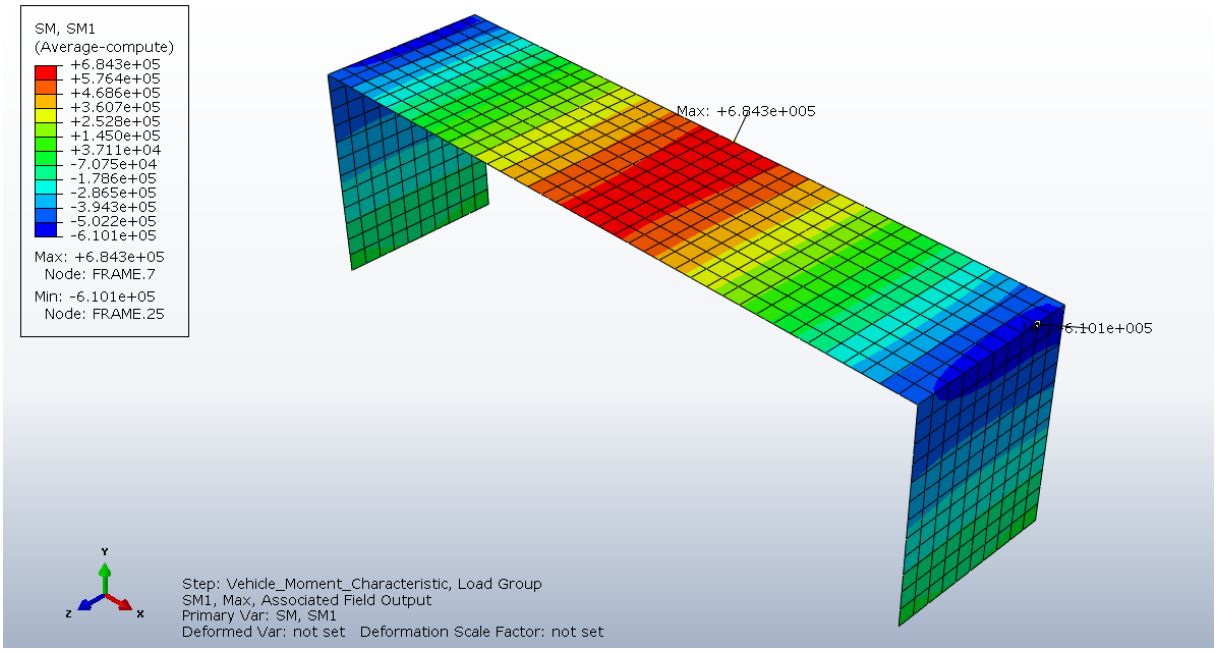

Difference field moment compared to frame analyses: 20%

Difference in corner moment compared to frame analyses: 18,6%

Brigade plus:

Traffic lane 1, w=3m, Q=270/2 kN, q=7.2 kN/m2

Traffic lane 2, w=3m, Q=270/2, , q=7.2 kN/m2

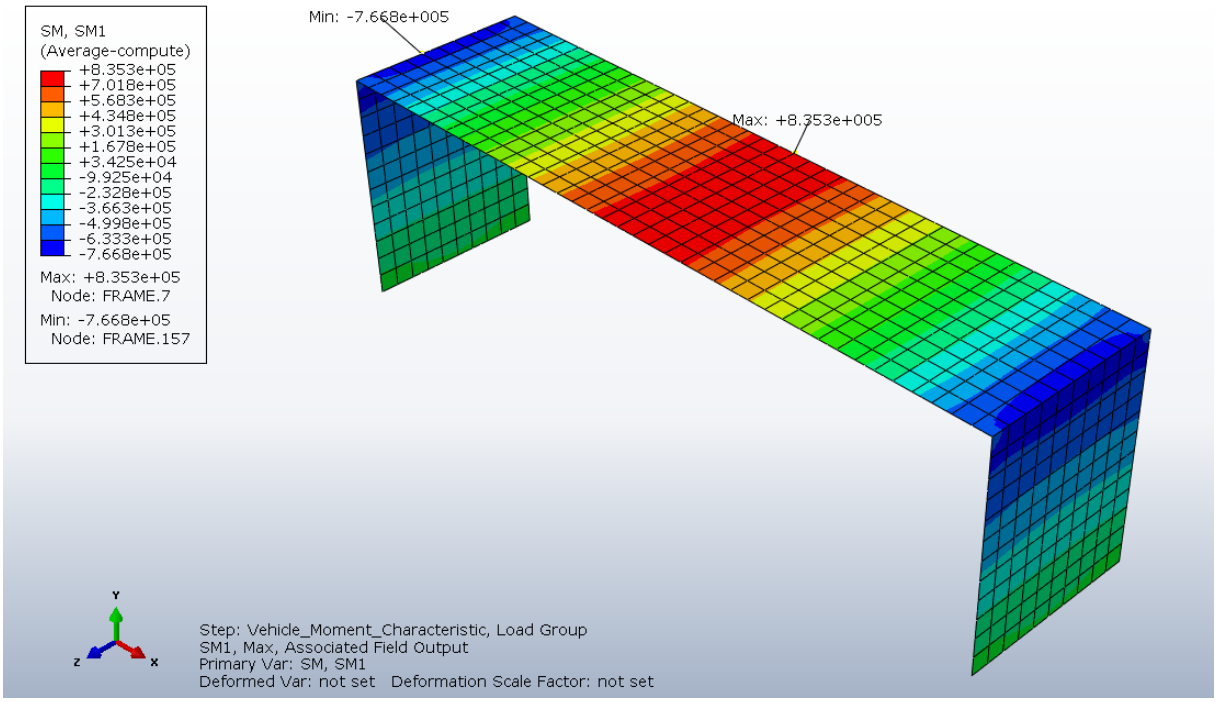

Difference field moment compared to frame analyses: 1,7%

Difference in corner moment compared to frame analyses: 6%

D

Analytical expressions for displacement of frame due to loads on frame legs

Expressions for horizontal displacement caused by embankment load and with fixed boundary conditions to the foundation:

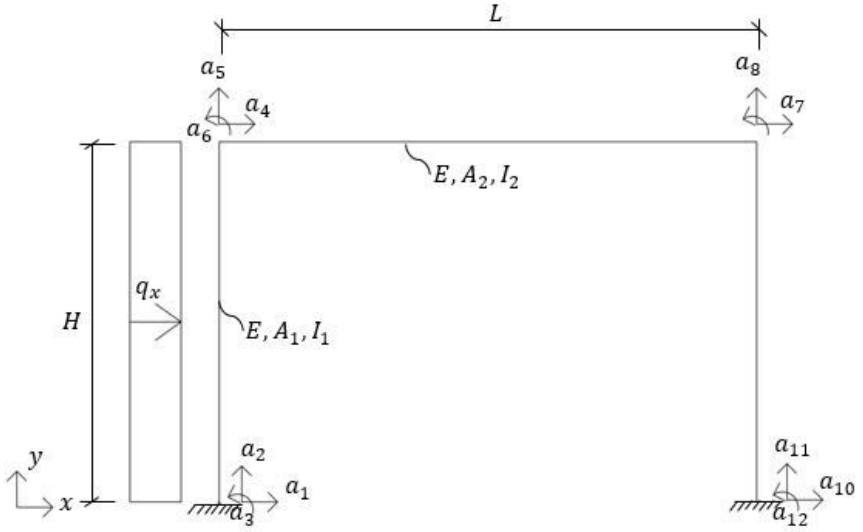

$$a_7 = \frac{q_x H^5 (24A_2H^4I_1I_2^2 + 2A_1A_2H^4I_2^2L^2 + 48A_2H^3I_1^2I_2L + 5A_1A_2H^3I_1I_2L^3 + 2A_1A_2H^2I_1^2L^4 + 96HI_1^2I_2^2L - 8A_1I_1^2I_2L^4)}{16EI_1\,(A_1I_1L^3 + 6A_1I_2HL^2 + 24I_1I_2H)(A_2I_2H^4 + 2A_2I_1H^3L + 6I_1I_2HL + 3I_1^2L^2)}$$

Expressions for horizontal displacement caused by counteracting earth pressure and with fixed boundary conditions to the foundation:

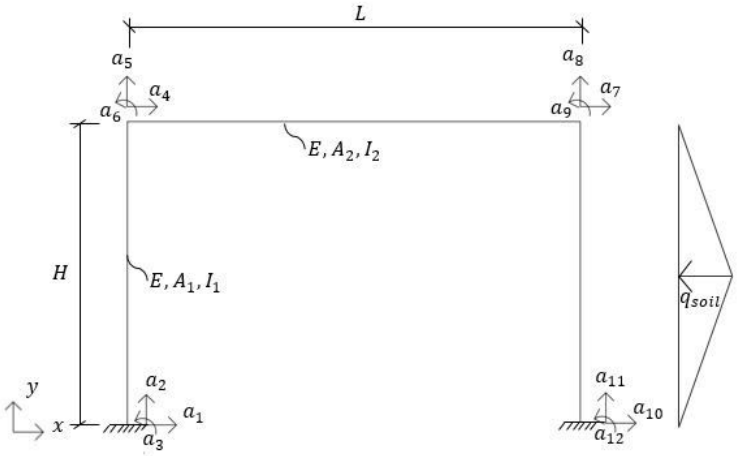

$$a_7 = -\frac{q_{soil} H^5 (264A_2H^4I_1I_2^2 + 24A_1A_2H^4I_2^2L^2 + 528A_2H^3I_1^2I_2L + 59A_1A_2H^3I_1I_2L^3 + 22A_1A_2H^2I_1^2L^4 + 1008HI_1^2I_2^2L - 84A_1I_1^2I_2L^4)}{384EI_1\,(A_1I_1L^3 + 6A_1I_2HL^2 + 24I_1I_2H)(A_2I_2H^4 + 2A_2H^3I_1L + 6I_1I_2HL + 3I_1^2L^2)}$$

Expressions for horizontal displacement caused by braking force and with fixed boundary conditions to the foundation:

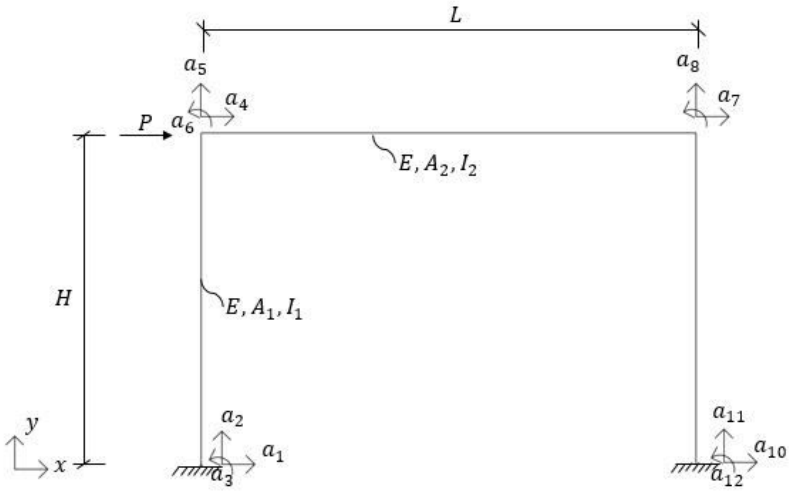

$$a_7 = \frac{PH^4(48A_2H^4I_1I_2^2 + 3A_1A_2H^4I_2^2L^2 + 96A_2H^3I_1^2I_2L + 8A_1A_2H^3I_1I_2L^3 + 4A_1A_2H^2I_1^2L^4 + 216HI_1^2I_2^2L - 18A_1I_1^2I_2L^4)}{12EI_1\,(A_1I_1L^3 + 6A_1I_2HL^2 + 24I_1I_2H)(A_2I_2H^4 + 2A_2I_1H^3L + 6I_1I_2HL + 3I_1^2L^2)}$$

Expressions for horizontal displacement caused by braking force and with pinned boundary conditions to the foundation:

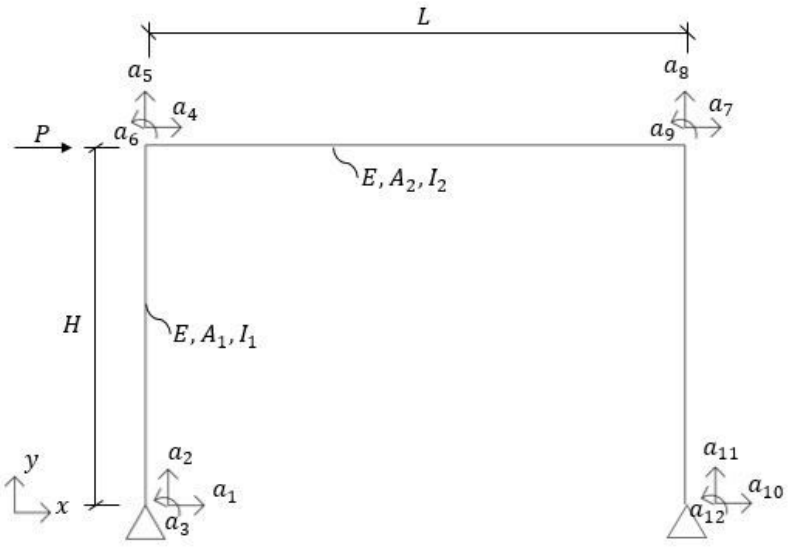

$$a_7 = \frac{PH^2(48A_2H^4I_1I_2^2 + 4A_1A_2H^4I_2^2L^2 + 72A_2H^3I_1^2I_2L + 8A_1A_2H^3I_1I_2L^3 + 3A_1A_2H^2I_1^2L^4 + 72HI_1^2I_2^2L - 6A_1I_1^2I_2L^4)}{12EI_1I_2A_1L^2(2A_2I_2H^3 + 3A_2I_1LH^2 + 3I_1I_2L)}$$

E

Calculation of Loads and load combination factors

Calculations of loads – Characteristic values

Self-weight: The self-weight of the bridges has been calculated assuming a unit weight of the reinforced concrete.

$$\rho_C = 25\ kN/m^3$$

By multiplying the unit-weight with the cross-sectional area of the member the self-weight is obtained as a line load.

$$G_k = t * B * \rho_c \qquad [kN/m]$$

Where t is the thickness parameter (optimization parameter) and B is the width of the bridge.

Earth pressure: The earth pressure has been assumed and calculated with Jaky's formula.

Earth pressure coefficient at rest:

$$K_0 = 1 - \sin(\phi') \qquad \text{where } \phi' = 45° \text{ (Assumed)}$$

The earth heaviness is defined in the document TSFS 2018:57 11 chap. 8§
(Transportstyrelsen. (2018). *TSFS2018:57 – Transportstyrelsens föreskrifter och allmänna råd om tillämpning av eurokoder*)
For a width of 6 m, Earth heaviness: $\gamma_s = 20\ kN/m^2$

Lateral earth pressure:

$$G_s = K_0 * \gamma_s * h(z) \qquad [kN/m]$$

Where $h(z)$ describes the depth (the height of the frame legs).

Pavement: The pavement has been assumed in the analyses and is given as a normal surface load per unit area.

$$q_{pav} = 2.72\ kN/m^2$$

Surcharge: The surcharge load is calculated with Jaky's formula for lateral earth pressure.

$$q_{sur,h} = K_0 * q_{sur,v} = 5.86\ kN/m^2 \qquad [kN/m^2]$$

Where

$$q_{sur,v} = 20\ kN/m^2$$

Counteracting (passive) earth pressure: The counteracting earth pressure has been calculated in several steps. First by assuming a magnitude of the earth pressure:

$$\Delta p = C\gamma_s \frac{10\ mm}{H} z \qquad (1)$$

Where C = 300/600 depending on if the load is considered as favourable/unfavourable.

The displacement of the frame caused by the assumed counteractive earth pressure ($\delta_{\Delta p}$) has either been calculated analytically or numerically. The actual magnitude of the counteracting earth pressure can be calculated as:

$$q_{res} = \frac{\delta_{sur}\frac{\Delta p}{10\ mm}}{1+\frac{\delta_{\Delta p}}{10\ mm}} \quad [kN/m] \qquad (2)$$

Temperature:

$$T_{max} = 35\ °C$$
$$T_{min} = -35\ °C$$

Adjusted temperature for concrete:

$$T_{max,c} = 35 + 2\ °C$$
$$T_{min,c} = -35 + 8\ °C$$

Casting & hydration:

$T_0 = 10\ °C$	Cast temperature
$\Delta T_{cTc} = T_0 - T_{min,c}$	Temperature difference for contraction
$\Delta T_{cTe} = T_{max,c} - T_0$	Temperature difference for expansion
$\Delta T_{tot} = \Delta T_{cTc} - \lvert\Delta T_{cTe}\rvert$	Total temperature difference

Horizontal expansion caused by temperature:

$$\Delta\delta_T = \frac{\alpha_{cT}\Delta T_{tot}L}{2}[m]$$

Where L is the span length and α_{cT} the coefficient of thermal expansion of concrete ($10^{-5}/°C$).

The counteractive earth pressure can be calculated in the same way as for the surcharge load, with (1) and (2).

Temperature gradient: When the bridge is subjected to a temperature gradient, the curvature is affected and thus internal restraints in frame corners.

$$\Delta T_h = 15\ °C$$
$$k_{sur,h} = 0.7 \qquad \text{(SS-EN 1991-1-5)}$$
$$\Delta T_c = -8\ °C$$
$$k_{sur,c} = 1.0 \qquad \text{(SS-EN 1991-1-5)}$$

$\Delta T_{pos} = \Delta T_h k_{sur,h} = 10.5\ °C$ (Higher temperature at the surface of the bridge deck)

$\Delta T_{neg} = \Delta T_c k_{sur,c} = -8\ °C$ (Lower temperature at the surface of the bridge deck)

Shrinkage: The drying shrinkage has been assumed since the drying shrinkage depends on the cross-section of the concrete members. The autogenous shrinkage has been calculated according to EC. The effect of shrinkage has been taken into account by calculating an equivalent temperature that gives the same effect as the shrinkage.

$$\varepsilon_{ca} = 2.5 * 10^{-6}(f_{ck} - 10)$$
$$\varepsilon_{cd} = 2 * 10^{-4} \text{ (Assumed)}$$

The equivalent temperature due to shrinkage:

$$\Delta T_{shrinkage} = \frac{\varepsilon_{ca} + \varepsilon_{cd}}{\alpha_{cT}}$$

Loads from wing-walls: When considering the wing loads, several load components are to be taken into account. The loads that acts on the wing walls can be applied as line loads in the transverse and longitudinal direction of the bridge, a bending moment and a traction caused by the self-weight of the wing walls.

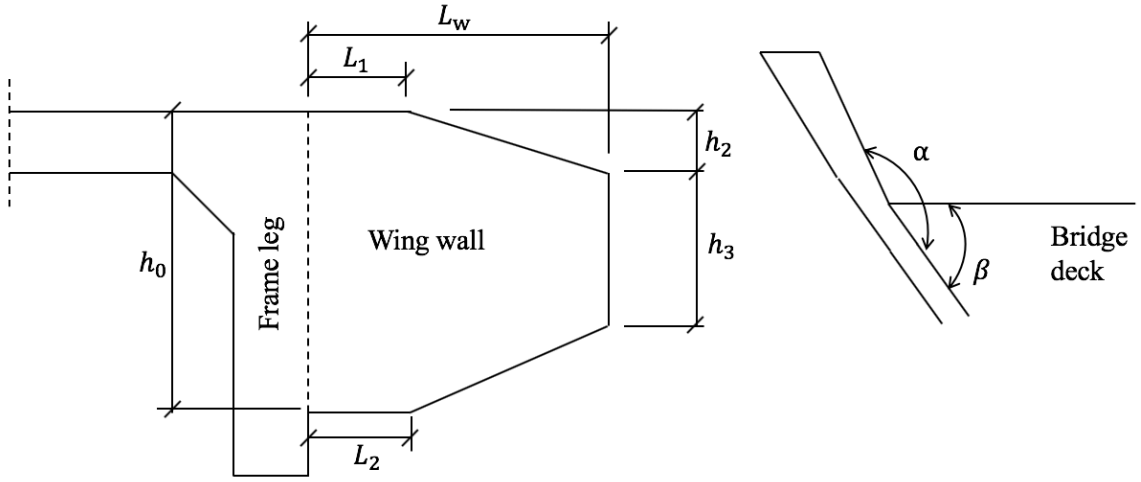

$h_0 = H - 500\ mm$ where H is the height of the frame legs
$L_w = 3\ m$ Predefined length of the wing walls
$h_3 = h_0 - \frac{3L_w}{2}$
$L_1 = 0$
$L_2 = 0$
$h_2 = 0$

The normal forces can be determined by mathematical operations and yields:

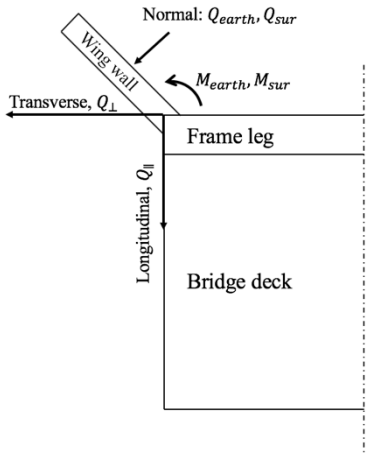

$$Q_{earth} = K_0 \gamma_s \frac{\frac{h_0^2 L_w}{3} - \frac{h_0 h_3 L_w}{3} + \frac{h_3^2 L_w}{3}}{H} \qquad [kN/m]$$

$$Q_{sur} = K_0 q_{sur} \frac{h_0 L_w - \frac{L_w(h_0 - h_3)}{2}}{H} \qquad [kN/m]$$

The forces can be divided in components in the longitudinal and transverse direction of the bridge, respectively.

$$Q_{\parallel,earth} = Q_{earth}\frac{\sqrt{2}}{2}, \qquad Q_{\parallel,sur} = Q_{sur}\frac{\sqrt{2}}{2}$$

$$Q_{\perp,earth} = Q_{earth}\frac{\sqrt{2}}{2}, \qquad Q_{\perp,sur} = Q_{sur}\frac{\sqrt{2}}{2}$$

The bending moment at the connection between the wing wall and the frame legs yields:

$$M_{earth} = K_0\gamma_s \frac{\frac{h_0^2 L_w^2}{12} - \frac{h_0 h_3 L_w^2}{6} + \frac{h_3^2 L_w^2}{4}}{H} \qquad [kNm/m]$$

$$M_{sur} = K_0 q_{sur} \frac{\frac{h_0 L_w^2}{2} - \frac{L_w^2(h_0 - h_3)}{3}}{H} \qquad [kNm/m]$$

The self-weight of the wing walls give rise to a line traction.

$t_w = 300\ mm$ Assumed thickness of wing walls

$$G_w = \rho_c t_w \frac{h_0 L_w - \frac{L_w(h_0 - h_3)}{2}}{H} \qquad [kN/m]$$

Vertical traffic load – LM1:

LM1 follows the requirements stated in EC. *(EN 1991-2 Eurocode 1: Actions on structures - Part 2: Traffic loads on bridges. CEN European Committee for Standardization. Brussels)*

$Q_{1k} = 300\ kN$ (Characteristic concentrated load per axle in lane 1, i.e., 150 kN per point load)
$Q_{2k} = 200\ kN$ (Characteristic concentrated load per axle in lane 2, i.e., 100 kN per point load)
$q_{1k} = 9\ kN/m^2$ (Characteristic uniformly distributed load in lane 1)
$q_{2k} = 2.5\ kN/m^2$ (Characteristic uniformly distributed load in lane 2)

$\alpha_{Q1} = \alpha_{Q2} = 0.9$ (Adaption factor for axle-loads)
$\alpha_{q1} = 0.8$ (Adaption factor for q_{1k})
$\alpha_{q2} = 1.0$ (Adaption factor for q_{2k})

Design traffic load for load model 1 (LM1):

$Q_{1d} = \frac{\alpha_{Q1} Q_{1k}}{2} = 135\ kN$ (Design concentrated load per wheel)
$Q_{2d} = \frac{\alpha_{Q2} Q_{2k}}{2} = 90\ kN$ (Design concentrated load per wheel)
$q_{1d} = \alpha_{q1} q_{1k} = 7.2\ kN/m^2$ (Design uniformly distributed load in lane 1)
$q_{2d} = \alpha_{q2} q_{2k} = 2.5\ kN/m^2$ (Design uniformly distributed load in lane 2)

Vertical traffic load – Vehicle model I:
The vertical traffic load that corresponds to vehicle model I is given by the Swedish transport Agency (Transportstyrelsen). *Transportstyrelsen. (2018). TSFS 2018:57 -Transportstyrelsens föreskrifter och allmänna råd om tillämpning av eurokoder.*

$B_k = 300\ kN$ (Characteristic concentrated axle load)
$q_k = 5\ kN/m^2$ (Characteristic concentrated axle load)
$\alpha_D = 1.25$ (Dynamic amplification factor)
$\alpha_{B1} = 1.0$ (Adaption factor for B_k in lane 1)
$\alpha_{q1} = 1.0$ (Adaption factor for q_k in lane 1)
$\alpha_{B2} = 0.8$ (Adaption factor for B_k in lane 2)
$\alpha_{q2} = 0.8$ (Adaption factor for q_k in lane 2)

Design traffic load for vehicle model I:

$B_{1d} = \frac{\alpha_{B1}\alpha_D B_k}{2} = 187.5\ kN$ (Design concentrated load per wheel in lane 1)
$B_{2d} = \frac{\alpha_{B2}\alpha_D B_k}{2} = 150\ kN$ (Design concentrated load per wheel in lane 2)
$q_{1d} = \alpha_{q1}\alpha_D q_k = 6.25\ kN/m^2$ (Design uniformly distributed load in lane 1)
$q_{2d} = \alpha_{q2}\alpha_{q2} q_k = 5\ kN/m^2$ (Design uniformly distributed load in lane 2)

Fatigue model: In the design checks for fatigue, the fatigue model 3 is used (*(EN 1991-2 Eurocode 1: Actions on structures - Part 2: Traffic loads on bridges. CEN European Committee for Standardization. Brussels)*)

$Q_{FAT} = \frac{120\ kN}{2} = 60\ kN$ (Characteristic concentrated load for fatigue design)

According to the Swedish national annex, NN2.1 (101) in SS-EN 1992-2, the characteristic value of the fatigue loads should be multiplied by a factor of 1.4. This should be done for fatigue checks regarding the damage equivalent stress range of reinforcement.

$Q_{FAT} = 1.4 * 60\ kN = 84\ kN$

Braking force: The axle-loads from vehicles should be considered as a surface traction acting over the bridge deck. The uniformly distributed loads from the vehicle models acts also as a surface traction over the bridge deck.

The braking force is calculated according to SS-EN-1991-2. 8(*(EN 1991-2 Eurocode 1: Actions on structures - Part 2: Traffic loads on bridges. CEN European Committee for Standardization. Brussels)*)

$Q_{1k} = 300\ kN$ (Characteristic value of axle-load)
$q_{1k} = 9\ kN/m^2$ (Characteristic uniformly distributed load)
$\alpha_{Q1} = 0.9$ (Adaption factor for axle-loads)
$\alpha_{q1} = 0.8$ (Adaption factor for uniformly distributed load)

$A_{bd} = bL = 6\ m * L$ (Surface area of bridge deck, $[m^2]$)

$q_{bfa,k} = \frac{0.6*\alpha_{Q1}*2*Q_{1k}}{A_{bd}} = \frac{324\ kN}{A_{bd}}$ (Surface traction from axle-loads $[kN/m^2]$)

$q_{bfu,k} = 0.1\alpha_{q1}q_{1k} = 0.72\ kN/m^2$ (Surface traction from uniformly distributed load, $[kN/m^2]$)

$q_{lk,min} = \frac{\alpha_{Q1}180\ kN}{A_{bd}} = \frac{162\ kN}{A_{bd}}$ (Minimum value of braking force, $[kN/m^2]$)

$q_{lk,max} = \frac{900\ kN}{A_{bd}}$ (Maximum value of braking force, $[kN/m^2]$)

$q_m = \max(q_{bfu,k}, q_{lk,min})$

$q_d = \min(q_m, q_{lk,max})$

Calculations of loads – Load Combinations

The load combination and following combination factors follows the recommendation given by EC (*EN 1991-1: Eurocode 1: Actions on structures – General actions – Densities, self-weight, imposed loads for buildings. CEN European Committee for Standardization. Brussels.* But also recommendations from Swedish Transport Agency (TSFS 2018:57) and from Swedish . Transport Administration (TDOK 2016:0204).

Q_k	Characteristic value
$\psi_0 Q_k$	Combined value
$\psi_1 Q_k$	Frequent value
$\psi_2 Q_k$	Quasi-permanent value

Permanent loads – SUP/INF values for permanent loads:

Load	SUP	INF
Self-weight	1.0	1.0
Pavement	1.1	0.9
Earth Pressure	1.0	1.0
Shrinkage	1.0	1.0
Differential settlements	1.0	1.0

Variable loads – combination factor ψ for variable loads:

Load	ψ_0	ψ_1	ψ_2
LM1 – Axle loads	0.75	0.75	0.0
LM1 – Uniformly distributed load	0.4	0.4	0.0
Vehicle model I	0.75	0.75	0.0
Surcharge	0.75	0.75	0.0
Temperature	0.6	0.6	0.5
Acceleration/braking	0.75	0.75	0.0

F

Design Checks

Design checks

This appendix presents the design checks that has been performed in the analyses. Material parameters and design checks are defined according to SS – EN 1992-1-1 and SS – EN 1992-2.

Material parameters:

$f_{ck} = 35\ MPa$	Characteristic concrete compressive strength (C35/45), *SS-EN 1992-1-1 tab. 3.1*
$f_{ctm} = 3.2\ MPa$	Mean concrete tensile strength (C35/45), *SS-EN 1992-1-1 tab. 3.1*
$f_{yk} = 500\ MPa$	Characteristic yield stress of reinforcement K500C-T
$E_{cm} = 34\ GPa$	Young's modulus for concrete (C35/45), *SS-EN 1992-1-1 tab. 3.1*
$E_s = 200\ GPa$	Young's modulus for reinforcing steel K550C-T
$\gamma_c = 1.5$	Partial factor for concrete, *SS-EN 1992-1-1 2.4.2.4 tab. 2.1N*
$\gamma_1 = 1.15$	Partial factor for reinforcing steel, *SS-EN 1992-1-1 2.4.2.4 tab. 2.1N*
$\gamma_{Ff} = 1.0$	Partial factor for fatigue loading, *SS-EN 1991-2 Appendix D2*
$\gamma_{Mf} = 1.15$	Partial factor for fatigue strength, *SS-EN 1993-1-9 tab. 3.1*
$\alpha_{cc} = 1.0$	Factor that takes strength reduction due to long term loading of concrete into account, *SS-EN 1992-1-1 3.1.6(1)*
$\varepsilon_{cc} = 3.5 * 10^{-3}$	Ultimate strain of concrete in compression [-], *SS-EN 1992-1-1 tab. 3.1*
$k_1 = 0.15$	Coefficient for mean concrete compressive strength [-], *SS-EN 1992-1-1 6.2.2*
$v = 0.6\left(1 - \frac{fck}{250MPa}\right)$	Strength reduction factor for concrete cracked in shear [-] with f_{ck} in [MPa], *SS-EN*
$C_{rd,c} = \frac{0.18}{\gamma_c}$	National parameter for shear design, recommended value [-], *SS-EN 1992-1-1 6.2.2*
$k = 1 + \sqrt{\frac{200}{d}} \leq 2.0$	National parameter for shear design [-], with d in [mm], *SS-EN 1992-1-1 6.2.2*
$v_{min} = 0.035k^{\frac{3}{2}}\sqrt{f_{ck}}$	National parameter for shear design, *SS-EN 1992-1-1 6.2.2 (6.3N)*
α_{cw}	Factor that takes initial stress state in concrete into account [-], *SS-EN 1992-1-1 6.2.3(3)*
$v_1 = 0.6$	For $f_{ck} \leq 60\ MPa$, *SS-EN 1992-1-1 6.2.3 (6.10aN)*
$\theta = 21.8°$	Shear failure angle
$\Delta\sigma_{Rsk} = 162.5\ MPa$	Resisting stress range at N number of cycles, *SS-EN 1992-1-1 tab. 6.3N*
D	Bending diameter of stirrups [mm]
ϕ_w	Diameter of stirrups [m]
u	Deflection of bridge deck in mid-span [m]
φ	Creep factor [-]

$E_{cm,eff} = \frac{E_{cm}}{1+\varphi}$	Effective Young's modulus for concrete, *SS-EN 1992-1-1 (7.20)*
$f_{cd} = \alpha_{cc}\frac{f_{cd}}{\gamma_c} = 23.33\ MPa$	Design concrete strength, *SS-EN 1992-1-1 3.1.6(1)*
$f_{yd} = \frac{f_{yk}}{\gamma_s} = 435\ MPa$	Design yield strength of reinforcing steel, *SS-EN 1992-1-1 3.2.7 (2)a*
$\varepsilon_{syd} = \frac{f_{yd}}{E_s} = 2.175 * 10^{-3}$	Yield strain of reinforcing steel [-]

Bending moment:

Height of compressive zone, assuming yielding of tensile reinforcement:

$$x_c = \frac{d}{2\beta} - \sqrt{\left(\frac{d}{2\beta}\right)^2 + \frac{N_{Ed}e}{\alpha f_{cd}\beta} - \frac{|M_{Ed}|}{\alpha f_{cd}\beta}}$$

Where:

d	Effective height [m]
b	Width of the bridge [m]
$e = d - \frac{t}{2}$	Eccentricity, reinforcement – gross centre of gravity [m]
N_{Ed}	Design normal force [N]
M_{Ed}	Design bending moment [Nm]
A_s	Cross-sectional area of tensile reinforcement [m^2]
$\alpha = 0.81$	Stress block factor [-]
$\beta = 0.416$	Stress block factor [-]

Check if reinforcement ends up in compressive zone of the cross-section:

if: $\left(\frac{d}{2\beta}\right)^2 + \frac{N_{Ed}e}{\alpha f_{cd}\beta} - \frac{|M_{Ed}|}{\alpha f_{cd}\beta} < 0.0 \rightarrow$ Increase thickness of cross-section

else:

$$x_c = \frac{d}{2\beta} - \sqrt{\left(\frac{d}{2\beta}\right)^2 + \frac{N_{Ed}e}{\alpha f_{cd}\beta} - \frac{|M_{Ed}|}{\alpha f_{cd}\beta}}$$

Check if reinforcement is yielding in layer two:

$\varepsilon_s = \frac{d_2 - x_c}{x_c}\varepsilon_{cc}$	Strain in reinforcement, layer two

if: $\varepsilon_s \geq \varepsilon_{syd}$

$F_d = \alpha f_{cd} b x_c + N_{Ed}$	Design tensile force that needs to be taken by the tensile reinforcement [N]

$F_c = A_S f_{yd}$ Reinforcement tensile capacity [N]

$\mu_M = \frac{F_d}{F_c}$ Utilization ratio, bending moment [-]

if: $0.90 \leq \mu_M \leq 0.97 \rightarrow$ return t, else: $t_{new} = t\,\frac{\mu_M}{0.94}$

If the tensile reinforcement has not reached yielding, the thickness of the cross-section is updated manually: $t_{new} = t + 10\ mm$

Shear check without shear reinforcement:

V_{Ed} Design shear force [N]

$\rho_l = \frac{A_s}{bd} \leq 0.02$ Reinforcement amount as a function of the cross-sectional area, with A_s as the tensile reinforcement, *SS-EN 1992-1-1 6.2.2 (6.2b)*

$\sigma_{cp} = \frac{N_{Ed}}{bt} \leq 0.2 f_{cd}$ Compressive stress from the design normal force, *SS-EN 1992-1-1 6.2.2 (6.2b)*

Shear capacity without shear reinforcement (shear sliding failure), *SS-EN 1992-1-1 6.2.2 (6.2a)*:

$$V_{Rd,cs} = \left(C_{rd,c} k (100 \rho_l f_{ck})^{\frac{1}{3}} - k_1 \sigma_{cp}\right) bd$$

With a minimum capacity of (*SS-EN 1992-1-1 6.2.2 (6.2b)*):

$$V_{Rd,cs} = \left(v_{min} - k_1 \sigma_{cp}\right) bd$$

Shear capacity without shear reinforcement (web shear compression failure), *SS-EN1992-1-1 6.2.2(6) (6.5)*:

$$V_{Rd,cw} = 0.5 v f_{cd} bd$$

Design shear resistance without shear reinforcement:

$$V_{Rd,c} = \min\left(V_{Rd,cs}, V_{Rd,cw}\right)$$

μ_V Utilization ratio, shear [-]

if: $0.90 \leq \mu_V \leq 0.97 \rightarrow$ return t, else: $t_{new} = t\,\frac{\mu_V}{0.94}$

Shear check with shear reinforcement:
SS-EN1992-1-1 6.2.3(3) (6.11.aN, 6.11.bN, 6.11.cN)

$\alpha_{cw} = 1 + \frac{\sigma_{cp}}{f_{cd}}$ $\quad if \quad 0 < \sigma_{cp} \leq 0.25 f_{cd}$

$\alpha_{cw} = 1.25$ $\quad if \quad 0.25 f_{cd} < \sigma_{cp} \leq 0.5 f_{cd}$

$\alpha_{cw} = 2.5\left(1 - \frac{\sigma_{cp}}{f_{cd}}\right)$ $\quad if \quad 0.5 f_{cd} < \sigma_{cp} < 1.0 f_{cd}$

Shear capacity with shear reinforcement:
(SS-EN1992-1-1 6.2.3 (6.8), (6.9))

$$V_{Rd,s} = \frac{A_{sw}}{s} z 0.8 f_{ywd} \cot(\theta)$$

$$V_{Rd,max} = \frac{\alpha_{cw} b z v_1 f_{cd}}{\cot(\theta) + \tan(\theta)}$$

Where:

A_{sw}	Cross-sectional area of shear reinforcement [m^2]
s	Spacing (longitudinally) of shear reinforcement [m]
z	Internal lever arm [m]

$$V_{Rd} = \min(V_{rd,s}, V_{Rd,max})$$

if: $0.90 \leq \mu_V \leq 0.97 \rightarrow$ return t, else: $t_{new} = t \frac{\mu_V}{0.94}$

Fatigue – Shear reinforcement:
The method for fatigue design of shear reinforcement follows the recommendations given by the Swedish Concrete Association in the handbook to Eurocode 2 (Volume 2), 2012.

When performing the fatigue check of shear reinforcement, one look at the stress range given as the difference between V_{max} and V_{min}. V_{max} is the upper design shear force for fatigue loading and V_{min} is the corresponding lower shear force.

$$\Delta\sigma_V = \frac{V_{max} - V_{min}}{\frac{A_{sw}}{s} z \cot(\theta)_{fat}}$$

Where

$\cot(\theta)_{fat} = \sqrt{\cot(\theta)}$

The stress range should be reduced due to bending of the stirrups.

$\xi = 0.35 + 0.026 \frac{D}{\phi_w} \rightarrow \Delta\sigma_{Rsk,red} = \xi \Delta\sigma_{Rsk}$

$\mu_{V,FAT} = \frac{\Delta\sigma_V}{\frac{\Delta\sigma_{Rsk,red}}{\gamma_{Mf}}}$ utilization ratio, fatigue of shear reinforcement

if: $0.90 \leq \mu_{V,FAT} \leq 0.97 \rightarrow$ return t, else: $t_{new} = t\frac{\mu_V}{0.94}$

Deflection of bridge deck in mid-span:

$$u_{max} = \frac{L}{400}$$

Where:

L	Span length of the bridge deck
$\mu_u = \frac{u}{u_{max}}$	utilization ratio, deflection

if: $0.90 \leq \mu_u \leq 0.97 \rightarrow$ return t, else: $t_{new} = \sqrt[3]{\left(\frac{t^3\mu_u}{0.94}\right)}$

Fatigue – Bending:

When performing the fatigue check due to bending of the member, one have to investigate the part of the cross-section subjected to tension and compression, respectively.

The stresses are calculated with Navier's formula, and the stress range is of interest, i.e., the difference in $\sigma_{FAT,max}$ and $\sigma_{FAT,min}$.

$$\sigma_{FAT,\max}(z) = \frac{N_{FAT,max}}{A_{II}} + \frac{M_{FAT,max}}{I_{FAT,max}}z$$
$$\sigma_{FAT,\min}(z) = \frac{N_{FAT,min}}{A_{II}} + \frac{M_{FAT,min}}{I_{FAT,min}}z$$

Where

z	Distance from the centre of gravity of the cross-section to the investigated fiber
$A_{II} = bd + \frac{E_s}{E_{cm,eff}}A_s$	Transformed concrete section, state two [m^2]
$M_{FAT,max}$, $N_{FAT,max}$	Is the upper design bending moment and normal force for fatigue design, respectively
$M_{FAT,min}$, $N_{FAT,min}$	Is the lower design bending moment and normal force for fatigue design, respectively
$I_{FAT,max}$, $I_{FAT,min}$	Is the second moment of area for upper and lower design forces, respectively

Factors for fatigue design:

$\lambda_{s1} = 1.22$ SS-EN 1992-1-1 tab 6.3(n)

$N_{obs} = 0.5 * 10^6$ Number of heavy vehicles per year, SS-EN 1991-2 tab 4.5(n)

$k_2 = 9.0$ SS-EN 1992-1-1 tab 6.3(n)

$Q = 0.82$ SS-EN 1992-2 tab NN.1

$N_{years} = 120$ Design life of the bridge [years]

$\lambda_{s2} = Q\left(\frac{N_{obs}}{2*10^6}\right)^{\frac{1}{k_2}}$ SS-EN 1992-1-1 (NN.103)

$\lambda_{s3} = \left(\frac{N_{years}}{100}\right)^{\frac{1}{k_2}}$ SS-EN 1992-2 (NN.103)

$\lambda_{s4} = 1.0$ SS-EN 1992-2 (NN.105)

$p_{fat} = 1.2$ SS-EN 1991-2 Appendix B(3)

$\lambda_s = p_{fat}\lambda_{s1}\lambda_{s2}\lambda_{s3}\lambda_{s4}$

$k_{1c} = 0.85$ SS-EN 1992-2, 6.8.7 (101)

$s = 0.25$ SS-EN 1992-1-1, 3.1.2(6)

$t_0 = 90$ Assumed time with fatigue loading [days]

$\beta_{cc} = e^{s\left(1.0-\sqrt{\frac{28}{t_0}}\right)}$ SS-EN 1992-1-1, 3.1.2(6)

$f_{cd,FAT} = k_{1c}\beta_{cc}f_{cd}\left(1.0 - \frac{fck}{250}\right)$ SS-EN 1992 (6.76)

Equivalent stress range for fatigue check of cross-section in tension:

$$\Delta\sigma_{t,equ} = \lambda_s\left(\sigma_{FAT,max} - \sigma_{FAT,min}\right)$$

$\mu_{Mt,FAT} = \frac{\Delta\sigma_{t,equ}}{\frac{\Delta\sigma_{Rsk}}{\gamma_{Mf}}}$ utilization ratio, fatigue due to bending stresses (tension)

if: $0.90 \leq \mu_{Mt,FAT} \leq 0.97 \rightarrow$ return t, else: $t_{new} = \sqrt[3]{\left(\frac{t^3\mu_{Mt,FAT}}{0.94}\right)}$

Check for cross-section in compression:

$$\frac{\sigma_{c,max}}{f_{cd,FAT}} \leq \max\left(0.5 + \frac{0.45\sigma_{c,min}}{f_{cd,FAT}}, 0.9\right)$$

$\mu_{Mc,FAT} = \frac{\sigma_{c,max}}{\max\left(0.5f_{cd,FAT}+0.45\sigma_{c,min}, 0.9f_{cd,FAT}\right)}$ utilization ratio, fatigue due to bending stresses (compression)

if: $0.90 \leq \mu_{Mc,FAT} \leq 0.97 \rightarrow$ return t, else: $t_{new} = \sqrt[3]{\left(\frac{t^3\mu_{Mc,FAT}}{0.94}\right)}$

Crack width:
The check of crack width is checked in all sections where part of the cross-section is subjected to tensile stresses, according to *SS-EN 1992-1-1 (7.3.4).*

Factors for crack width design:

$k_t = 0.4$ *SS-EN1992-1-1 7.3.3(2)*

$k_{1c} = 0.8$ *SS-EN1992-1-1 7.3.3(2)*

$k_{2c} = 0.5$ *SS-EN1992-1-1 7.3.3(3)*

$c_{k3} = 7D$ Where D is the diameter of the tensile reinforcement, *SS-EN1992-1-1 7.3.3(3)Note*

$\rho_{eff} = \frac{A_s}{A_{eff}}$ Where A_{eff} is the effective area of the cross-section. *SS-EN1992-1-1 7.3.4 (7.10)*

$f_{ct,eff} = \max(f_{ctm}, (1.6 - t)f_{ctm}$ Where t is the optimization parameter (thickness) of the cross-section.

$S_{r,max} = Cc * C_{k3} * k_{1c} * k_{2c} * k_{4t} * \frac{D}{\rho_{eff}}$ Maximum allowed crack spacing, *SS-EN1992-1-1 7.3.4 (7.11)*

$\varepsilon_{sm,cm} = \max\left(\frac{\left(\sigma - k_t\left(\frac{f_{ct,eff}}{\rho_{eff}}\right)\left(1+\frac{E_s}{E_{cm,eff}}\rho_{eff}\right)\right)}{E_s}, \frac{0.6\sigma}{E_s}\right)$ Where σ is the applied stress, *SS-EN1992-1-1 7.3.4 (7.9)*

$w_k = \varepsilon_{sm,cm} S_{r,max}$ Crack width, *SS-EN1992-1-1 7.3.4 (7.8)*

The maximum allowed crack width depends on the exposure class of the section.

In this thesis, following values of the maximum allowed crack width has been used:

Mid-span of bridge deck: $w_{max} = 0.3\ mm$

Frame corner – (End of haunch (bridge deck)): $w_{max} = 0.2\ mm$

Frame corner – (Top of frame leg): $w_{max} = 0.2\ mm$

Frame leg – mid: $w_{max} = 0.3\ mm$

Frame leg – at bottom slab: $w_{max} = 0.3\ mm$

$\mu_w = \frac{w_k}{w_{max}}$ utilization ratio, crack width

if: $0.90 \leq \mu_w \leq 0.97 \rightarrow$ return t, else: $t_{new} = t\,\frac{\mu_w}{0.94}$

G

Results - Optimized dimensions

Table F.1 Thicknesses and utilization ratios, H= 4m, Pinned BC

L [m]	t_s[mm]	**η** [%]	$\mathbf{t_{sh}}$[mm]	**η** [%]	t_{f2}[mm]	**η** [%]	t_{fmid} [mm]	**η** [%]	t_{f1}[mm]	**η** [%]
6	300	29.4 (M)	800	6.6 (M)	300	56.3 (V)	300	40.0 (FAT)	300	22.0 (V)
7	300	37.8 (M)	800	7.7 (M)	300	63.1 (V)	300	25.7 (FAT)	300	24.2 (V)
8	320	41.1 (M^*)	820	8.8 (M)	300	69.5 (V)	300	43.8 (V)	300	27.2 (V)
9	330	47.1 (M^*)	830	9.9 (M)	300	75.8 (V)	300	48.5 (V)	300	33.9 (V)
10	350	52.2 (M^*)	850	10.7 (M)	300	80.3 (V)	300	51.8 (V)	300	36.1 (V)
11	370	55.9 (M^*)	870	11.5 (M)	300	85.0 (V)	300	56.2 (V)	300	39.0 (V)
12	390	58.2 (M^*)	890	12.7 (M)	300	92.5 (V)	300	62.7 (V)	300	43.2 (V)
13	380	57.3 (M^*)	480	47.2 (M)	420	92.5 (V)	360	64.2 (V)	300	54.3 (V)
14	390	59.2 (M^*)	490	53.0 (M)	460	94.0 (V)	380	68.5 (V)	300	61.7 (V)
16	430	66.4 (M^*)	530	68.9 (M)	580	96.1 (V)	440	80.8 (V)	300	80.2 (V)

M = Bending moment, M^* = Bending moment, yielding of reinforcement in both layers,

FAT = Fatigue, V = Shear force

Table F.2 Thicknesses and utilization ratios, H= 6m, Pinned BC

L [m]	t_s[mm]	**η** [%]	$\mathbf{t_{sh}}$[mm]	**η** [%]	t_{f2}[mm]	**η** [%]	t_{fmid} [mm]	**η** [%]	t_{f1}[mm]	**η** [%]
6	300	23.3 (M)	800	8.8 (M)	300	79.9 (V)	300	33.9 (V)	300	37.4 (V)
7	300	33.2 (M)	800	9.8 (M)	300	75.6 (V)	300	35.7 (V)	300	37.8 (V)
8	310	40.1 (M^*)	810	10.7 (M)	300	82.1 (V)	300	38.8 (V)	300	38.1 (V)
9	330	46.4 (M^*)	830	11.0 (M)	300	84.0 (V)	300	41.0 (V)	300	38.5 (V)
10	350	50.2 (M^*)	850	12.1 (M)	300	89.9 (V)	300	44.5 (V)	300	39.0 (V)
11	370	56.0 (M^*)	870	12.3 (M)	300	91.8 (V)	300	46.6 (V)	300	39.5 (V)
12	380	58.0 (M^*)	880	14.4 (M)	330	91.9 (V)	330	47.1 (V)	330	28.8 (V)
13	390	58.9 (M^*)	490	46.0 (M)	400	92.3 (V)	350	48.9 (V)	300	35.1 (V)
14	400	61.8 (M^*)	500	51.0 (M)	430	92.6 (V)	365	51.7 (V)	300	38.1 (V)
16	440	70.1 (M^*)	540	66.4 (M)	530	94.0 (V)	415	61.4 (V)	300	43.3 (V)
18	460	76.0 (M^*)	560	80.3 (M)	620	95.1 (V)	460	67.9 (V)	300	55.6 (V)
20	480	76.6 (M^*)	590	93.5 (M)	740	95.4 (V)	520	74.0 (V)	300	72.0 (V)
22	490	80.8 (M^*)	670	94.3 (M)	880	91.5 (V)	590	82.0 (V)	300	77.3 (V)
24	500	81.3 (M^*)	770	91.1 (M)	980	89.3 (V)	660	92.5 (V)	340	96.6 (V)

M = Bending moment, M^* = Bending moment, yielding of reinforcement in both layers,

FAT = Fatigue, V = Shear force

Table F.3 Thicknesses and utilization ratios, H= 8m, Pinned BC

L [m]	t_s[mm]	**η** [%]	$\mathbf{t_{sh}}$[mm]	**η** [%]	t_{f2}[mm]	**η** [%]	t_{fmid} [mm]	**η** [%]	t_{f1}[mm]	**η** [%]
6	300	9.4 (M)	800	13.5 (M)	380	92.1 (V)	380	29.9 (V)	380	38.6 (V)
7	300	18.4 (M)	800	14.3 (M)	380	94.3 (V)	380	29.9 (V)	380	39.5 (V)
8	300	38.8 (M^*)	800	15.1 (M)	390	94.4 (V)	390	30.2 (V)	390	39.7 (V)
9	310	35.8 (M^*)	810	16.0 (M)	400	94.2 (V)	400	30.4 (V)	400	39.4 (V)
10	320	42.9 (M^*)	820	17.1 (M)	410	94.6 (V)	410	32.0 (V)	410	39.1 (V)
11	340	46.7 (M^*)	840	18.0 (M)	430	91.9 (V)	430	32.2 (V)	430	36.9 (V)
12	360	49.2 (M^*)	860	19.1 (M)	450	91.7 (V)	450	33.1 (V)	450	29.4 (V)
13	360	50.0 (M^*)	460	73.4 (M)	530	91.6 (V)	415	35.0 (V)	300	32.6 (V)
14	370	53.9 (M^*)	480	74.5 (M^*)	560	90.1 (V)	430	35.5 (V)	300	32.2 (V)
16	420	64.8 (M^*)	530	85.6 (M^*)	630	96.8 (V)	465	42.4 (V)	300	36.9 (V)
18	440	71.2 (M^*)	570	91.2 (M)	720	95.9 (V)	510	46.2 (V)	300	43.0 (V)
20	460	75.2 (M^*)	630	93.0 (M)	820	93.4 (V)	560	51.0 (V)	300	48.2 (V)
22	480	80.7 (M^*)	690	94.6 (M)	880	93.6 (V)	590	56.7 (V)	300	55.6 (V)
24	500	82.5 (M^*)	780	92.5 (M)	950	90.0 (V)	640	65.8 (V)	300	57.2 (V)
25	510	83.7 (M^*)	820	93.3 (M)	1030	90.0 (V)	680	69.7 (V)	300	62.0 (V)

M = Bending moment, M^* = Bending moment, yielding of reinforcement in both layers,

FAT = Fatigue, V = Shear force

Table F.4 Thicknesses and utilization ratios, H= 4m, Fixed BC

L [m]	t_s[mm]	**η** [%]	$\mathbf{t_{sh}}$[mm]	**η** [%]	t_{f2}[mm]	**η** [%]	t_{fmid} [mm]	**η** [%]	t_{f1}[mm]	**η** [%]
6	300	27.7 (M)	800	5.6 (M)	300	60.8 (V)	300	46.9 (V)	300	49.9 (V)
7	300	35.1 (M)	800	6.8 (M)	300	70.1 (V)	300	54.5 (V)	300	58.2 (V)
8	310	39.7 (M^*)	810	8.1 (M)	300	80.9 (V)	300	63.8 (V)	300	66.8 (V)
9	330	42.2 (M^*)	830	9.0 (M)	300	89.2 (V)	300	71.1 (V)	300	74.6 (V)
10	340	46.1 (M^*)	840	10.6 (M)	330	94.4 (V)	330	76.0 (V)	330	75.5 (V)
11	350	49.6 (M^*)	850	12.0 (M)	370	96.0 (V)	370	77.8 (V)	370	88.4 (V)
12	360	50.9 (M^*)	860	13.3 (M)	440	94.7 (V)	440	77.0 (V)	440	69.8 (V)
13	370	48.3 (M^*)	470	54.7 (M)	560	91.2 (V)	450	80.8 (V)	340	21.5 (M^*)
14	370	53.2 (M^*)	470	63.9 (M)	610	93.0 (V)	480	84.1 (V)	350	25.9 (M^*)
16	410	57.4 (M^*)	530	84.2 (M^*)	1070	96.3 (V)	805	87.3 (V)	540	24.9 (M^*)

M = Bending moment, M^* = Bending moment, yielding of reinforcement in both layers,

FAT = Fatigue, V = Shear force

Table F.5 Thicknesses and utilization ratios, H= 6m, Fixed BC

L [m]	t_s[mm]	**η** [%]	$\mathbf{t_{sh}}$[mm]	**η** [%]	t_{f2}[mm]	**η** [%]	t_{fmid} [mm]	**η** [%]	t_{f1}[mm]	**η** [%]
6	300	26.2 (M)	800	7.6 (M)	300	55.3 (V)	300	25.7 (V)	300	45.8 (V)
7	300	35.2 (M)	800	8.4 (M)	300	59.0 (V)	300	29.7 (V)	300	45.8 (V)
8	310	41.0 (M^*)	810	9.7 (M)	300	68.1 (V)	300	35.2 (V)	300	44.7 (V)
9	330	46.4 (M^*)	830	11.2 (M)	300	72.0 (V)	300	39.2 (V)	300	43.7 (V)
10	350	49.1 (M^*)	850	11.4 (M)	300	80.4 (V)	300	45.2 (V)	300	41.8 (V)
11	370	54.3 (M^*)	870	11.7 (M)	300	84.5 (V)	300	49.4 (V)	300	43.6 (V)
12	380	58.8 (M^*)	880	13.3 (M)	300	94.2 (V)	300	56.5 (V)	300	52.2 (V)
13	390	55.6 (M^*)	490	45.3 (M)	400	93.5 (V)	350	57.0 (V)	300	56.0 (V)
14	390	58.4 (M^*)	490	54.1 (M)	450	92.8 (V)	375	60.7 (V)	300	63.6 (V)
16	420	66.6 (M^*)	520	73.6 (M)	580	94.6 (V)	450	71.1 (V)	320	34.6 (M^*)
18	440	71.1 (M^*)	540	89.7 (M)	700	96.5 (V)	530	76.1 (V)	94.0	55.6 (V)
20	460	70.7 (M^*)	600	94.4 (M)	920	96.2 (V)	695	81.4 (V)	460	91.4 (V)
22	480	70.9 (M^*)	680	94.2 (M)	1210	91.9 (V)	870	90.5 (V)	530	92.2 (V)
24	490	71.3 (M^*)	770	96.4 (M)	1600	98.2 (V)	1090	98.5 (V)	580	23.3 (M^*)

M = Bending moment, M^* = Bending moment, yielding of reinforcement in both layers,

FAT = Fatigue, V = Shear force

Table F.6 Thicknesses and utilization ratios, H= 8m, Fixed BC

L [m]	t_s[mm]	**η** [%]	$\mathbf{t_{sh}}$[mm]	**η** [%]	t_{f2}[mm]	**η** [%]	t_{fmid} [mm]	**η** [%]	t_{f1}[mm]	**η** [%]
6	300	17.9 (M)	800	10.9 (M)	390	61.2 (V)	390	16.6 (V)	390	57.5 (M*)
7	300	26.6 (M)	800	11.7 (M)	390	60.7 (V)	390	16.8 (V)	390	57.9 (M*)
8	300	35.0 (M*)	800	13.2 (M)	390	68.0 (V)	390	16.6 (V)	390	57.8 (M*)
9	320	31.9 (M*)	820	14.1 (M)	390	71.4 (V)	390	17.8 (V)	390	57.0 (M*)
10	330	45.3 (M*)	830	15.3 (M)	390	75.5 (V)	390	21.1 (V)	390	56.3 (M*)
11	350	48.5 (M*)	850	16.4 (M)	390	79.3 (V)	390	24.5 (V)	390	55.2 (M*)
12	370	51.9 (M*)	870	17.4 (M)	390	83.4 (V)	390	28.0 (V)	390	53.8 (M*)
13	380	51.4 (M*)	480	56.4 (M)	460	89.3 (V)	415	30.7 (V)	370	52.2 (M*)
14	380	57.9 (M*)	480	63.4 (M*)	470	92.6 (V)	420	34.3 (V)	370	50.5 (M*)
16	420	66.1 (M*)	520	81.1 (M*)	590	94.1 (V)	480	42.3 (V)	370	48.8 (M*)
18	440	71.1 (M*)	550	93.7 (M)	700	94.8 (V)	530	47.4 (V)	360	42.4 (M*)
20	460	73.9 (M*)	610	95.3 (M)	810	94.9 (V)	585	53.8 (V)	360	38.4 (M*)
22	470	75.3 (M*)	700	92.4 (M)	950	91.4 (V)	655	61.7 (V)	360	28.7 (M*)
24	490	78.8 (M*)	780	92.0 (M)	990	92.3 (V)	675	72.5 (V)	360	33.2 (M*)
25	500	81.2 (M*)	800	96.0 (M)	1030	93.0 (V)	705	77.1 (V)	380	35.6 (M*)

M = Bending moment, M* = Bending moment, yielding of reinforcement in both layers,

FAT = Fatigue, V = Shear force

H

Case Study - Comparison of Carbon Dioxide Impact

Environmental Impact Comparison

General input:

$\rho_{steel} = 7800 \quad kg/m^3$

$EMC_{concrete} = 360 \quad kg/m^3$

$EMC_{reinforcement} = 1.03 * \rho_{steel} = 8034 \quad kg/m^3$

Bridge: L 814

Current design according to SRA

Dimensions:

$L = 6\,m$

$H = 6m$

$B = 6\,m$

$t_s = 350\,mm$

$t_{sh} = 850\,mm$

$t_{f1} = 400\,mm$

$t_{f2} = 400\,mm$

Pinned boundary condition

Required Reinforcement:

$As_{field} = \ 1.53 * 10^{-3} \ \frac{m^2}{m}$ (0.6 lager ϕ16 s85)

$As_{corner} = \ 1.94 * 10^{-3} \ \frac{m^2}{m}$ (0.8 lager ϕ16 s85)

$As_{mid} = \ 1.98 * 10^{-3} \ \frac{m^2}{m}$ (0.8 lager ϕ16 s85)

$Asw =$ 0 mm

$n_{stirrup} = 0$ *number if stirrups in longitudinal direction*

Concrete Volume:

$$V_{frame,leg} = B * \left(\left(t_{f1} * H \right) + \frac{(t_{f2} - t_{f1}) * H}{2} \right) * 2$$

$$V_{Bridge,deck} = B * \left((t_s * L) + 2 * \frac{0.5 * 0.5}{2} \right)$$

$$V_{concrete} = V_{frame,leg} + V_{Bridge,deck}$$

Reinforcement Volume:

$V_{rein,long,field} = As_{field} * \frac{L}{2} + \frac{As_{field}}{4} * \frac{L}{2}$

$V_{rein,long,corner} = As_{corner} * \frac{L}{4} * 2 + \frac{As_{corner}}{4} * \frac{L}{4} * 2 + As_{corner} * \frac{H}{4} * 2 + \frac{As_{corner}}{4} * \frac{H}{4} * 2$

$V_{rein,long,mid} = As_{mid} * \frac{H}{2} * 2 + \frac{As_{mid}}{4} * \frac{L}{2} * 2$

$V_{reinforcement} = V_{rein,long,field} + V_{rein,long,corner} + V_{rein,long,mid}$

Total Carbon Dioxide Impact

$Carbon\ impact\ concrete = V_{concrete} * EMC_{concrete}$

$Carbon\ impact\ reinforcement = V_{reinforcement} * EMC_{reinforcement}$

$Total\ carbon\ impact = Carbon\ impact\ concrete + Carbon\ impact\ reinforcement$

$\boldsymbol{Total\ carbon\ impact}$ **= 14454 kg CO_2-eq**

<u>Optimized design</u>

Dimensions:

$L = 6\ m$

$H = 6\ m$

$B = 6\ m$

$t_s = 300\ mm$

$t_{sh} = 800\ mm$

$t_{f1} = 300\ mm$

$t_{f2} = 300\ mm$

Pinned boundary condition

Required Reinforcement:

$As_{field} = 1.94 * 10^{-3}\ \frac{m^2}{m}$ (0.5 $lager\ \phi 20$ s88)

$As_{corner} = 3.07 * 10^{-3}\ \frac{m^2}{m}$ (0.8 $lager\ \phi 20$ s88)

$As_{mid} = 2.45 * 10^{-3}\ \frac{m^2}{m}$ (0.7 $lager\ \phi 20$ s88)

Stirrups : double loop

$Asw = 0.0785 * 10^{-3}\ m^2$ (5 x ϕ10 s220)

$n_{stirrup} = 2 * 5 = 10\ st$ *number if stirrups in longitudinal direction*

$n_{transverse} = 2.5\ st$ *number of stirrup-bars in transverse direction/m*

$$L_{stirrup} = \left(2 * b_{stirrup} + 2 * (t_{sh} - 2 * c_c) + 2 * l_{lap}\right) * n_{transverse}$$

Concrete Volume:

$$V_{frame,leg} = B * \left(\left(t_{f1} * H\right) + \frac{(t_{f2} - t_{f1}) * H}{2}\right) * 2$$

$$V_{Bridge,deck} = B * \left((t_s * L) + 2 * \frac{0.5 * 0.5}{2}\right)$$

$$V_{concrete} = V_{frame,leg} + V_{Bridge,deck}$$

Reinforcement Volume:

$$V_{rein,long,field} = As_{field} * \frac{L}{2} + \frac{As_{field}}{4} * \frac{L}{2}$$

$$V_{rein,long,corner} = As_{corner} * \frac{L}{4} * 2 + \frac{As_{corner}}{4} * \frac{L}{4} * 2 + As_{corner} * \frac{H}{4} * 2 + \frac{As_{corner}}{4} * \frac{H}{4} * 2$$

$$V_{rein,long,mid} = As_{mid} * \frac{H}{2} * 2 + \frac{As_{mid}}{4} * \frac{L}{2} * 2$$

$$V_{rein,stirrup} = Asw * n_{stirrups} * L_{stirrups} = 0\ m^2$$

$$V_{reinforcement} = V_{rein,long,field} + V_{rein,long,corner} + V_{rein,long,mid} + V_{rein,stirrup}$$

Total Carbon Dioxide Impact

$$Carbon\ impact\ concrete = V_{concrete} * EMC_{concrete}$$

$$Carbon\ impact\ reinforcement = V_{reinforcement} * EMC_{reinforcement}$$

$$Total\ carbon\ impact = Carbon\ impact\ concrete + Carbon\ impact\ reinforcement$$

$\boldsymbol{Total\ carbon\ impact}$ **= 11648 kg $\boldsymbol{CO_2}$-eq**

Bridge: Y 1283

Current design according to SRA

Dimensions:

$L = 10\ m$

$H = 6m$

$B = 6\ m$

$t_s = 450\ mm$

$t_{sh} = 950\ mm$

$t_{f1} = 400\ mm$

$t_{f2} = 400\ mm$

Pinned boundary condition

Required Reinforcement:

As_{field} = $2.93 * 10^{-3}\ \frac{m^2}{m}$ (0.8 lager ϕ20 s87.5)

As_{corner} = $3.48 * 10^{-3}\ \frac{m^2}{m}$ (1.0 lager ϕ20 s87.5)

As_{mid} = $1.40 * 10^{-3}\ \frac{m^2}{m}$ (0.6 lager ϕ16 s85)

Asw = 0 mm

$n_{stirrup}$= 0 *number if stirrups in longitudinal direction*

Concrete Volume:

$$V_{frame,leg} = B * \left(\left(t_{f1} * H \right) + \frac{(t_{f2} - t_{f1}) * H}{2} \right) * 2$$

$$V_{Bridge,deck} = B * \left((t_s * L) + 2 * \frac{0.5 * 0.5}{2} \right)$$

$$V_{concrete} = V_{frame,leg} + V_{Bridge,deck}$$

Reinforcement Volume:

$$V_{rein,long,field} = As_{field} * \frac{L}{2} + \frac{As_{field}}{4} * \frac{L}{2}$$

$$V_{rein,long,corner} = As_{corner} * \frac{L}{4} * 2 + \frac{As_{corner}}{4} * \frac{L}{4} * 2 + As_{corner} * \frac{H}{4} * 2 + \frac{As_{corner}}{4} * \frac{H}{4} * 2$$

$$V_{rein,long,mid} = As_{mid} * \frac{H}{2} * 2 + \frac{As_{mid}}{4} * \frac{L}{2} * 2$$

$V_{reinforcement} = V_{rein,long,field} + V_{rein,long,corner} + V_{rein,long,mid}$

Total Carbon Dioxide Impact

$Carbon\ impact\ concrete = V_{concrete} * EMC_{concrete}$

$Carbon\ impact\ reinforcement = V_{reinforcement} * EMC_{reinforcement}$

$Total\ carbon\ impact = Carbon\ impact\ concrete + Carbon\ impact\ reinforcement$

$\boldsymbol{Total\ carbon\ impact}$ **= 19918 kg CO_2-eq**

Optimized design

Dimensions:

$L = 10\ m$

$H = 6\ m$

$B = 6\ m$

$t_s = 350\ mm$

$t_{sh} = 850\ mm$

$t_{f1} = 300\ mm$

$t_{f2} = 300\ mm$

Pinned boundary condition

Required Reinforcement:

$As_{field} = 4.23 * 10^{-3}\ \frac{m^2}{m}$ (0.9 $lager\ \phi 25$ s99)

$As_{corner} = 5.5 * 10^{-3}\ \frac{m^2}{m}$ (1.1 $lager\ \phi 25$ s99)

$As_{mid} = 2.01 * 10^{-3}\ \frac{m^2}{m}$ (0.9 $lager\ \phi 16$ s85)

Stirrups : double loop

$Asw = 0.0785 * 10^{-3}\ m^2$, 5 $x\ \phi 10$ s220

$n_{stirrup} = 2 * 6 = 12\ st$ *number if stirrups in longitudinal direction*

$n_{transverse} = 2.5\ st$ *number of stirrup-bars in transverse direction/m*

$$L_{stirrup} = \left(2 * b_{stirrup} + 2 * (t_{sh} - 2 * c_c) + 2 * l_{lap}\right) * n_{transverse}$$

Concrete Volume:

$$V_{frame,leg} = B * \left(\left(t_{f1} * H\right) + \frac{(t_{f2} - t_{f1}) * H}{2}\right) * 2$$

$$V_{Bridge,deck} = B * \left((t_s * L) + 2 * \frac{0.5 * 0.5}{2}\right)$$

$$V_{concrete} = V_{frame,leg} + V_{Bridge,deck}$$

Reinforcement Volume:

$$V_{rein,long,field} = As_{field} * \frac{L}{2} + \frac{As_{field}}{4} * \frac{L}{2}$$

$$V_{rein,long,corner} = As_{corner} * \frac{L}{4} * 2 + \frac{As_{corner}}{4} * \frac{L}{4} * 2 + As_{corner} * \frac{H}{4} * 2 + \frac{As_{corner}}{4} * \frac{H}{4} * 2$$

$$V_{rein,long,mid} = As_{mid} * \frac{H}{2} * 2 + \frac{As_{mid}}{4} * \frac{L}{2} * 2$$

$$V_{rein,stirrup} = Asw * n_{stirrups} * L_{stirrups} = 0\ m^2$$

$$V_{reinforcement} = V_{rein,long,field} + V_{rein,long,corner} + V_{rein,long,mid} + V_{rein,stirrup}$$

Total Carbon Dioxide Impact

$$Carbon\ impact\ concrete = V_{concrete} * EMC_{concrete}$$

$$Carbon\ impact\ reinforcement = V_{reinforcement} * EMC_{reinforcement}$$

$$Total\ carbon\ impact = Carbon\ impact\ concrete + Carbon\ impact\ reinforcement$$

$$\boldsymbol{Total\ carbon\ impact} = \textbf{15201 kg } \boldsymbol{CO_2}\textbf{-eq}$$

Bridge: Z 1060

Current design according to SRA

Dimensions:

$L = 14.5\ m$

$H = 6\ m$

$B = 6\ m$

$t_s = 550\ mm$

$t_{sh} = 750\ mm$

$t_{f1} = 400\ mm$

$t_{f2} = 500\ mm$

Pinned boundary condition

Required Reinforcement:

As_{field} = $4.06 * 10^{-3}\ \frac{m^2}{m}$ (0.8 lager ϕ25)

As_{corner} = $2.77 * 10^{-3}\ \frac{m^2}{m}$ (0.6 lager ϕ25)

As_{mid} = $1.38 * 10^{-3}\ \frac{m^2}{m}$ (0.6 lager ϕ16)

Asw = 0 mm

$n_{stirrup}$= 0 *number if stirrups in longitudinal direction*

Concrete Volume:

$$V_{frame,leg} = B * \left(\left(t_{f1} * H\right) + \frac{(t_{f2} - t_{f1}) * H}{2} \right) * 2$$

$$V_{Bridge,deck} = B * \left((t_s * L) + 2 * \frac{(t_{sh} - t_s) * \frac{L}{4}}{2} \right)$$

$$V_{concrete} = V_{frame,leg} + V_{Bridge,deck}$$

Reinforcement Volume:

$$V_{rein,long,field} = As_{field} * \frac{L}{2} + \frac{As_{field}}{4} * \frac{L}{2}$$

$$V_{rein,long,corner} = As_{corner} * \frac{L}{4} * 2 + \frac{As_{corner}}{4} * \frac{L}{4} * 2 + As_{corner} * \frac{H}{4} * 2 + \frac{As_{corner}}{4} * \frac{H}{4} * 2$$

$V_{rein,long,mid} = As_{mid} * \frac{H}{2} * 2 + \frac{As_{mid}}{4} * \frac{L}{2} * 2$

$V_{rein,stirrup} = Asw * n_{stirrups} * L_{stirrups} = 0\ m^2$

$V_{reinforcement} = V_{rein,long,field} + V_{rein,long,corner} + V_{rein,long,mid}$

Total Carbon Dioxide Impact

$Carbon\ impact\ concrete = V_{concrete} * EMC_{concrete}$

$Carbon\ impact\ reinforcement = V_{reinforcement} * EMC_{reinforcement}$

$Total\ carbon\ impact = Carbon\ impact\ concrete + Carbon\ impact\ reinforcement$

$\boldsymbol{Total\ carbon\ impact}$ **= 30011 kg $\boldsymbol{CO_2}$-eq**

<u>Optimized design</u>

Dimensions:

$L = 14.5\ m$

$H = 6\ m$

$B = 6\ m$

$t_s = 410\ mm$

$t_{sh} = 510\ mm$

$t_{f1} = 300\ mm$

$t_{f2} = 450\ mm$

Pinned boundary condition

Required Reinforcement:

$As_{field} = 5.57 * 10^{-3}\ \frac{m^2}{m}$ (1.1 $lager\ \phi 25\ s99$)

$As_{corner} = 4.78 * 10^{-3}\ \frac{m^2}{m}$ (1.0 $lager\ \phi 25\ s99$)

$As_{mid} = 1.94 * 10^{-3}\ \frac{m^2}{m}$ (0.5 $lager\ \phi 20$)

$Asw = 0$

$n_{stirrup} = 0$ *number if stirrups in longitudinal direction*

Concrete Volume:

$$V_{frame,leg} = B * \left(\left(t_{f1} * H \right) + \frac{(t_{f2} - t_{f1}) * H}{2} \right) * 2$$

$$V_{Bridge,deck} = B * \left((t_s * L) + 2 * \frac{(t_{sh} - t_s) * \frac{L}{4}}{2} \right)$$

$$V_{concrete} = V_{frame,leg} + V_{Bridge,deck}$$

Reinforcement Volume:

$$V_{rein,long,field} = As_{field} * \frac{L}{2} + \frac{As_{field}}{4} * \frac{L}{2}$$

$$V_{rein,long,corner} = As_{corner} * \frac{L}{4} * 2 + \frac{As_{corner}}{4} * \frac{L}{4} * 2 + As_{corner} * \frac{H}{4} * 2 + \frac{As_{corner}}{4} * \frac{H}{4} * 2$$

$$V_{rein,long,mid} = As_{mid} * \frac{H}{2} * 2 + \frac{As_{mid}}{4} * \frac{L}{2} * 2$$

$$V_{rein,stirrup} = Asw * n_{stirrups} * L_{stirrups} = 0\ m^2$$

$$V_{reinforcement} = V_{rein,long,field} + V_{rein,long,corner} + V_{rein,long,mid}$$

Total Carbon Dioxide Impact

$$Carbon\ impact\ concrete = V_{concrete} * EMC_{concrete}$$

$$Carbon\ impact\ reinforcement = V_{reinforcement} * EMC_{reinforcement}$$

$$Total\ carbon\ impact = Carbon\ impact\ concrete + Carbon\ impact\ reinforcement$$

$$\boldsymbol{Total\ carbon\ impact} = \textbf{23490 kg } \boldsymbol{CO_2}\textbf{-eq}$$

Bridge: Y 1217

Current design according to SRA

Dimensions:

$L = 18\ m$

$H = 6\ m$

$B = 6\ m$

$t_s = 730\ mm$

$t_{sh} = 930\ mm$

$t_{f1} = 400\ mm$

$t_{f2} = 500\ mm$

Pinned boundary condition

Required Reinforcement:

As_{field} = $6.15 * 10^{-3}\ \frac{m^2}{m}$ (1.7 lager ϕ20 s87.5)

As_{corner} = $2.75 * 10^{-3}\ \frac{m^2}{m}$ (0.7 lager ϕ20 s87.5)

As_{mid} = $2.34 * 10^{-3}\ \frac{m^2}{m}$ (0.6 lager ϕ20 s87.5)

Asw = 0 mm

$n_{stirrup}$= 0 *number if stirrups in longitudinal direction*

Concrete Volume:

$$V_{frame,leg} = B * \left(\left(t_{f1} * H \right) + \frac{(t_{f2} - t_{f1}) * H}{2} \right) * 2$$

$$V_{Bridge,deck} = B * \left((t_s * L) + 2 * \frac{(t_{sh} - t_s) * \frac{L}{4}}{2} \right)$$

$$V_{concrete} = V_{frame,leg} + V_{Bridge,deck}$$

Reinforcement Volume:

$$V_{rein,long,field} = As_{field} * \frac{L}{2} + \frac{As_{field}}{4} * \frac{L}{2}$$

$$V_{rein,long,corner} = As_{corner} * \frac{L}{4} * 2 + \frac{As_{corner}}{4} * \frac{L}{4} * 2 + As_{corner} * \frac{H}{4} * 2 + \frac{As_{corner}}{4} * \frac{H}{4} * 2$$

$V_{rein,long,mid} = As_{mid} * \frac{H}{2} * 2 + \frac{As_{mid}}{4} * \frac{L}{2} * 2$

$V_{reinforcement} = V_{rein,long,field} + V_{rein,long,corner} + V_{rein,long,mid}$

Total Carbon Dioxide Impact

$Carbon\ impact\ concrete = V_{concrete} * EMC_{concrete}$

$Carbon\ impact\ reinforcement = V_{reinforcement} * EMC_{reinforcement}$

$Total\ carbon\ impact = Carbon\ impact\ concrete + Carbon\ impact\ reinforcement$

$\boldsymbol{Total\ carbon\ impact}$ = **42200 kg CO_2-eq**

<u>Optimized design</u>

Dimensions:

$L = 18\ m$

$H = 6\ m$

$B = 6\ m$

$t_s = 460\ mm$

$t_{sh} = 560\ mm$

$t_{f1} = 300\ mm$

$t_{f2} = 620\ mm$

Pinned boundary condition

Required Reinforcement:

$As_{field} = 7.31 * 10^{-3}\ \frac{m^2}{m}$ (1.5 $lager\ \phi 25$ s99)

$As_{corner} = 7.93 * 10^{-3}\ \frac{m^2}{m}$ (1.6 $lager\ \phi 25$ s99)

$As_{mid} = 3.08 * 10^{-3}\ \frac{m^2}{m}$ (0.6 $lager\ \phi 25$ s99)

$Asw = 0.0785 * 10^{-3}\ m^2$ (5 $x\ \phi 10$ s250)

$n_{stirrup} = 2 * 9 = 18\ st$ *number if stirrups in longitudinal direction*

$n_{transverse} = 2.5\ st$ *number of stirrup-bars in transverse direction/m*

$$L_{stirrup} = \left(2 * b_{stirrup} + 2 * (t_{sh} - 2 * c_c) + 2 * l_{lap}\right) * n_{transverse}$$

Concrete Volume:

$$V_{frame,leg} = B * \left(\left(t_{f1} * H\right) + \frac{(t_{f2} - t_{f1}) * H}{2}\right) * 2$$

$$V_{Bridge,deck} = B * \left((t_s * L) + 2 * \frac{(t_{sh} - t_s) * \frac{L}{4}}{2}\right)$$

$$V_{concrete} = V_{frame,leg} + V_{Bridge,deck}$$

Reinforcement Volume:

$$V_{rein,long,field} = As_{field} * \frac{L}{2} + \frac{As_{field}}{4} * \frac{L}{2}$$

$$V_{rein,long,corner} = As_{corner} * \frac{L}{4} * 2 + \frac{As_{corner}}{4} * \frac{L}{4} * 2 + As_{corner} * \frac{H}{4} * 2 + \frac{As_{corner}}{4} * \frac{H}{4} * 2$$

$$V_{rein,long,mid} = As_{mid} * \frac{H}{2} * 2 + \frac{As_{mid}}{4} * \frac{L}{2} * 2$$

$$V_{rein,stirrup} = Asw * n_{stirrups} * L_{stirrups} = 0\ m^2$$

$$V_{reinforcement} = V_{rein,long,field} + V_{rein,long,corner} + V_{rein,long,mid} + V_{rein,stirrup}$$

Total Carbon Dioxide Impact

$$Carbon\ impact\ concrete = V_{concrete} * EMC_{concrete}$$

$$Carbon\ impact\ reinforcement = V_{reinforcement} * EMC_{reinforcement}$$

$$Total\ carbon\ impact = Carbon\ impact\ concrete + Carbon\ impact\ reinforcement$$

$\boldsymbol{Total\ carbon\ impact}$ **= 32013 kg $\boldsymbol{CO_2}$-eq**

Bridge: A

Current design

Dimensions:

$L = 11.5\ m$

$H = 8.363\ m$

$B = 6\ m$

$t_s = 600\ mm$

$t_{sh} = 1100\ mm$

$t_{f1} = 550\ mm$

$t_{f2} = 550\ mm$

Pinned boundary condition

Used Reinforcement:

As_{field} = $2.86 * 10^{-3}\ \frac{m^2}{m}$ (ϕ20 s110)

As_{corner} = $3.49 * 10^{-3}\ \frac{m^2}{m}$ (ϕ25 s110)

As_{mid} = $1.75 * 10^{-3}\ \frac{m^2}{m}$ (ϕ20 s110)

As_{sup} = $1.12 * 10^{-3}\ \frac{m^2}{m}$ (ϕ16 s180)

Asw = 0 mm

$n_{stirrup}$= 0 st *number if stirrups in longitudinal direction*

Concrete Volume:

$$V_{frame,leg} = B * \left(\left(t_{f1} * H \right) + \frac{(t_{f2} - t_{f1}) * H}{2} \right) * 2$$

$$V_{Bridge,deck} = B * \left((t_s * L) + 2 * \frac{0.5 * 0.5}{2} \right)$$

$$V_{concrete} = V_{frame,leg} + V_{Bridge,deck}$$

Reinforcement Volume:

$$V_{rein,long,field} = As_{field} * \frac{L}{2} + \frac{As_{field}}{4} * \frac{L}{2}$$

$$V_{rein,long,corner} = As_{corner} * \frac{L}{4} * 2 + \frac{As_{corner}}{4} * \frac{L}{4} * 2 + As_{corner} * \frac{H}{4} * 2 + \frac{As_{corner}}{4} * \frac{H}{4} * 2$$

$V_{rein,long,mid} = As_{mid} * \frac{H}{2} * 2 + \frac{As_{mid}}{4} * \frac{L}{2} * 2$

$V_{reinforcement} = V_{rein,long,field} + V_{rein,long,corner} + V_{rein,long,mid}$

Total Carbon Dioxide Impact

$Carbon\ impact\ concrete = V_{concrete} * EMC_{concrete}$

$Carbon\ impact\ reinforcement = V_{reinforcement} * EMC_{reinforcement}$

$Total\ carbon\ impact = Carbon\ impact\ concrete + Carbon\ impact\ reinforcement$

$\boldsymbol{Total\ carbon\ impact}$ = **34664 kg CO_2-eq**

<u>Optimized design</u>

Dimensions:

$L = 11.5\ m$

$H = 8.363$

$B = 6\ m$

$t_s = 350\ mm$

$t_{sh} = 850\ mm$

$t_{f1} = 440\ mm$

$t_{f2} = 440\ mm$

Fixed boundary condition

Required Reinforcement:

$As_{field} = 3.9 * 10^{-3}\ \frac{m^2}{m}$ (0.8 $lager\ \phi 25\ s99$)

$As_{corner} = 4.34 * 10^{-3}\ \frac{m^2}{m}$ (0.9 $lager\ \phi 25\ s99$)

$As_{mid} = 4.19 * 10^{-3}\ \frac{m^2}{m}$ (0.8 $lager\ \phi 25$ s99)

$Asw = 0.0785 * 10^{-3}\ m^2$ (5 $x\ \phi 10$ s200)

$n_{stirrup} = 2 * 8 = 16\ st$ *number if stirrups in longitudinal direction*

$n_{transverse} = 2.5\ st$ *number of stirrup-bars in transverse direction/m*

$$L_{stirrup} = \left(2 * b_{stirrup} + 2 * (t_{sh} - 2 * c_c) + 2 * l_{lap}\right) * n_{transverse}$$

Concrete Volume:

$$V_{frame,leg} = B * \left(\left(t_{f1} * H\right) + \frac{(t_{f2} - t_{f1}) * H}{2}\right) * 2$$

$$V_{Bridge,deck} = B * \left((t_s * L) + 2 * \frac{0.5 * 0.5}{2}\right)$$

$$V_{concrete} = V_{frame,leg} + V_{Bridge,deck}$$

Reinforcement Volume:

$$V_{rein,long,field} = As_{field} * \frac{L}{2} + \frac{As_{field}}{4} * \frac{L}{2}$$

$$V_{rein,long,corner} = As_{corner} * \frac{L}{4} * 2 + \frac{As_{corner}}{4} * \frac{L}{4} * 2 + As_{corner} * \frac{H}{4} * 2 + \frac{As_{corner}}{4} * \frac{H}{4} * 2$$

$$V_{rein,long,mid} = As_{mid} * \frac{H}{2} * 2 + \frac{As_{mid}}{4} * \frac{L}{2} * 2$$

$$V_{rein,stirrup} = Asw * n_{stirrups} * L_{stirrups}$$

$$V_{reinforcement} = V_{rein,long,field} + V_{rein,long,corner} + V_{rein,long,mid} + V_{rein,stirrup}$$

Total Carbon Dioxide Impact

$$Carbon\ impact\ concrete = V_{concrete} * EMC_{concrete}$$

$$Carbon\ impact\ reinforcement = V_{reinforcement} * EMC_{reinforcement}$$

$$Total\ carbon\ impact = Carbon\ impact\ concrete + Carbon\ impact\ reinforcement$$

$\boldsymbol{Total\ carbon\ impact}$ **= 25200 kg $\boldsymbol{CO_2}$-eq**

Bridge: B

Current design

Dimensions:

$L = 13.6\ m$

$H = 5.676\ m$

$B = 6\ m$

$t_s = 666\ mm$

$t_{sh} = 866\ mm$

$t_{f1} = 600\ mm$

$t_{f2} = 600\ mm$

Fixed boundary condition

Used Reinforcement:

$As_{field} = \ 3.49 * 10^{-3}\ \frac{m^2}{m}$ (ϕ20 s90)

$As_{corner} = \ 3.49 * 10^{-3}\ \frac{m^2}{m}$ (ϕ20 s90)

$As_{mid} = \ 1.12 * 10^{-3}\ \frac{m^2}{m}$ (ϕ16 s180)

$As_{sup} = \ 1.12 * 10^{-3}\ \frac{m^2}{m}$ (ϕ16 s180)

Stirrups : inclined G-bars

$Asw = 0.201 * 10^{-3} m^2$ (6 x ϕ16 s360)

$n_{stirrup} = 2 * 6 = 12\ st$ *number if stirrups in longitudinal direction*

$n_{transverse} = 2.78\ st$ *number if stirrups in transverse direction / m*

$L_{stirrup} = \frac{t_{sh}}{cos45°} + 0.45 + 0.35$

Concrete Volume:

$V_{frame,leg} = B * \left(\left(t_{f1} * H \right) + \frac{(t_{f2} - t_{f1}) * H}{2} \right) * 2$

$V_{Bridge,deck} = B * \left((t_s * L) + 2 * \frac{(t_{sh} - t_s) * \frac{L}{4}}{2} \right)$

$V_{concrete} = V_{frame,leg} + V_{Bridge,deck}$

Reinforcement Volume:

$V_{rein,long,field} = As_{field} * \frac{L}{2} + \frac{As_{field}}{4} * \frac{L}{2}$

$V_{rein,long,corner} = As_{corner} * \frac{L}{4} * 2 + \frac{As_{corner}}{4} * \frac{L}{4} * 2 + As_{corner} * \frac{H}{4} * 2 + \frac{As_{corner}}{4} * \frac{H}{4} * 2$

$V_{rein,long,mid} = As_{mid} * \frac{H}{2} * 2 + \frac{As_{mid}}{4} * \frac{L}{2} * 2$

$V_{rein,stirrup} = Asw * n_{stirrups} * L_{stirrups} * n_{transverse}$

$V_{reinforcement} = V_{rein,long,field} + V_{rein,long,corner} + V_{rein,long,mid} + V_{rein,stirrup}$

Total Carbon Dioxide Impact

$Carbon\ impact\ concrete = V_{concrete} * EMC_{concrete}$

$Carbon\ impact\ reinforcement = V_{reinforcement} * EMC_{reinforcement}$

$Total\ carbon\ impact = Carbon\ impact\ concrete + Carbon\ impact\ reinforcement$

$\boldsymbol{Total\ carbon\ impact}$ = **34447 kg CO_2-eq**

<u>Optimized design</u>

Dimensions:

$L = 13.6\ m$

$H = 5.676$

$B = 6\ m$

$t_s = 390\ mm$

$t_{sh} = 490\ mm$

$t_{f1} = 300\ mm$

$t_{f2} = 450\ mm$

Fixed boundary condition

Required Reinforcement:

$As_{field} = 4.68 * 10^{-3}\ \frac{m^2}{m}$ ($0.9\ lager\ \phi 25$)

As_{corner} = $4.45 * 10^{-3}$ $\frac{m^2}{m}$ (0.9 $lager\ \phi 25$)

As_{mid} = $0.88 * 10^{-3}$ $\frac{m^2}{m}$ (0.4 $lager\ \phi 16$)

Stirrups : double loops

Asw =$0.0785 * 10^{-3}$ m^2 (5 $x\ \phi 10$ s250)

$n_{stirrup} = 2 * 7 = 14\ st$ *number if stirrups in longitudinal direction*

$n_{transverse} = 2.5\ st$ *number of stirrup-bars in transverse direction/m*

$$L_{stirrup} = \left(2 * b_{stirrup} + 2 * (t_{sh} - 2 * c_c) + 2 * l_{lap}\right) * n_{transverse}$$

Concrete Volume:

$$V_{frame,leg} = B * \left(\left(t_{f1} * H\right) + \frac{(t_{f2} - t_{f1}) * H}{2}\right) * 2$$

$$V_{Bridge,deck} = B * \left((t_s * L) + 2 * \frac{(t_{sh} - t_s) * \frac{L}{4}}{2}\right)$$

$$V_{concrete} = V_{frame,leg} + V_{Bridge,deck}$$

Reinforcement Volume:

$$V_{rein,long,field} = As_{field} * \frac{L}{2} + \frac{As_{field}}{4} * \frac{L}{2}$$

$$V_{rein,long,corner} = As_{corner} * \frac{L}{4} * 2 + \frac{As_{corner}}{4} * \frac{L}{4} * 2 + As_{corner} * \frac{H}{4} * 2 + \frac{As_{corner}}{4} * \frac{H}{4} * 2$$

$$V_{rein,long,mid} = As_{mid} * \frac{H}{2} * 2 + \frac{As_{mid}}{4} * \frac{L}{2} * 2$$

$$V_{rein,stirrup} = Asw * n_{stirrups} * L_{stirrups} = 0\ m^2$$

$$V_{reinforcement} = V_{rein,long,field} + V_{rein,long,corner} + V_{rein,long,mid} + V_{rein,stirrup}$$

Total Carbon Dioxide Impact

$$Carbon\ impact\ concrete = V_{concrete} * EMC_{concrete}$$

$$Carbon\ impact\ reinforcement = V_{reinforcement} * EMC_{reinforcement}$$

$$Total\ carbon\ impact = Carbon\ impact\ concrete + Carbon\ impact\ reinforcement$$

$\boldsymbol{Total\ carbon\ impact}$ = **21315 kg $\boldsymbol{CO_2}$-eq**

DEPARTMENT OF ARCHITECTURE AND CIVIL ENGINEERING
CHALMERS UNIVERSITY OF TECHNOLOGY
Gothenburg, Sweden
www.chalmers.se

CHALMERS
UNIVERSITY OF TECHNOLOGY